GEOPHYSICAL INVESTIGATION FOR FOUNDATION STUDIES OF THE PHASE II SITE, AHMADU BELLO UNIVERSITY, ZARIA USING MULTI-CHANNEL ANALYSIS OF SURFACE WAVES

BY

FAHAD ABUBAKAR

DEPARTMENT OF PHYSICS,

FACULTY OF PHYSICAL SCIENCE,

AHMADU BELLO UNIVERSITY, ZARIA

NIGERIA

MARCH, 2021

GEOPHYSICAL INVESTIGATION FOR FOUNDATION STUDIES OF THE PHASE II SITE, AHMADU BELLO UNIVERSITY, ZARIA USING MULTI-CHANNEL ANALYSIS OF SURFACE WAVES

BY

FAHAD ABUBAKAR

P16PSPY8043

BEING A DISSERTATION SUBMITTED TO THE SCHOOL OF POSTGRADUATE STUDIES, AHMADU BELLO UNIVERSITY, ZARIA

IN PARTIAL FULFILMENT OF THE REQUIREMENTS FOR THE AWARD OF MASTER OF SCIENCE DEGREE IN APPLIED GEOPHYSICS.

DEPARTMENT OF PHYSICS,

FACULTY OF PHYSICAL SCIENCE,

AHMADU BELLO UNIVERSITY, ZARIA

NIGERIA.

MARCH, 2021

DECLARATION

I declare that the work in this dissertation entitled "GEOPHYSICAL INVESTIGATION FOR FOUNDATION STUDIES OF THE PHASE II SITE, AHMADU BELLO UNIVERSITY, ZARIA USING MULTI-CHANNEL ANALYSIS OF SURFACE WAVES" has been carried out by me in the Department of Physics under the supervision of Dr. A.L. Ahmed and Prof. K.M. Lawal. The information derived from literature has been duly acknowledged in the text and a list of references provided. No part of this thesis was previously presented for another degree or diploma at this or any other institution.

ABUBAKAR FAHAD	_____	_____
Name of Student	Signature	Date

CERTIFICATION

This dissertation entitled "GEOPHYSICAL INVESTIGATION FOR FOUNDATION STUDIES OF THE PHASE II SITE, AHMADU BELLO UNIVERSITY, ZARIA USING MULTI-CHANNEL ANALYSIS OF SURFACE WAVES" by Fahad ABUBAKAR meets the regulations governing the award of the degree of Masters of Science in Applied Geophysics of Ahmadu Bello University, Zaria and is approved for its contribution to knowledge and literary presentation.

Dr. A.L. Ahmed	_____	_____
Chairman, Supervisory Committee	Signature	Date
Prof. K. Lawal	_____	_____
Member, Supervisory Committee	Signature	Date
Prof. N. Rabiu	_____	_____
Head of Department	Signature	Date
Prof. S.A. Abdullahi	_____	_____
Dean, School of Postgraduate Studies	Signature	Date

DEDICATION

I dedicated this research work to my mum, Abubakar Bilikisu, and also in honor of my late father, Abubakar Aliyu.

ACKNOWLEDGMENT

All thanks and adoration are due to Almighty ALLAH (SWT), the lord of the world who has given me the strength to rise height despite all odds and granted me the opportunity to complete this dissertation.

My profound gratitude goes to my supervisors, Dr. A.L. Aminu and Prof. K.M. Lawal for their technical guidance, constructive comments, critical reading, and directions during the period of this research.

My heartfelt appreciation goes to the Head of Department (H.O.D) of Physics, Prof. Rabiu Nasir, the Postgraduate coordinator, Dr. N.N. Garba, the coordinator of the Applied Geophysics unit, Dr. R. Jimoh, the Seminar coordinator, Dr. A.A. Khalid, and the technical staff of the physics department, Ahmadu Bello University, Zaria for their efforts in ensuring a successful running of my M.Sc. program.

Special appreciation goes to all of my lecturers, including, Prof. K.M. Lawal, Dr. P. Sule, Dr. A.L. Aminu, Dr. R. Jimoh, Mr. J. Osumeje, and Malam B. Bala for the educative and quality knowledge of Geophysics they exposed me to.

Further appreciation goes to my course mates, friends, and senior colleagues: Muhammad Tyabo Usman, Olayinka Adesina Lukman, Eugene Anibe, Kabir Momoh Onotu, Bello Yusuf Ayoola, Abubakar Aliyu, Enesi, Babangida.

Deep appreciation goes to my Mum, Mrs. Abubakar, and my lovely siblings; my one and only sister, Mariam, my outstanding brothers, Mushood and Sheriff, for their moral and financial support.

Special appreciation goes to my wife, Munirah Abdulsalam Fahad for her moral and spiritual support to the completion of the program.

Undoubtedly, I appreciate the effort of my lecturer and my technical adviser, Dr. I.A. Isiaka of the Geology Department, Ahmadu Bello University, Zaria for the technical and intellectual support throughout this dissertation.

Sincere appreciation goes to the Kogi State University, Anyigba for the financial support.

Also, I appreciate the Head of Geology Department, Kogi State University, Anyigba, Dr. A.O. Omali, Mr. Ahmed Jimoh, and the lecturers of the Geology Department, Kogi State University for their support, understanding, and cooperation throughout this program.

Although many people have contributed in various ways to the actualization of this dissertation, the list is almost endless, such is my debt of gratitude and as such, I will like to observe protocol, "Out of sight is not out of mind". May Allah bless you all.

ABSTRACT

The Multi-channel Analysis of Surface Waves (MASW) was employed at the Ahmadu Bello University, Zaria Phase II site to characterize the site for foundation studies. The dispersive nature of the Rayleigh wave was used to estimate the average shear wave velocities (down to 30 m) of the site, using both the 1-dimensional (1D) and 2-dimensional (2D) shear wave velocity models. The average shear wave velocity distribution of the site shows that the soil thickness increases eastwards. Employing the borehole log data and shear wave velocities of soil/rock as control, the 2D models reveal a first layer (topsoil and laterite) with shear wave velocity (V_S) in the range of 158 to 290 m/s and corresponding thickness of 0 to 6 m. The second layer (clayey sand) shows a V_S of 180 to 270 m/s with a corresponding thickness range of 2 to 7 m. The third layer, which is the weathered basement shows a V_S of 250 to 500 m/s and a thickness range of 4 to 18 m. The fourth layer (fractured basement) has a thickness of 2 to 8 m and V_S of 400 to 650 m/s. The fifth layer with the highest V_S (> 650 m/s) is assumed to be the fresh basement (bedrock), which was delineated at 24 m depth in some of the areas. The average V_{s30} obtained for the site varies between 273.5 m/s to 446.2 m/s, which reveals the site class of C and D following the National Earthquake Hazard Reduction Program (NEHRP) provision. Following this provision, the site is can be assumed for engineering construction. Nonetheless, we recommend that the clayey material observed should be excavated or densified (perhaps using rock chips) before embarking on construction on the site.

TABLE OF CONTENTS

Title	Page
Cover page	i
Fly page	ii
Title page	iii
Declaration	iv
Certification	v
Dedication	vi
Acknowledgment	vii
Abstract	ix
Table of content	x
List of Figures	xiii
List of Plates	xvi
List of Tables	xvii
List of Abbreviations, Symbols, and Definition	xviii
List of Appendices	xxi

CHAPTER ONE: INTRODUCTION

1.1 General Overview 1

1.2 Location of the Study Area 3

1.3 Geology of the Study Area 4

1.4 Statement of Problem 5

1.5 Justification for the Research 6

1.6 Aim and Objectives 6

CHAPTER TWO: LITERATURE REVIEW

2.1 Previous Works on MASW Survey 7

2.2 Other Related Geophysical Works 8

2.3 Seismic Method 9

2.3.1 Application of the seismic method 13

2.3.2 The Theory of Elasticity 15

2.3.2.1 Huygens principle 23

2.3.2.2 Partitioning of seismic body waves at a boundary 25

2.3.3 Surface waves (Rayleigh type) 26

2.3.3.1 Dispersion spectrum 27

2.3.3.2 Inversion analysis 33

2.3.4 Multi-channel Analysis of Surface Waves (MASW) 37

CHAPTER THREE: MATERIALS AND RESEARCH METHODOLOGY

3.1 Materials 39

3.1.1 Software 39

3.1.2 Description of materials 39

3.2 Methodology 39

3.2.1 Desk studies 39

3.2.2 Reconnaissance visit 40

3.2.3 Data acquisition 40

CHAPTER FOUR: DATA PROCESSING, RESULTS, AND INTERPRETATION

4.1 Data Processing 44

4.2 Results and Interpretation 47

CHAPTER FIVE: DISCUSSION, CONCLUSION, AND RECOMMENDATION

5.1 Discussion 61

5.2 Conclusion 62

5.3 Recommendation 62

REFERENCES 63

LIST OF FIGURES

Figures **Page**

Figure 1.1: Layout Plan of the Study Area 3

Figure 1.2: Geological Map Showing the Study Area 5

Figure 2.1 Elastic Deformations and Ground Particle Motions Associated with the Passage of Body Waves 10

Figure 2.2: Surface Waves 12

Figure 2.3: Elastic Deformations and Ground Particle Motions Associated with the Passage of Surface Waves 13

Figure 2.4 Stress Components Acting on an Infinitesimally Small Volume Surrounding a Point within an Elastic Solid 16

Figure 2.5: Two points P and Q within a Solid Body Subject to a Stress Field 17

Figure 2.6. Deformation Caused by Stress 18

Figure 2.7: Reflected and Refracted P-wave Rays 24

Figure 2.8: The Generation of Reflected and Refracted P- and S-waves from a P-wave Incident on a Plane Interface 26

Figure 2.9: A Seismic Source (s) Generates Waves that Propagate in all Directions; Waves Traveling in Different Directions are Recorded at Different Receiver's Locations (r) 28

Figure 2.10: Dispersion Spectrum 31

Figure 2.11: Dispersion Spectrum Showing Fundamental and Higher mode 32

Figure 2.12: A Layered Earth Model with Parameters of Shear-wave Velocity, Compressional Wave Velocity, Density, and Thickness 34

Figure 3.1: Schematic Illustration for the Multi-channel Analysis of Surface Waves (MASW) Data Acquisition 41

Figure 3.2: Standard Roll-along Configuration for 2-D MASW Survey 42

Figure 4.1-1: Profile 1 (A-A^1), 1st shot gather analysis 48

Figure 4.1-2: Profile 1 (A-A^1), 10th shot gather analysis 49

Figure 4.1-3: Profile 1 (A-A^1), 15th shot gather analysis 50

Figure 4.1-4: Profile 3 (C-C^1), 1st shot gather analysis 51

Figure 4.1-5: Profile 3 (C-C^1), 7th shot gather analysis 52

Figure 4.1-6: Profile 3 (C-C^1), 15th (last) shot gather analysis 53

Figure 4.2: Borehole log data 55

Figure 4.3-1: 2D shear wave velocity model with inferred layers for profile 1 (A-A^1) 56

Figure 4.3-2: 2D shear wave velocity model with inferred layers for profile 2 (B-B^1) 56

Figure 4.3-3: 2D shear wave velocity model with inferred layers for profile 3 (C-C^1) 56

Figure 4.3-4: 2D shear wave velocity model with inferred layers for profile 4 (D-D^1) 57

Figure 4.3-5: 2D shear wave velocity model with inferred layers for profile 5 (E-E^1) 57

Figure 4.3-6: 2D shear wave velocity model with inferred layers for profile 6 (F-F^1) 57

Figure 4.3-7: 2D shear wave velocity model with inferred layers for profile 7 (G-G^1) 58

Figure 4.4: Map of the study area showing the average shear wave velocity distribution 58

LIST OF PLATES

Plates **Page**

Plate 3.1: Seismic survey 43

LIST OF TABLES

Tables **Page**

Table 3.1: Description of Materials 39

Table 3.2: Acquisition parameters 41

Table 4.1: Site Classification, according to the NEHRP provisions 59

Table 4.2: The site classification of the study area, based on the NEHRP provision 59

Table 4.3: RMSE for the 2D models 60

LIST OF ABBREVIATIONS, SYMBOLS AND DEFINITIONS

'	Minutes
°	Degrees
1D	One-Dimension
2D	Two-Dimension
ABU	Ahmadu Bello University
BSSC	Building Seismic Safety Council
DC	Direct current
E	East
Eqn	Equation
et al.	and others
etc.	et cetera (and other similar things)
E-W	East-West
Fig.	Figure
ft	Feet
GPS	Global Positioning System
Hz	Hertz
Km	Kilometer

lb	Pounds (in weight)
LMO	Linear moveout
m	Metre
m/s	Metre per second
MASW	Multi-channel Analysis of Surface Waves
ms	Milliseconds
N	North
NEHRP	National Earthquake Hazards Reduction Program
N-S	North-South
P-wave	Primary wave
RMSE	Root-mean square error
S	South
SH	Horizontally transverse
SV	Vertically transverse
SVD	Singular-value decomposition
S-wave	Shear wave
V	Volt
V_s	Shear wave velocity

V_{s30}	Shear wave velocity down to 30 m
W	West
E	Young's modulus
K	Bulk modulus
σ	Poisson's ratio

LIST OF APPENDICES

Appendices **Page**

Appendix I – Shot Gather 69

Appendix II – Picked Rayleigh Wave Fundamental Mode 86

Appendix III – 1-Dimensional Shear Wave Velocity Model 95

CHAPTER ONE

INTRODUCTION

1.1 General Overview

Site characterization is a process that entails developing an understanding of the geologic and engineering properties of a site. In the process of characterizing a site, priority is given to cost-benefit (Bowles, 1984). Although, there have been advancements in the field of engineering geology sequel to soil data collection (in-situ). Nonetheless, the result obtained (upon analysis) reveals the condition of the subsurface limited to the portion or area under examination. however, when considering engineering design purposes, data must be obtained for a whole soil mass. Undetected anomalies, either natural or man-made can invalidate the earth's assumptions usually adopted during geotechnical data analysis (Abubakar *et al*., 2020). Stumbling upon an anomaly when a site is already at the development stage, perhaps the construction stage can disrupt a project, or may result in additional cost or labour.

To curb some of these challenges resulting from data collection at points, which is the conventional geotechnical field operations, there is a need to bridge the gap in a cost-effective, swift, and snappy manner.

Geophysicists have made several advancements in near-surface analytical methods to imaging subsurface conditions. According to steeples (2001), these advancements in geophysical data acquisition and interpretation have proven geophysical surveys to be very effective and cost-efficient in engineering projects. The multi-channel analysis of surface waves (MASW) is a geophysical method that operates upon seismic principles. It uses the Rayleigh type surface waves to estimate the shear wave velocity of soil or rock under

investigation. It has been proven to be consistently reliable in site characterization (Long and Donohue, 2007; Neelima and Rao, 2008; Mohamed *et al*., 2013; Yilmaz, 2015; Anand and Parul, 2018).

Subsurface instabilities and foundation failure assessment are of great concern to engineers and geoscientists all over the world. In the Zaria area, many buildings are affected by foundation-based structural defects, usually as a result of the poor subsurface conditions, which have sometimes led to the collapse of the affected parts of buildings (Egwuonwu and Osazuwa, 2011). The Foundation of any structure is meant to transfer the load of the structure to the ground without causing the ground to respond to an uneven and excessive movement (Blyth and Freitas, 1984). In order to achieve this, one must understand the characteristics and distribution of the subsurface layers and also the probable cause of the rampant failure of building foundations due to subsurface movements that give rise to cracks in buildings. Foundation studies of a site using the appropriate geophysical methods and giving the acquired data a substantial analysis and interpretation will give an insight into the subsurface condition and its aerial information.

1.2 Location of the Study Area

The study area is the Ahmadu Bello University, Zaria Phase II site (Figure 1.1).

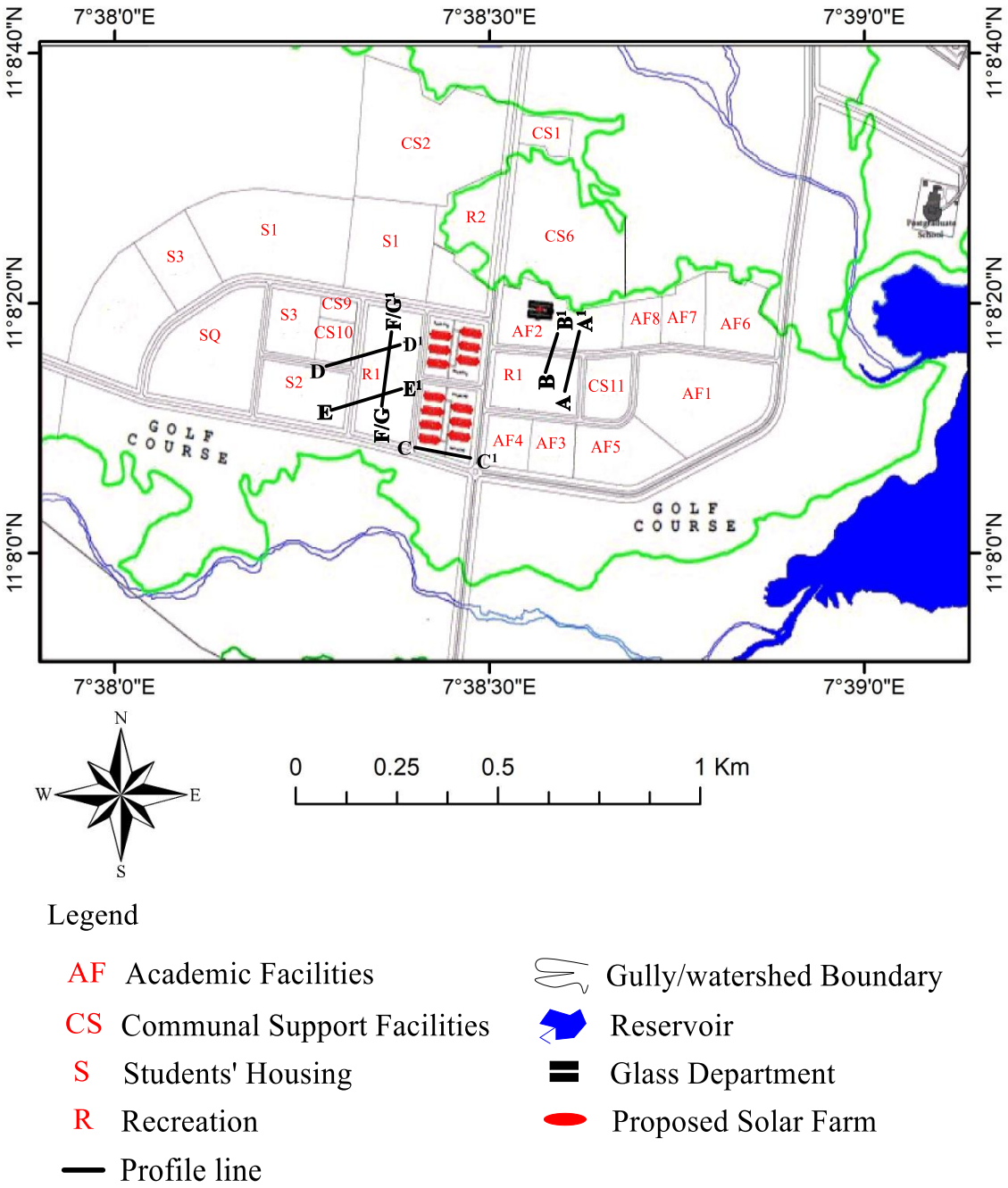


Figure 1.1: Layout Plan of the Study Area (After Physical Planning and Municipal Services, ABU Zaria, 2017).

1.3 Geology of the Study Area

The Zaria area is underlain by Basement rocks of Precambrian age. They are mainly granites and gneisses but also include rock types such as schist and quartzite (McCurry, 1970). Bands of migmatite are mostly confined to the granite gneiss boundary. The crystalline rocks of the Zaria area are part of the Nigerian Basement Complex that covers the western part of the country. Several workers on the Nigerian Basement Complex (including Truswell and Cope, 1963; Oyawoye, 1964) established its relationship with the West African Basement. This is as a result of the entire region been involved in a single set of orogeny, which is the Pan African orogeny. Oyawoye (1964) reported that at least two major phases of deformation affected the Nigerian Basement (study area inclusive).

The study area is predominated by Biotite Gneiss (Figure 1.2) which extends westwards to form a gradational boundary with the Quartz-Mica Schist and extends eastwards, which is occasionally broken up by similar older granites (McCurry, 1970). The outcrops are mostly in stream valleys, where they are deeply weathered. The gneiss complex are medium to coarse-grained and are moderate to weakly foliated rocks. They are principally composed of quartz, oligoclase, and mica (Wright and McCurry, 1970). The area represents part of the Kubanni river basin (Figure 1.2). The superficial deposits that cover most of the basement rocks in the basin act as recharge areas where they are underlain by weathered basement (Eigbefo, 1978), water percolates through them to the main aquifer (the weathered basement). The superficial deposits consist of the Older laterite and the Quarternary deposits. Tokarski (1972) classified the elements of the Quarternary deposits in the area as Aeolian cover, Upper Savannah Loam, Lower Savannah Loam, and Younger Laterite.

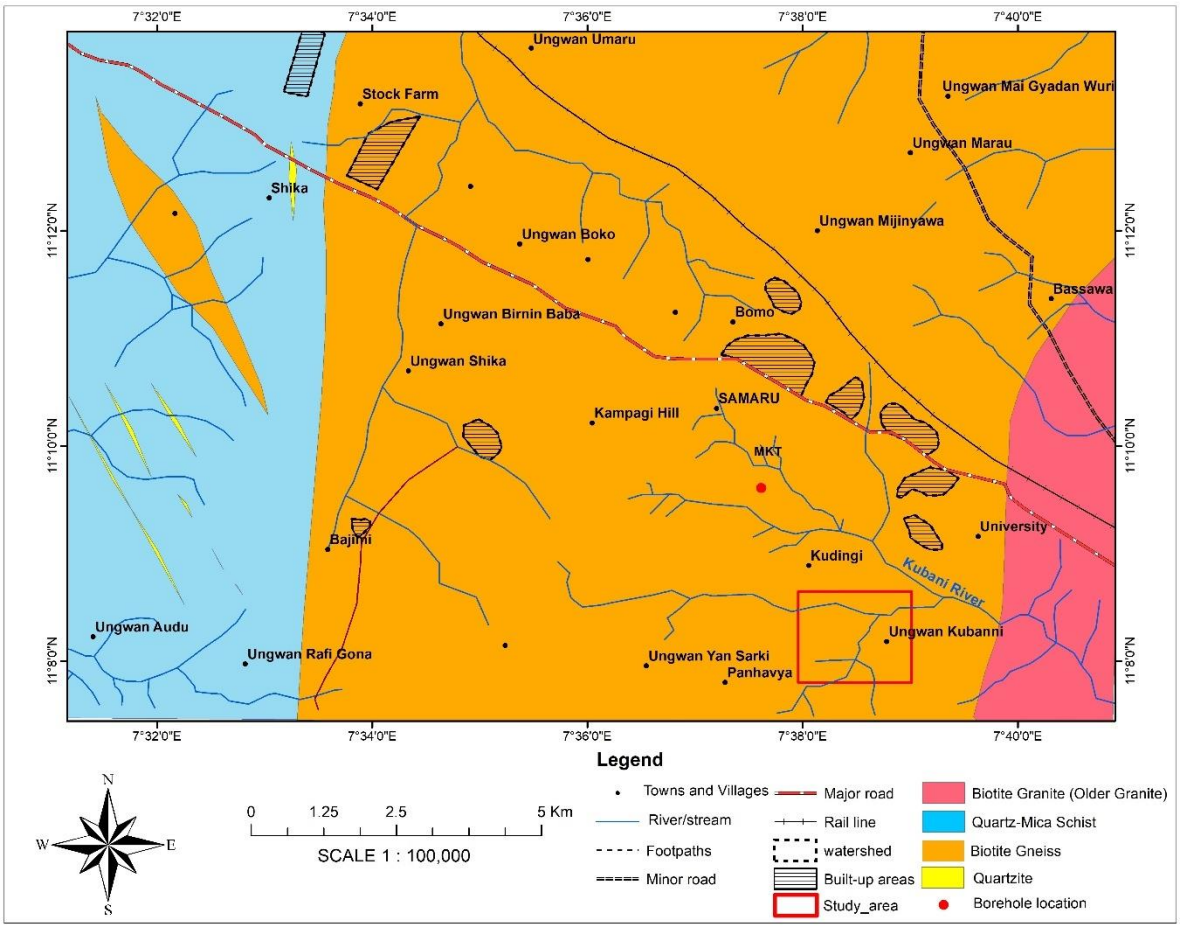


Figure 1.2: Geological Map Showing the Study Area (After McCurry, 1970).

The superficial deposits cover almost everywhere within the weathered basement (Wright and McCurry, 1970). Some exposure reveals sections of lateritic soil, measuring up to 3 m in thickness around the study area.

1.4 Statement of Problem

Poor knowledge of the subsurface condition is a potential threat to engineering structures. The failure of building structures within the Zaria area has been attributed to be a result of poor subsurface conditions (Egwuonwu and Osazuwa, 2011). This structural failure has sometimes resulted in the loss of lives and properties (Premium times, 2018).

Data collection at points, of the customary geotechnical field operation, can be accurate but lacks spatial resolution. This is because the information obtained upon analysis reveals only the condition of the portion examined. There is every possibility for undetected anomalies within the subsurface to disrupt or pose threat to engineering structures that would be erected.

1.5 Justification for the Research

The phase II site, ABU, Zaria is a site where lots of engineering structures would be erected. The need for pre-foundation studies has therefore become imperative as the knowledge of the subsurface conditions will serve as a guide to engineers on the building foundation, the architect, and the chief planner on the proper design for the engineering site.

1.6 Aim and Objectives

This work aims to evaluate the stability of soil to host engineering structures sequel to the foundation at the ABU (Phase II) site, using Multi-channel Analysis of Surface Waves (MASW). Below are the objectives to achieving the aim;

1. To generate 1D and 2D shear wave velocity model of the subsurface layers to a depth of 30 m and to estimate its average shear wave velocity.
2. To produce a shear wave velocity map of the survey area.
3. To classify the site following the National Earthquake Hazards Reduction Program (NEHRP) Provisions on mean shear-wave velocity down to 30 m (Vs_{30}).

CHAPTER TWO

LITERATURE REVIEW

2.1 Previous Works on MASW Survey

Lin *et al*. (2004) assessed the soil liquefaction potential at several sites in central-western Taiwan using the MASW method. Conclusively, they emphasized the MASW imaging being an effective tool for estimating the extent of potential liquefaction hazard.

Watabe and Sassa (2008) used the MASW method in the identification of a tidal flat stratigraphy and its geoenvironmental interpretation. The result obtained by the MASW was consistent with the morphological soil structures that manifested themselves under relevant geoenvironmental dynamics.

Anbazhagan and Sitharam (2006) evaluated the dynamism in the properties of soil using the MASW method and established a correlation with the standard penetration test of the soil.

Mohamed *et al*. (2013) carried out site-specific shear wave velocity investigation for geotechnical engineering applications using seismic refraction and 2D MASW. This was done to quantify the near-surface seismic properties (P- and S-wave velocities, and the dynamic elastic properties) with respect to the depth at a specific area. The V_{S30} was obtained using the MASW technique and the studied area demonstrates site classes of C and D following the National Earthquake Hazard Reduction Program (NEHRP). The layering from the models generated demonstrates a top layer of medium to coarse sand with a shear wave velocity (Vs) range of 250-350 m/s. The second layer (i.e. clayey sand) has a Vs of about 200 m/s. The third layer is gravely-coarse sand with Vs in the range of 400 – 500 m/s. The fourth layer has a Vs of 650 m/s which is dense coarse sand. The fifth layer with a high Vs > 1300

m/s is assumed to be the bedrock velocity. Anand and Parul (2018); Ashraf *et al*. (2017); Neelima and Rao (2008); Long and Donohue (2007) also employed the MASW method in site characterization.

Collins (2014) investigated the safety of the dam, Ahmadu Bello University using the MASW method. The obtained values were compared with the normal range of dam embankment, which he concluded that the dam embankment is in a good condition and also that an MASW method is an effective tool in characterizing the strength of material for engineering.

Duffy *et al.* (2014) used the MASW to delineate fault avoidance zones and correlated the MASW survey's result with geotechnical parameters obtained from the survey area.

Kalinina and Ammosov (2015) used the MASW for solving seismic micro-zonation problems in different locations of the Russian Federation. The results obtained from the MASW method were stable for the complex geological sections. Anukwu *et al.* (2017) also utilized the MASW method in characterizing a complex geological terrain.

2.2 Other Related Geophysical Works

Chiemeke and Osazuwa (2007) applied the seismic refraction method in imaging the subsurface within the Basawa area of Zaria. From the result obtained, the depth of the fresh basement was estimated to be about 17.09 m.

Jimoh (2011) employed the electrical resistivity method at the Ahmadu Bello University wastewater treatment site. From the result obtained, the weathered basement was delineated to be in a range of about 5.3 to 24.6 m, the fractured basement at about 23 m, and the fresh basement at about 27.5 m.

Egwuonwu *et al*. (2011) carried out a geophysical assessment of foundation depths around a leaning superstructure in the Zaria area using Electrical Resistivity Tomography (ERT). The result of the tomogram reveals that the vertical, diagonal, and horizontal cracks which are shown on most parts of the building walls were a result of failure entrenched on the subsurface. Adewoyin *et al*. (2017); Arjwech and Everett (2015); Ayolabi *et al*. (2012); Kabir *et. al*. (2011) also utilized the 2-D Electrical resistivity method for geotechnical investigation.

2.3 Seismic Method

Seismology is the study of Earthquakes and seismic waves that move through and around the Earth. Seismic waves are the waves of energy caused by the sudden breaking of rock within the Earth or an explosion. They are the energy that travels through the Earth which is recorded on a seismograph. Seismic waves induce elastic deformation of particles (i.e. a type of deformation that vanishes upon removal of the stress that caused it) (Yilmaz,2015), represented by an infinitesimally small volume around a point, within the rock and soil column along the propagation path in the subsurface. There are two main types of seismic waves; body waves and surface waves.

Body waves are the fastest kind of seismic wave. It travels within solids and fluids. Body wave propagation gives rise to reflection, diffraction, and refraction phenomena. There are two types of body waves, namely; the P-waves and the S-waves (Yilmaz, 2015).

P-waves (or equivalently, longitudinal waves, compressional waves, or dilatational waves), for which the displacement of particle associated with it is in the direction of propagation (Figure 2.1a); compressional stress causes a change in the particle dimension or volume. The more the rock or soil column resists the compressional stress, the higher the compressional wave velocity. S-waves (or equivalently, transverse waves, shear waves, or rotational waves),

for which the displacement of particles is in the direction perpendicular to the direction of propagation (Figure 2.1b); the displacement can be horizontally transverse (SH-wave) or vertically transverse (SV-wave) to the direction of propagation (Yilmaz, 2015). Shear stress causes a change in the particle shape. The more the rock or soil column resists the shear stress, the higher the shear-wave velocity.

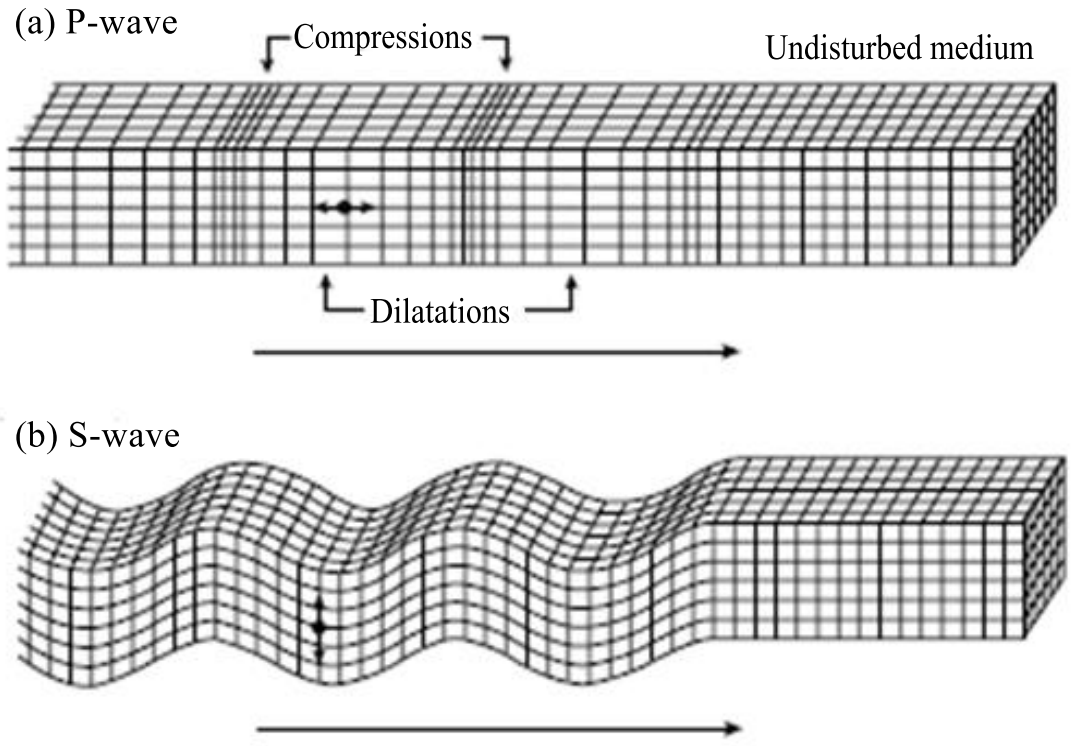


Figure 2.1 Elastic deformations and ground particle motions associated with the passage of body waves. (a) P-wave. (b) S-wave. (From Bolt 1982).

The relationships between the physical properties and the velocity of the wave propagation are independent of the frequency of the waves. Body waves are non-dispersive; which implies that all frequency components in a wave train travel through any material at the same velocity, determined only by the elastic moduli and density of the material.

Surface waves are known to propagate along the free surface and the boundary of a solid (bounded elastic solid) whose depth of penetration is wavelength dependent; which implies that the longer the wavelength the deeper portion of the earth is influenced (Figure 2.2a). Surface waves are characterized as dispersive (Figure 2.2b); which implies, each frequency component travels at a different speed. This dispersion is directly attributable to the variation of velocity with depth in the interior of the Earth. There are two types of surface waves namely, Rayleigh waves and Love waves.

Rayleigh waves travel along the free surface associated with an elastic layer over an elastic half-space and give rise to particle motion that is in a vertical plane that contains the direction of wave propagation (2.3a). Particle motion is elliptical, retrograde, and prograde with respect to the direction of propagation (Rayleigh, 1885). Rayleigh waves are coupled P- and SV-waves trapped within the near-surface traveling in the horizontal direction along the free surface. Love waves travel along the free surface associated with an elastic layer over an elastic half-space and give rise to particle motion that is horizontal and transverse to the direction of propagation (Figure 2.3b). Love waves are SH-waves trapped within the near-surface traveling in the horizontal direction along the free surface. They are polarized shear waves, which are second sets of surface waves generated when the surface layer shear wave velocity is lower than that of the underlying layer.

Surface waves are restricted to a low-velocity near-surface layer, for example; a soil column. Surface waves travel in a horizontal direction with frequency-dependent phase velocities (Yilmaz, 2015). This type of propagation of waves makes the surface waves dispersive in nature. The phase velocities for surface waves are less than P-wave velocities and equal to or less than S-wave velocities (Bolt,1993).

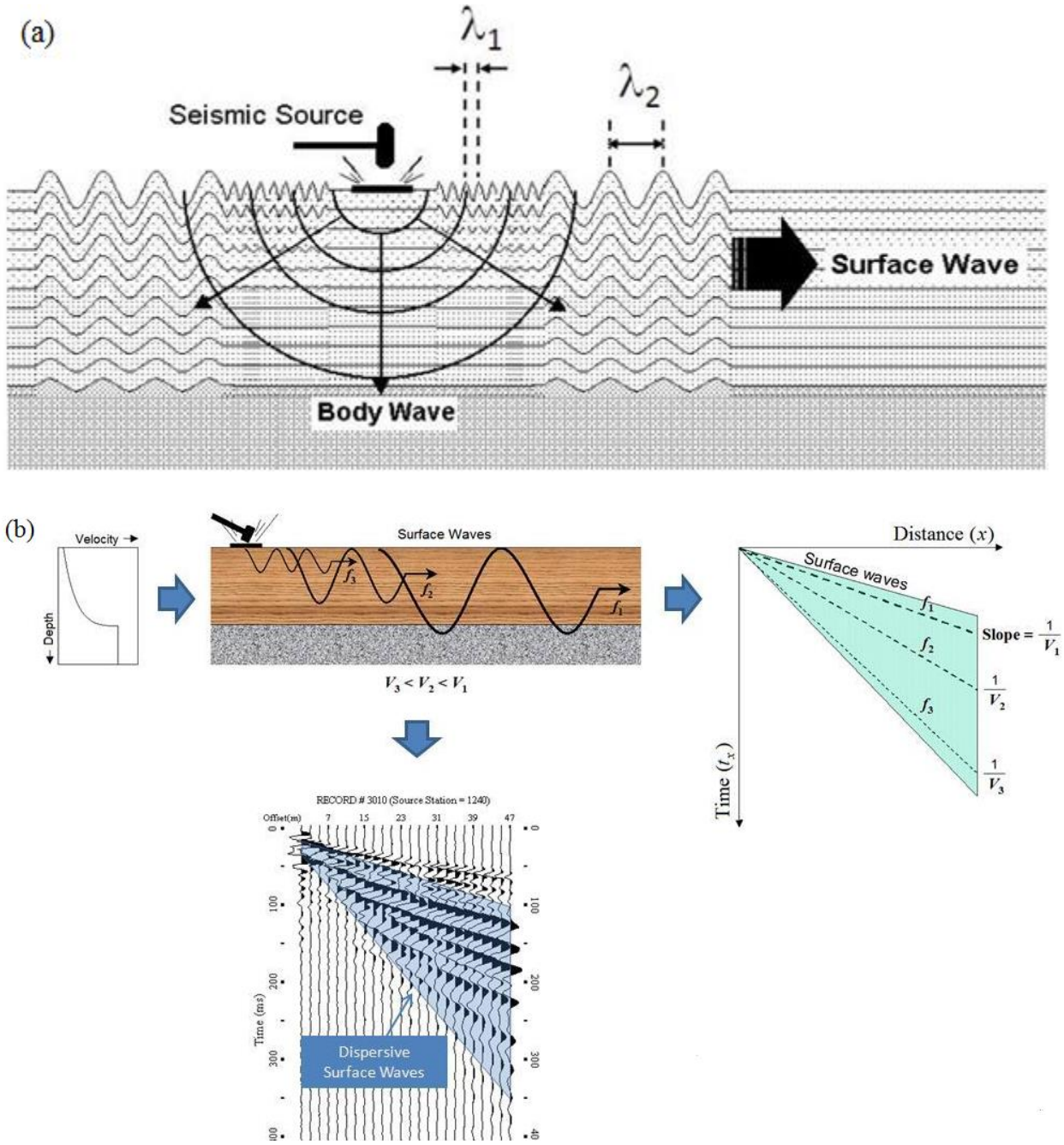


Figure 2.2: Surface waves (a) longer wavelength surface waves influence deeper depth of subsurface materials (b) illustrating seismic velocity increasing with depth, longer wavelengths (lower frequencies) of surface waves penetrating deeper depths travel with faster velocity than shorter wavelengths (higher frequencies) do. Thus, different frequencies arrive at different times on a seismic record, making a dispersive seismic event. (after Park, 2019).

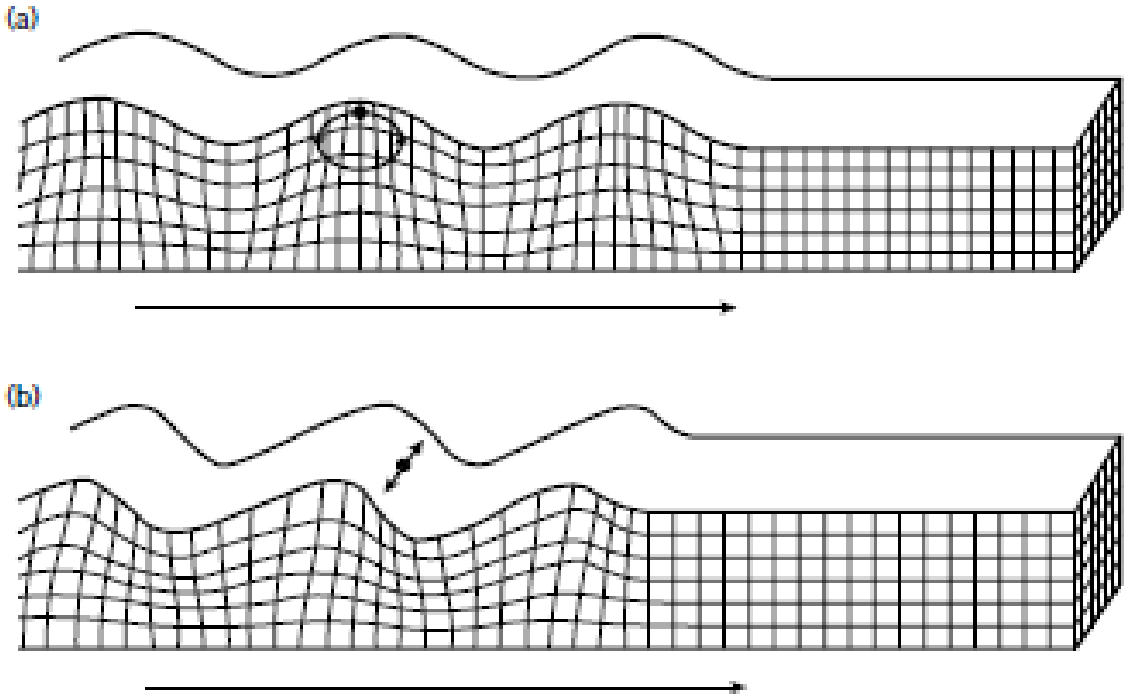


Figure 2.3: Elastic deformations and ground particle motions associated with the passage of surface waves (a) Rayleigh wave. (b) Love wave (From Bolt 1982).

2.3.1 Application of the seismic method

The seismic method is applied in three different categories. Firstly, earthquake seismology, of which is used to investigate the deeper interior and the Earth's crustal structure. Secondly, exploration seismology, of which it is applied to the exploration and development of oil and gas fields. Lastly, engineering seismology. Here, it is applied to the delineation of near-surface geology for site investigations, groundwater, mineral, and geothermal exploration. The seismic method uses refraction, reflection, and diffraction phenomena associated with body-wave propagation, and the dispersive phenomenon associated with surface wave propagation for the aforementioned applied seismology. For this research, emphasis will be laid on engineering seismology.

In engineering seismology, for site investigation required for civil engineering structures, the Rayleigh wave or Love wave dispersion curves are used to estimate an S-wave velocity-depth model for the soil column. The surface wave dispersion is also used in detecting karst cavities within shallow bedrock. The first arrival times associated with the refracted waves are used to estimate a P-wave velocity-depth model and shallow reflections to derive a seismic image for the near-surface (Yilmaz, 2015). Thence, we can delineate the geometry of the layers and faults within the soil column and the geometry of the soil-bedrock interface. Considering the horizontal scale of recording in the application of seismology, it is on the order of thousands of kilometers around the globe in the case of earthquake seismology, several kilometers in the case of exploration seismology, and several tens of meters in the case of engineering seismology. Also, the scale observation time is on the order of several hours, several seconds, and only a second in the case of earthquake seismology, exploration seismology, and engineering seismology respectively. In all three cases, Rayleigh waves exhibit themselves in the form of a prominently dispersive wave package. There is also a difference in scale with respect to the thickness of the near-surface layer. In engineering seismology, the near-surface is defined as the layer below the free surface with a few tens of meters of thickness (Yilmaz, 2015), it is usually composed of a soil column of fine-grained material (silt, clay, and sand), coarse-grained material (gravel, cobble, and conglomerate), and it may also include low velocity, unconsolidated, heterogeneous, highly weathered, and poorly cohesive rocky soil. Unlike the earthquake and exploration seismology which the near-surface is considered to be approximately 30km (i.e. the Earth's crust) and 300m thick respectively (Yilmaz, 2015). The subsurface, which is often referred to as the bedrock, is composed of relatively high-velocity consolidated layers of crystalline and sedimentary rocks. The bedrock in engineering seismology is referred to as geotechnical bedrock, while

in exploration seismology, it is referred to as geological bedrock. Specifically, when a shear wave velocity of 700m/s is reached in a soil column, it is assumed to have entered the geotechnical bedrock, which does not require any soil remediation. Coincidentally, this velocity often corresponds to a depth of nearly 100 ft or 30 m (Yilmaz, 2015). Hence, a significant seismic parameter for the geotechnical engineer is the mean shear wave velocity V_{S30} within a soil column of 30 m thickness.

2.3.2 The Theory of Elasticity

Seismic waves are generally regarded as elastic waves because they induce elastic deformation. the term "elastic" refers to the kind of deformation that vanishes upon removal of the stress that causes it. The term "deformation" refers to the alternating compression and dilatation that take place as the particles respond to forces associated with the propagated waves (Telford *et al*., 1990). Since this propagation depends upon the elastic properties of the rocks, the basic concept of elasticity becomes imperative to be understood.

The theory relates the forces which are applied to the external surface of a body to the resulting changes in size and shape. The relation between the force applied and the deformations are most conveniently expressed in terms of the concept of stress and strain.

Stress is force per unit area. Considering a particle represented by an infinitesimally small volume around a point within a solid body with dimensions (dx, dy, dz) as illustrated in Figure 2.4. The stress acting upon any of the surfaces, like $dy - dz$, can be in some arbitrary direction.

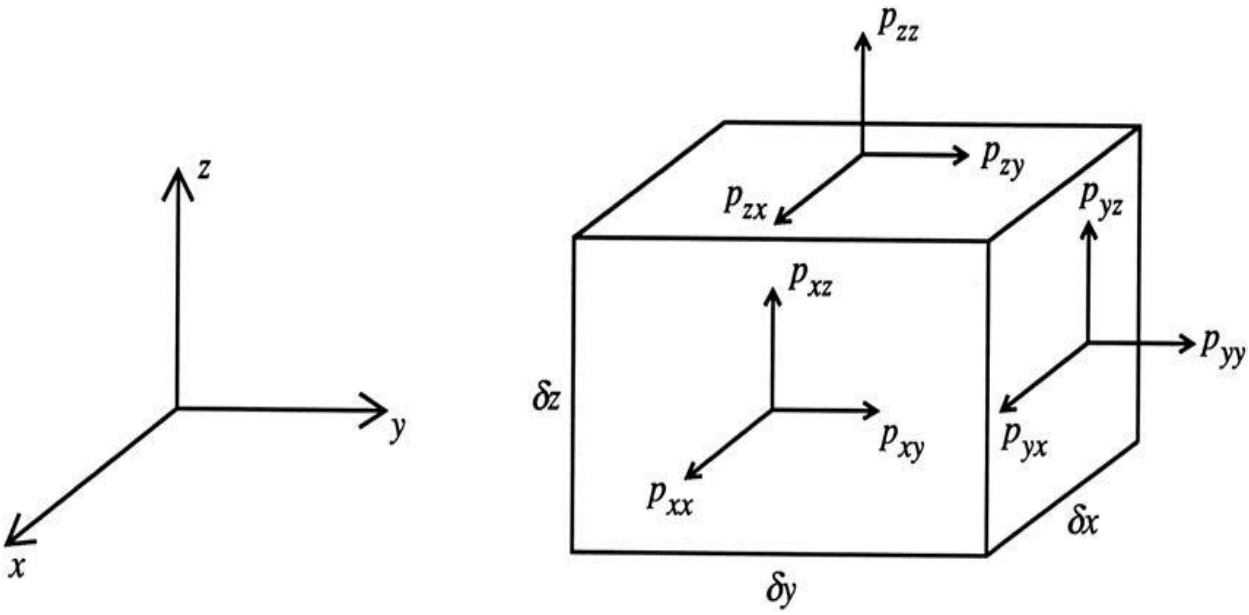


Figure 2.4. stress components acting on an infinitesimally small volume surrounding a point within an elastic solid (after Sheriff and Geldart, 1982).

The particle motion in any arbitrary direction resolved into three components – one which is normal to the surface (P_{xx}) and two which are tangential to the surface (P_{xy} and P_{xz}) (Figure 2.3). The normal component of the stress is called the normal stress and the tangential components are called the shear stress. A normal stress component is tensional if it is positive and compressional if it negative. Fluids cannot support shear stress. In a fluid medium, only one independent stress component exists, which is the hydrostatic pressure (Yilmaz, 2015).

Strain is the fractional change in dimension or volume induced by stress. Strain is a dimensionless quantity. The stress field away from the typical seismic source is so small that it does not cause any permanent deformation on rock particles along the propagation path. Hence, the strain induced by seismic waves is very small, usually around 10^{-6} (Yilmaz, 2015). Considering two points, P and Q, within a solid body as indicated in Figure 2.5

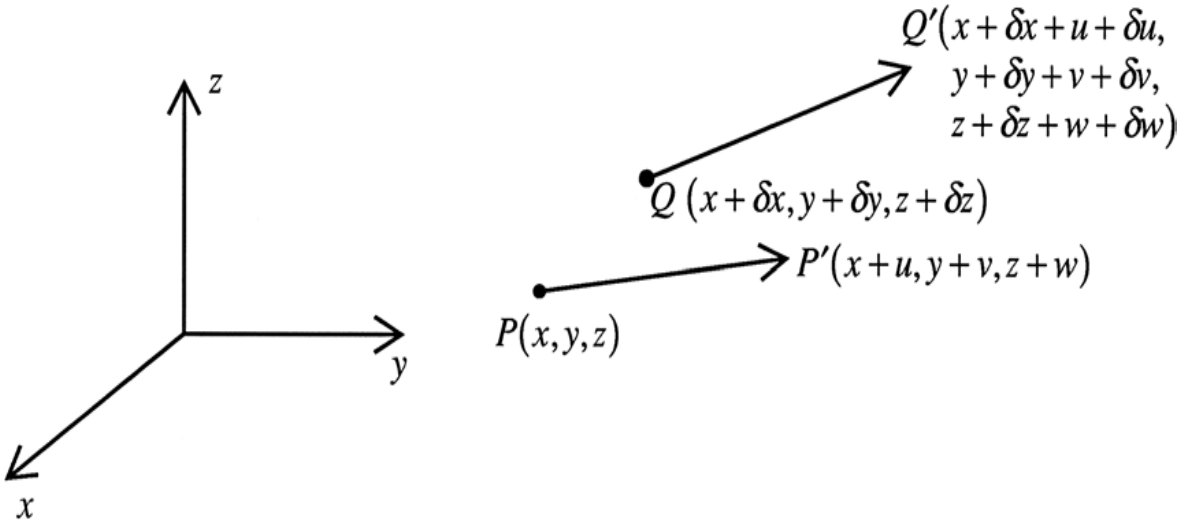


Figure 2.5: Two points P and Q within a solid body subject to a stress field. The solid is deformed in some manner and the particles at points P and Q are displaced to new locations P' and Q'. if we define u, v, and w, as the components of displacement for point P, then the components of displacement for point Q are u + ∂u, v + ∂v, and w + ∂w.

Consider the deformations of specific types illustrated in Figure 2.6. The simplest deformation is the extension in one direction as a result of tensional stress in Figure 2.6a (For simplicity, only the surface of the volume in Figure 2.4 is considered). The fractional change in length in the x-direction is $\partial u/\partial x$ which, in the limit as the volume becomes infinitesimally small, is defined as the normal strain component. The fractional change in length in a given direction is defined as the principal strain component. A positive strain refers to an extension and a negative strain refers to a contraction. Other types of deformation are caused by shearing (Figure 2.6b), rotation (Figure 2.6c), and a combination of the two (Figure 2.6d). These angular deformations are called shear strains because they result in the shearing of the volume around a point within a solid body (Figure 2.6b).

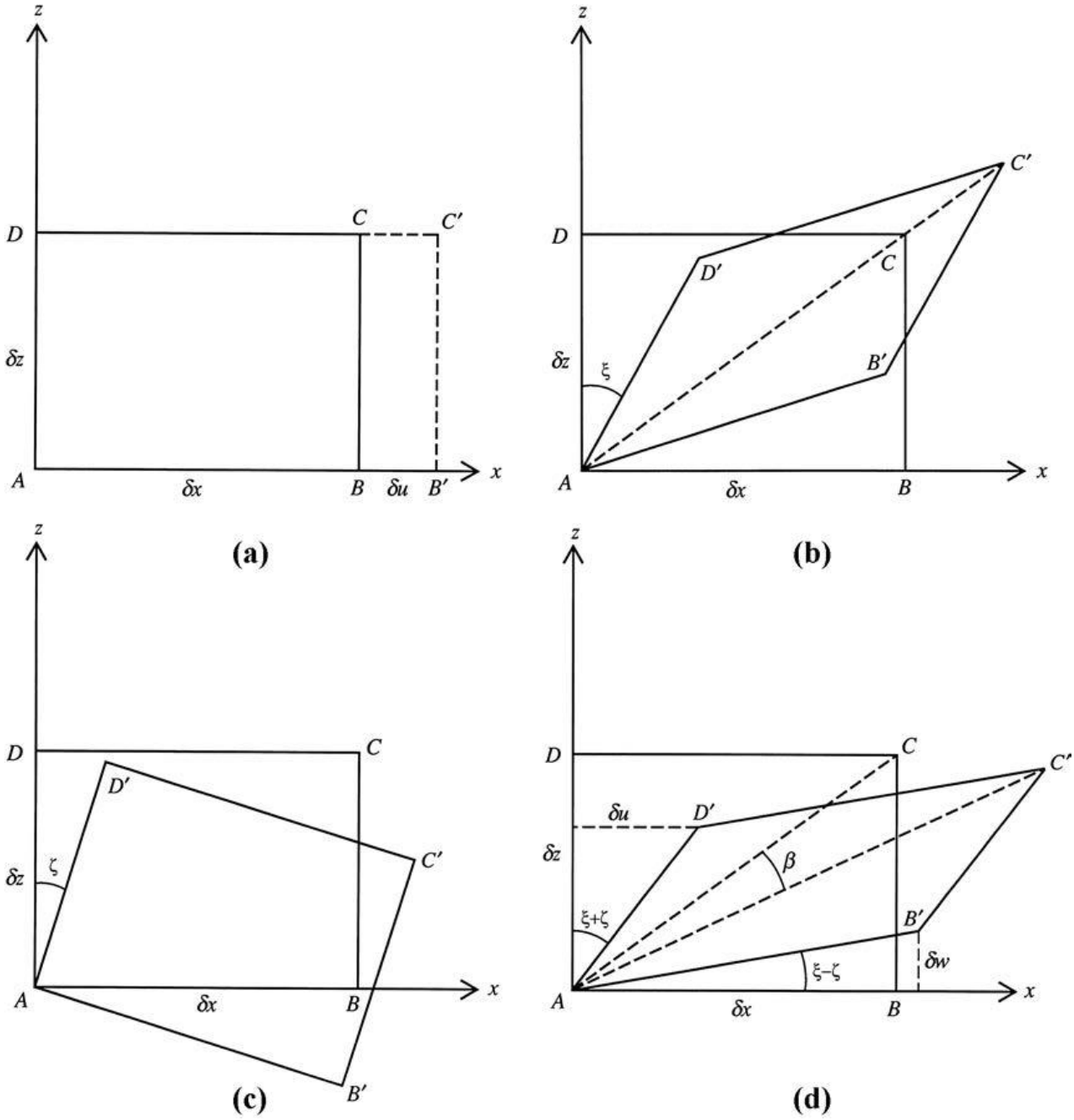


Figure 2.6. Deformation caused by stress acting on one surface of the volume in Figure 3.3: (a) Linear deformation that results in extension of the side AB in the x-direction by an amount BB' ; (b) shearing only; (c) rotation only; (d) combined angular deformation (α) and rotation (β).

Mathematically, The P-wave velocity (V_p) is given by

$$V_p = \sqrt{\frac{\lambda + 2\mu}{\rho}} \tag{2.1}$$

and the S-wave velocity (V_s) is given by

$$V_s = \sqrt{\frac{\mu}{\rho}} \tag{2.2}$$

where λ and μ are Lame's constants and ρ is density.

Elastic moduli are quantities that measure an object or substance's resistance to being deformed elastically when stress is applied to it. A stiffer material will have a higher elastic modulus (Yilmaz, 2015). The elastic moduli are material constants that describe stress-strain relations, below are some expressions for the elastic moduli:

$$K = \lambda + \frac{2\mu}{3} \tag{2.3a}$$

$$E = \frac{\mu(3\lambda + 2\mu)}{\lambda + \mu} \tag{2.3b}$$

$$\sigma = \frac{\lambda}{2(\lambda + \mu)} \tag{2.3c}$$

where K is the bulk modulus, E is Young's modulus and σ is the Poisson's ratio

Conversely, the elastic parameters can be expressed as a function of P- and S-wave velocities:

$$\frac{\lambda}{\rho} = V_P^2 - 2V_S^2 \tag{2.4a}$$

$$\frac{\mu}{\rho} = V_S^2 \tag{2.4b}$$

Substituting equation 2.4a and 2.4b in 2.3a, 2.3b and 2.3c, gives equation 2.4c, 2.4d and 2.4e respectively.

$$\frac{\kappa}{\rho} = V_P^2 - \frac{4}{3}V_S^2 \tag{2.4c}$$

$$\frac{E}{\rho} = V_S^2\left(\frac{3V_P^2 - 4V_S^2}{V_P^2 - V_S^2}\right) \tag{2.4d}$$

and

$$\sigma = \frac{V_P^2 - 2V_S^2}{2(V_P^2 - V_S^2)} \tag{2.4e}$$

where $\lambda' = \frac{\lambda}{\rho}$ and $\mu' = \frac{\mu}{\rho}$ are the normalized Lame's constants $\kappa' = \frac{\kappa}{\rho}$ is the normalized bulk modulus, $E' = \frac{E}{\rho}$ is the normalized Young's modulus and σ is the Poisson's ratio. μ is the modulus of rigidity which is also known as the shear modulus. It should be noted that the normalized elastic parameters with respect to density provide the relationship in terms of P-wave and S-wave velocities.

E is Young's modulus, it is a measure of the stiffness of an elastic solid, such as a soil column. The stiffness is directly proportional to the resistance of the soil column, the larger the stiffness, the more the soil column resists elastic deformation. The equation (2.4d) it shows that the magnitude of E depends strongly on the S-wave velocity than the P-wave velocity. Distinctively, the magnitude of E is proportional to the square of the Shear wave velocity. Hence, a decrease in the S-wave velocity (V_S) will result in a corresponding decrease in stiffness of the soil column.

The shear modulus/modulus of rigidity (μ) which is the object's tendency to shear (the deformation of shape at constant volume) when acted upon by opposing forces, can be seen from equation (2.4b) that the magnitude of the modulus of rigidity is directly proportional to the V_S and is independent of the P-wave velocity. Therefore, a decrease in the S-wave velocity will result in a corresponding decrease in the modulus of rigidity μ, and therefore a significant decrease in resistance of the soil column to shear deformation. In order to increase the shear resistance of the soil column, one will have to increase the shear wave velocity by way of densification or precompression (Coduto, 1999). Equation (2.4b) and (2.4d) shows that the V_S governs the behavior of the soil column when it is subjected to principal and shear stresses. This makes it evident that the most important parameter for the geotechnical engineer is the shear wave velocity (V_S).

Hooke's law happens to be the foundation of linear elastic theory. To calculate the strains when the stresses are known, we must know the relationship between stress and strain. When the strains or the elastic deformations in solid are infinitesimally small, this relation is given by Hooke's law, which states that each stress component can be expressed as a linear combination of all the strain components (Officer, 1958). The stiffness matrix $\{c_{ij}\}$ relates the stress components to the strain components (equation 2.5a) (Officer, 1958).

$$\{c_{ji}\} = \begin{pmatrix} c_{11} & c_{12} & c_{13} & c_{14} & c_{15} & c_{16} \\ c_{21} & c_{22} & c_{23} & c_{24} & c_{25} & c_{26} \\ c_{31} & c_{32} & c_{33} & c_{34} & c_{35} & c_{36} \\ c_{41} & c_{42} & c_{43} & c_{44} & c_{45} & c_{46} \\ c_{51} & c_{52} & c_{53} & c_{54} & c_{55} & c_{56} \\ c_{61} & c_{62} & c_{63} & c_{64} & c_{65} & c_{66} \end{pmatrix} \qquad (2.5a)$$

The elements of the stiffness matrix are the elastic constants of an elastic solid. Because this matrix is symmetric, $\{c_{ij}\} = \{c_{ji}\}$, therefore there are 21 independent constants for a general

Hookean solid. These constants must be known to define the elastic properties of a medium. For an isotropic solid, the number of independent constants is reduced to two – Lame's constants λ and μ. Hence, the stiffness matrix given by equation 2.5a reduces to the special form (Yilmaz, 2015).

$$\{c_{ji}\} = \begin{pmatrix} \lambda+2\mu & \lambda & \lambda & 0 & 0 & 0 \\ \lambda & \lambda+2\mu & \lambda & 0 & 0 & 0 \\ \lambda & \lambda & \lambda+2\mu & 0 & 0 & 0 \\ 0 & 0 & 0 & 2\mu & 0 & 0 \\ 0 & 0 & 0 & 0 & 2\mu & 0 \\ 0 & 0 & 0 & 0 & 0 & 2\mu \end{pmatrix} \qquad (2.5b)$$

Now, substitute equations (2.4a) and (2.4b) to obtain

$$\{c_{ji}\} = \rho \begin{pmatrix} V_P^2 & V_P^2-2V_S^2 & V_P^2-2V_S^2 & 0 & 0 & 0 \\ V_P^2-2V_S^2 & V_P^2 & V_P^2-2V_S^2 & 0 & 0 & 0 \\ V_P^2-2V_S^2 & V_P^2-2V_S^2 & V_P^2 & 0 & 0 & 0 \\ 0 & 0 & 0 & 2V_S^2 & 0 & 0 \\ 0 & 0 & 0 & 0 & 2V_S^2 & 0 \\ 0 & 0 & 0 & 0 & 0 & 2V_S^2 \end{pmatrix} \qquad (2.5c$$

This is the stiffness matrix and its elements expressed in terms of P-wave (V_P) and S-wave velocity (V_S) with the density (ρ) factored out. It states that the principal stress component depends on both V_P and V_S, and the shear stress components depend only on V_S.

For weak soils without cohesion, $V_S << V_P$. therefore, the equation can be further simplified as follows:

$$\{c_{ji}\} = \rho \begin{pmatrix} V_P^2 & V_P^2 & V_P^2 & 0 & 0 & 0 \\ V_P^2 & V_P^2 & V_P^2 & 0 & 0 & 0 \\ V_P^2 & V_P^2 & V_P^2 & 0 & 0 & 0 \\ 0 & 0 & 0 & 2V_S^2 & 0 & 0 \\ 0 & 0 & 0 & 0 & 2V_S^2 & 0 \\ 0 & 0 & 0 & 0 & 0 & 2V_S^2 \end{pmatrix} \qquad (2.5d)$$

This equation states that, for weak soils without cohesion, the principal stress components depend only on V_P and the shear stress components depend only on V_S (Yilmaz, 2015).

For fluids, the stiffness matrix is given by equation (2.5d) becomes

$$\{c_{ji}\} = \rho \begin{pmatrix} V_P^2 & V_P^2 & V_P^2 & 0 & 0 & 0 \\ V_P^2 & V_P^2 & V_P^2 & 0 & 0 & 0 \\ V_P^2 & V_P^2 & V_P^2 & 0 & 0 & 0 \\ 0 & 0 & 0 & 0 & 0 & 0 \\ 0 & 0 & 0 & 0 & 0 & 0 \\ 0 & 0 & 0 & 0 & 0 & 0 \end{pmatrix} \quad (2.5e)$$

This shows that fluids can only support principle stress (hydrostatic pressure). When soil is liquefied, it cannot support shear stress.

The stiffness matrix expressed in terms of seismic velocities is meaningful if normalized by density.

2.3.2.1 Huygens Principle

The Huygens principle is derived from the principle of optics. It is applied to any kind of wave phenomenon. Huygens principle states that "All points on a wavefront can be regarded as point sources for the production of new spherical waves; the new wavefront is the tangential surface (or envelope) of the secondary wavelets". This principle is used to derive the laws of reflection and refraction of seismic waves at an interface, and also to describe the process of diffraction by which a wave is deflected at a comer or the edge of an object in its path. The laws of reflection and refraction can be expressed using Huygens's principles. The law of reflection states that the angle of reflection (θ_1) is equal to the angle of incidence (θ_1). Furthermore, the incident ray reflected ray, and the normal all lie in the same plane (Figure 2.7).

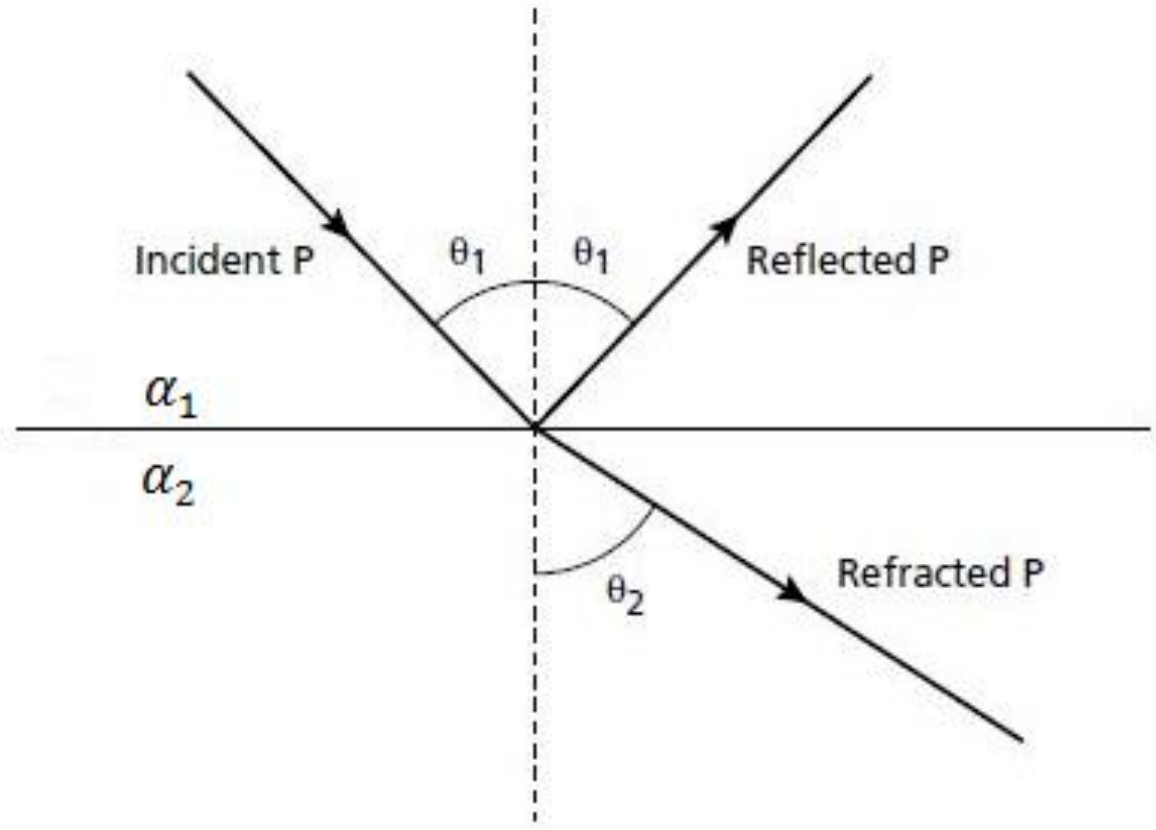


Figure 2.7: Reflected and refracted P-wave rays

The law of refraction is also known as Snell's law states that the ratio of the sines of the angles of incidence and refraction is equivalent to the ratio of phase velocities in the two media. Consequently,

$$\frac{\sin \theta_1}{\sin \theta_2} = \frac{\alpha_1}{\alpha_2} \tag{2.6}$$

2.3.2.2 Partitioning of seismic body waves at a boundary

Considering a P-wave incident at an angle i_P (Figure 2.8) on an interface between two media of acoustic impedance contrast (Z), which is defined as the product of the density and its wave velocity; thus, $Z = \rho V$, the energy is partitioned at the point of incidence i_P (Figure 2.8). At this point of incidence, the earth material is not only compressed but also sheared (Aki and Richards, 1980; Bolt, 1993). As a result, the reflected and transmitted waves will be of both compressional and shear-type (Yilmaz, 2015). At non-normal incidence, the P-wave is partitioned into four components at the interface (Figure 2.8): reflected P-wave, reflected SV type S-wave, transmitted compressional P-wave (refracted P-wave), and transmitted SV-type shear wave (refracted S-wave) (Aki and Richards, 1980; Udias,1999). Applying Snell's law to both the reflected and the reflected and refracted P- and S-waves gives

$$\frac{\sin i_P}{\alpha_1} = \frac{\sin i_s}{\beta_1} = \frac{\sin r_P}{\alpha_2} = \frac{\sin r_s}{\beta_2} \tag{2.7}$$

It is also evident that an incident SV-type shear wave would also be partitioned into four components: reflected SV-type shear wave, reflected compressional P-wave, transmitted SV-type shear wave, and transmitted compressional P-wave (Yilmaz, 2015). But the situation is different for an incident SH type wave, no mode conversion occurs at the interface (Aki and Richards, 1980), only reflected SH wave and refracted SH wave would be created. However, mode conversion can occur in the presence of a dipping layer (Xia *et. al*., 2002).

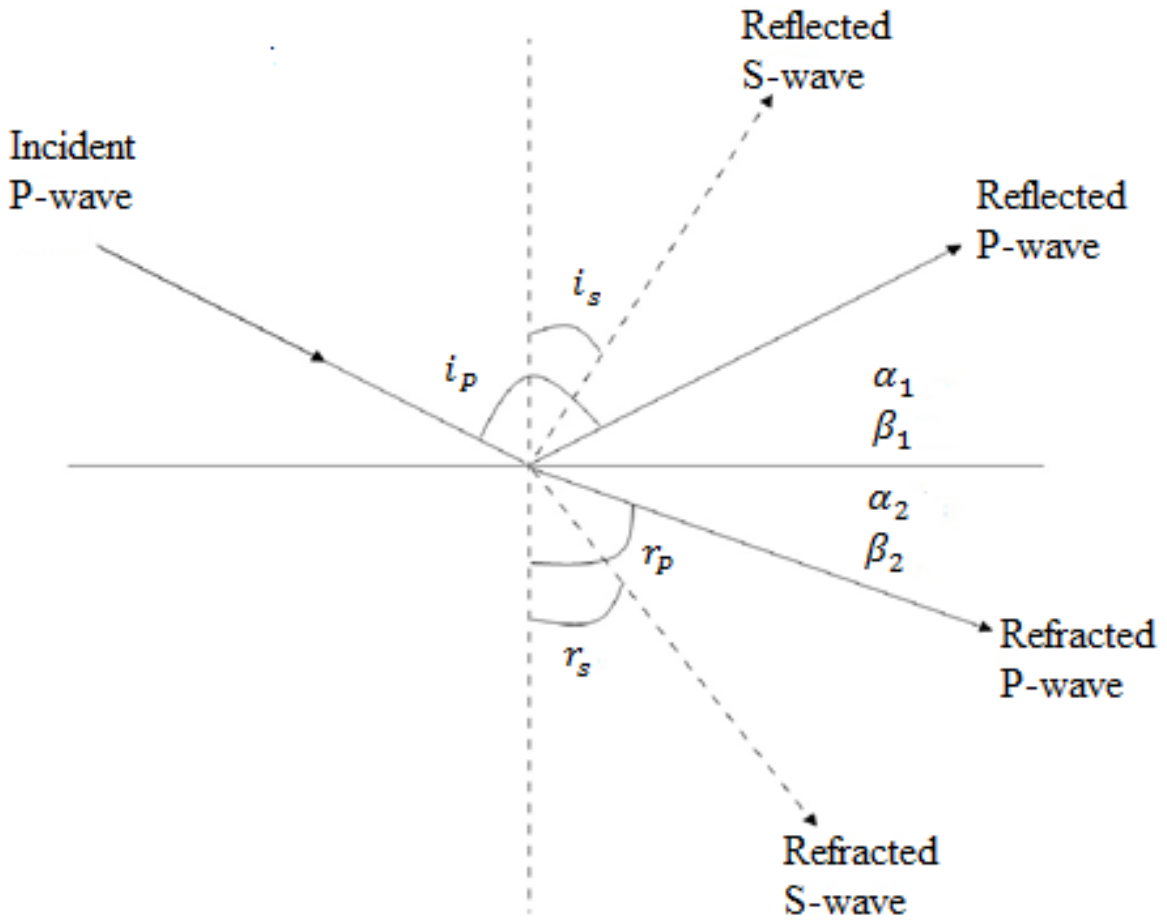


Figure 2.8: The generation of reflected and refracted P- and S-waves from a P-wave incident on a plane interface

2.3.3 Surface Waves (Rayleigh type)

As previously described, If the compressional wave energy is partitioned at the soil-bedrock interface, then the P-to-P reflected and P-to-SV mode-converted wave energy beyond the critical angle of propagation are trapped within the soil column and thereby, travel along the free surface in the form of Rayleigh waves with coupled P-SV-type particle motion-oriented in a vertical plane that contains the direction of wave propagation, and elliptical, prograde

and retrograde with respect to the direction of propagation (Yilmaz, 2015). This particle motion is also referred to as ground roll.

The amplitudes of Rayleigh waves are strongly influenced by the geometry of the soil column and lateral heterogeneity within the soil column. The Rayleigh waves amplitude decays rapidly with depth. At the surface, the vertical component of seismographs would record strong Rayleigh waves. This implies that a seismograph would record strong surface waves at a soil site and virtually no surface waves at a rock site. The closer the source is to the free surface, the higher the surface-wave amplitudes. If a source is placed at a depth of 33m, in that case, no surface wave is generated (Yilmaz, 2015).

2.3.3.1 Dispersion Spectrum

The 2-D Fourier transform is a way in which one uses to decompose a wavefield into its plane-wave components, each with a unique frequency and each traveling at a unique angle from the vertical direction. Plane-wave decomposition of a wavefield, such as common shot gather, can be achieved by applying linear moveout and summing amplitudes over the offset axis. This procedure is called slant stacking (Claerbout, 1978). The slant stacking assumption is that of a horizontally layered earth model. Slant stacking replaces the offset axis with the ray parameter p axis. A group of traces with a range of p values is called a slant-gather (Yilmaz, 2015). Each trace in a gather represents a plane wave that propagates at a certain angle vertically. For example, when an explosive source explodes, the energy propagates at all angles (Figure 2.9).

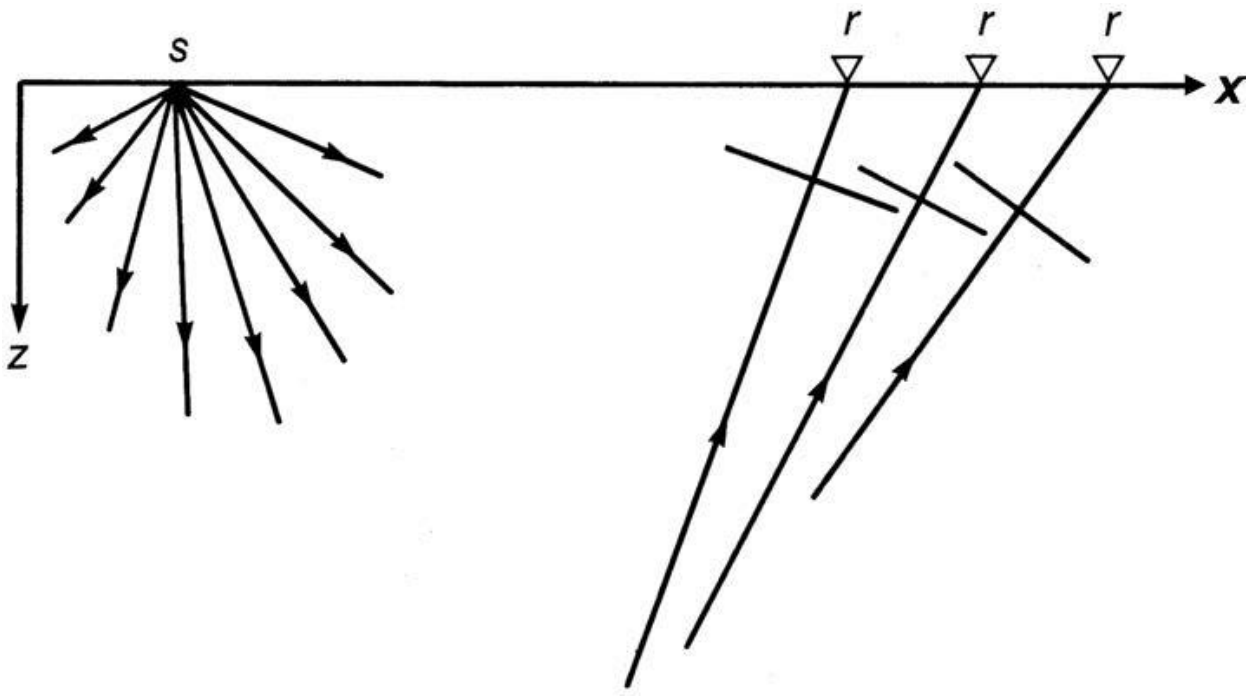


Figure 2.9: A seismic source (s) generates waves that propagate in all directions; waves traveling in different directions are recorded at different receivers' locations (r). (After Yilmaz, 2001)

The reflected energy arrives at different receiver groups at different angles because of the offset between the source and receiver locations. The farther the offset or the shallower the reflecting interface, the more oblique the angle of the upcoming wavefront. This plane wave reflects from an interface and is recorded by a receiver at the surface.

Slant-stack transformation

The plane waves are synthesized, by the application of linear moveout (LMO) correction to the common-shot gather data $d(x,t)$ based on a coordinate transformation defined by

$$\tau = t - px \tag{2.8a}$$

where p is the ray parameter, x is the offset, t is the two-way travel time, and is the intercept time at p =0. Next, the data are summed over the offset axis by

$$u(p,\tau) = \sum_{x} d(x, \tau + px) \qquad 2.8b$$

Where $u(p,\tau)$ represents a plane wave with ray parameter $p = \sin\theta/v$. By repeating the LMO correction for a range of p values and performing the summation in equation (2.8b), a complete slant-stack gather is constructed. A slant-stack gather, in practice, alternatively is referred to as the $\tau - p$ gather, it consists of all the dip components within the specified range of p values in the original shot gather data $d(x,t)$.

The discrete form of the slant-stack gather $u(p,\tau)$ can be written as

$$u(p,\tau) = \sum_{x} u_k(p)\delta(\tau - k\Delta\tau)\,, k = 0,1,2\ldots, \qquad 2.9$$

Where $u_k(p)$, for a trace with a given p value, are the discrete samples of $u(p,\tau)$ along the time axis $\tau, \Delta\tau$ is the sampling interval and $\delta(\tau - k\Delta\tau)$ is the Dirac delta function

$$\delta(\tau) = \begin{cases} 1, & \tau/0 \\ 0, & otherwise \end{cases} \qquad 2.10$$

To compute the dispersion spectrum of $d(x,t)$, perform a discrete Fourier transform of $u(p,\tau)$ in the direction of the time variable τ, for each of the $p - traces$,

$$u(p,\omega) = \sum_{x} u_k(p) exp(-i\omega k\Delta\tau)\,, k = 0,1,2\ldots, \qquad 2.11$$

Where ω is the Fourier dual of the time variable t. Next, compute the amplitude spectrum $A(p,\omega)$ from the complex Fourier transform function $u(p,\omega)$ for each of the p-traces. Finally, take the inverse of the ray parameter $p = \sin\theta/v$ to map the amplitude spectrum $A(p,\omega)$ to $A(c,\omega)$, where $c = 1/p$, the horizontal phase velocity, and $A(c,\omega)$ is the dispersion spectrum of the shot gather data $d(x,t)$.

Computing the dispersion spectrum by way of slant-stack transformation is based on the horizontally layered earth assumption. Thus, the shear-wave velocity-depth profile estimated by inversion of the fundamental-mode dispersion curve (Figure 2.10) picked from the dispersion spectrum represents a horizontally layered soil column.

The surface waves need to be isolated from the refracted and leaky-mode surface waves by outside mute, and from the reflected waves by inside mute. Then the isolated surface waves are bandpass filtered to remove low and high-frequency noise.

Leaky-mode surface waves are similar in particle motion to that of Rayleigh waves but have a faster phase velocity than the maximum phase velocity of the Rayleigh waves. They exist in the near-surface layer (Schroder and Scott, 2001). They are confined to near-offset traces and can easily be confused with direct waves. They can also contaminate the lower end of the dispersion spectrum and bias the dispersion curve for the fundamental mode, making the phase velocity higher. Thus, if leaky-mode surface waves are not muted, there can be overestimation in the shear wave velocity by the Rayleigh wave inversion.

Another aspect of the dispersion spectrum that requires attention when picking the dispersion curve for the fundamental mode is the phenomenon of mode interference, commonly known as mode-kissing" (Xia *et al*., 2012). A likely example of mode interference is shown in Fig. 2.10. Mode interference commonly occurs with Rayleigh-wave dispersion, primarily caused by the influence of the P-wave particle motion. Whereas, mode interference does not occur with Love-wave dispersion, because Love waves are independent of P-waves.

Excellent quality of data can yield a dispersion spectrum such that the fundamental mode and the higher modes (Fig. 2.11) can be depicted with confidence. The energy strongly associated with the P-to-SV conversion is confined to the fundamental mode. The higher mode contains a P-wave component of Rayleigh waves (Yilmaz, 2015).

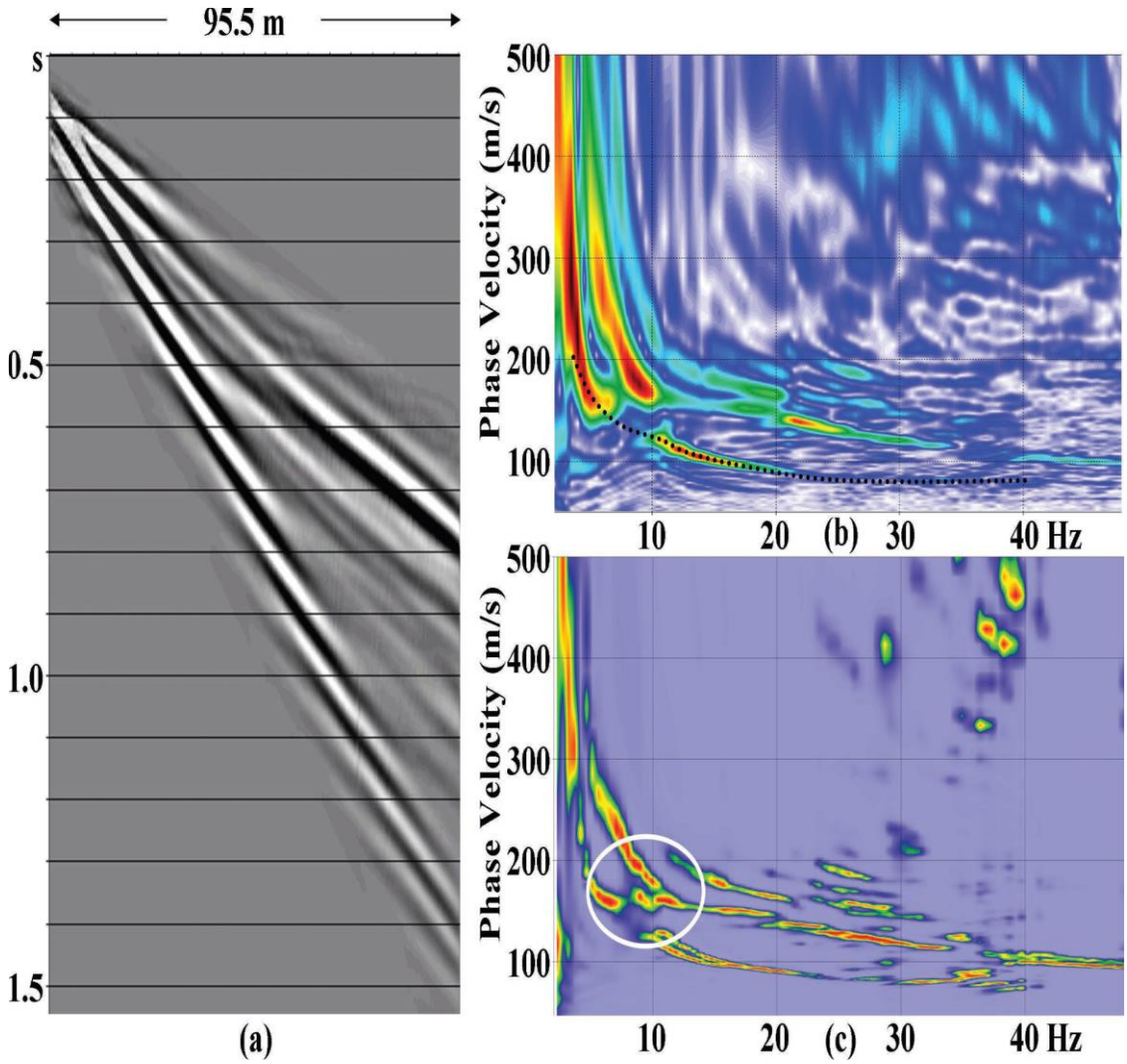


Figure 2.10: Dispersion spectrum (a) A field record acquired by using a 95.5-m receiver spread of 192 4.5-Hz geophones at 0.5-m intervals, and a buffalo gun explosive charge at 30-cm depth and 2m to the left of the receiver spread. The dispersion spectra of the shot gather in (a) computed by (b) conventional slant stack transformation. The curve picked from the dispersion spectrum in (b) corresponds to the fundamental mode of the Rayleigh waves. The region inside the white ellipse in (c) exhibits a likely interference of the fundamental mode and the first higher mode in the neighborhood of 10 Hz. (after Yilmaz, 2015).

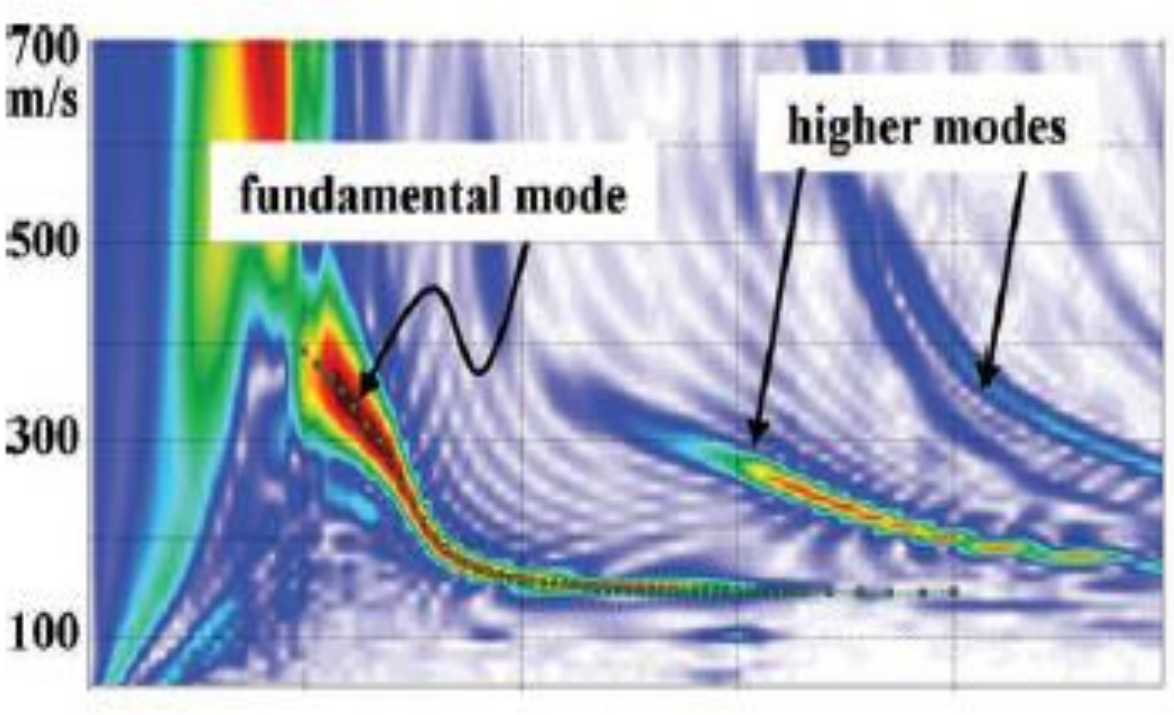


Figure 2.11: Dispersion spectrum showing fundamental and higher mode (Yilmaz, 2015)

The higher-mode Rayleigh waves are more sensitive to S-wave velocities than P-wave velocities (Kennett and Clarke, 1983). This implies that the higher-modes of Rayleigh waves may be included in the procedure of inversion to enhance the depth accuracy in S-wave estimation (Xia *et al*., 2003; Xia *et al.*, 2004). Despite that, the higher modes are not usually easy to pick from the dispersion spectrum. In contrast, picking the fundamental mode alone provides a reliable inversion for Vs estimation (Yilmaz, 2015).

2.3.3.2 Inversion Analysis

Commonly, for an Engineering site, the Rayleigh wave dispersion curves are used (by way of inversion) to estimate the shear wave velocity-depth model for the soil column. From this, the geometry of the layers and weak zones (such as faults and fractures) can be delineated within the soil column, and also the soil-bedrock interface can be delineated.

Generally, inverse problems consist of utilizing the results of measurements (observed) to estimate the values of the parameters that characterize the system under investigation. A forward problem is used to address the reverse. Specifically, the inverse problem in the MASW method consists of estimating the set of parameters that describe the soil column based on the observed dispersion curve.

According to Ryden and Park (2006), inverse problems based on wave propagation theory cannot be solved directly due to non-linearity. Therefore, iterative methods whereby a theoretical dispersion curve is determined for a given layer model and used in comparison with the observed dispersion curve.

Theory (Inversion of dispersion curve)

For a layered earth model (Figure 2.12), Rayleigh-wave dispersion curves can be calculated using Knopoff's method (Schwab and Knopoff, 1972). Rayleigh-wave phase velocity, c_{Rj}, is determined by a characteristic equation (2.12) in its nonlinear, implicit form:

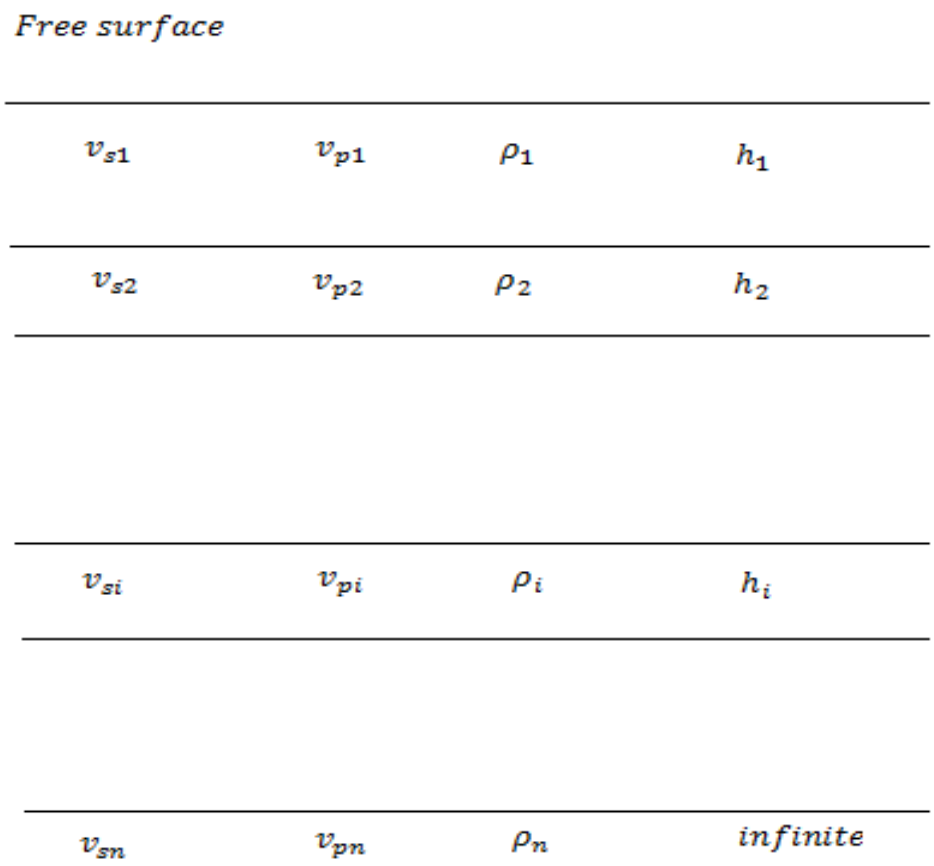


Figure 2.12: A layered earth model with parameters of shear-wave velocity (v_s), compressional wave velocity (v_p), density (ρ), and thickness (h).

For forward calculation, according to Xia *et al*. (1999),

$$F\left(f_j, c_{Rj}, v_s, v_p, \rho, h\right) = 0, (j = 1,2, \dots, m) \qquad 2.12$$

where m is the number of data points, f_j is the frequency, c_{Rj} is the Rayleigh wave phase velocity, $v_s(v_{s1}, v_{s2}, \dots, v_{sn})^T$ is the S-wave velocity vector, with v_{si} the shear wave velocity of the ith layer while n is the number of layers; $v_p\left(v_{p1}, v_{p2}, \dots, v_{pn}\right)^T$ is the P-wave velocity vector, with v_{pi} the P-wave velocity of the ith layer; $\rho(\rho_1, \rho_2, \dots, \rho_n)^T$ is the density vector, with ρ_i the density of the ith layer and $h(h_1, h_2, \dots, h_{n-1})^T$ is the thickness vector, with h_i

the thickness of the ith layer. For a given set of model parameters (v_s, v_p, ρ, h) and a specific frequency f_j, the roots of equation (2.12) are the phase velocities. For the fundamental mode, if the dispersion curve consists of m data points, a set of m equations in the form of equation (2.12) can be used to find phase velocities at frequencies f_j $(j = 1,2, \dots, m)$ using the bisection method (Press *et al*., 1992).

Accuracy of the partial derivatives is key in determining modifications to the earth model parameters and dramatically affects the convergence of the inverse procedure (Xia, 1986). To calculate the partial derivatives of equation 2.12, Ridder's method of polynomial extrapolation is used to calculate the partial derivative (or Jacobian matrix) during the inversion

The sensitivity of Earth Model Parameters

The Rayleigh-wave phase velocity is the function of four parameters: S-wave velocity, P-wave velocity, density, and thickness of the layer (equation 2.12). Each parameter has a unique contribution to the dispersion curve (Xia *et al*.,1999). S-wave velocity is the dominant property for the fundamental mode of high-frequency Rayleigh wave dispersion data.

Variations in S-wave velocities have a dramatic effect on Rayleigh-wave phase velocities. The Jacobian matrix of a model with respect to S-wave velocity J_s at frequencies f_j can be expressed as follows:

$$J_s = \left[-\frac{\partial F / \partial v_{si}}{\partial F / \partial c_R} \Big|_{f = f_j} \right] \qquad 2.13$$

Inversion algorithms

The inversion algorithm assumes that the S-wave velocities fundamentally control changes in Rayleigh-wave phase velocities for a layered earth model. This implies that S-wave velocities can be inverted adequately from Rayleigh-wave phase velocities.

The S-wave wave velocities (earth model parameters) can be represented as the elements of a vector x of length n or $x = [v_{s1}, v_{s2}, v_{s3} \dots, v_{sn}]^T$. Similarly, the data measurements of Rayleigh-wave phase velocities at m different frequencies can be represented as the elements of a vector b of length m or $b = [b_1, b_2, b_3 \dots, b_m]^T$. Since the model c_R(equation 2.12) is a nonlinear function, it must be linearized by Taylor-series expansion to employ the matrix theory:

$$J\Delta x = \Delta b \qquad 2.14$$

where $\Delta b = b - c_R(x_0)$ and is the difference between measured data and model response to the initial estimation, in which $c_R(x_0)$ is the model response to the initial S-wave velocity estimates, x_0; Δx is a modification of the initial estimation; and J is the Jacobian matrix with m rows and n columns ($m > n$), equation 2.14 is solved by optimization techniques

According to Xia *et al.* (1999), the objective function is given as:

$$\Phi = \|J\Delta x - \Delta b\|_2 W \|J\Delta x - \Delta b\|_2 + \lambda \|\Delta x\|_2^2 \qquad 2.15$$

where $\| \|_2$ is the ℓ_2-norm length of a vector, λ is the damping factor, and W is a weighting matrix. Since the weighting matrix W(equation 2.15) is both diagonal and positive, $W = L^T L$, where L is also a diagonal matrix. According to Marquardt (1963), The damping factor controls the direction of Δx and the speed of convergence.

The Solution for Δx is:

$$\Delta x = V(\Lambda^2 + \lambda I)^{-1}\Lambda U^T d \qquad 2.16$$

where d is the vector of difference between modeled and measured data, $V, \Lambda,$ and U are the Singular-value decomposition (SVD) techniques of the weighted Jacobian matrix.

2.3.4 Multi-channel Analysis of Surface Waves (MASW)

In the MASW methods, Rayleigh-type surface waves are generated and used to infer the shear wave velocity profile of the site to be surveyed as a function of depth. The shear wave velocity of individual soil layers is directly proportional to their shear modulus, which is their stiffness. The MASW method is low-cost, as well as being non-invasive and environmental-friendly since they neither require heavy machinery nor leave lasting marks on the ground surface. Moreover, it has been shown to provide consistently reliable results (Park *et al*., 1997; Xia *et al*., 2002). In the MASW method, the fundamental mode extracted from the dispersion curve obtained from the inverted shot records is used (Xia *et al*., 2000) to obtain the subsurface velocity model. The entire process involves three major steps, which are: acquisition of the data, construction of dispersion curve (phase velocity versus frequency), and inversion process to get the velocity model. This method provides a reliable estimate of shear wave velocity profiles within the upper 30m below the ground surface. The method can be used for effective site characterization (Yilmaz, 2015), seismic characterization of pavements (Park *et al*., 2001), to study Poisson's ratio (Ivanov *et al*., 2000), seismic investigation of sea bottom sediments (Park *et al*., 2000; Ivanov *et al*., 2000), mapping bedrock surface, detecting dissolution features (Miller *et al*., 1999) and generation of shear wave velocity profiles (Xia *et al*., 1999). The extraction of an accurate dispersion curve is a

very important step in the MASW method because an error in the dispersion curve would cause an inversion to produce an inaccurate value of shear wave velocity (Park *et al*., 1999).

CHAPTER THREE

MATERIALS AND METHODOLOGY

3.1 Materials

3.1.1 Software

- Seisimager/SW
- ReflexW
- Surfer
- ArcGis

3.1.2 Description of Materials

Table 3.1: Description of Materials

Acquisition Materials	Description
Seismograph	24 channel seismograph
Geophone type	10 Hz vertical geophones
Source	Sledgehammer (14 lb)
Cable	24 channel cable reel
G.P.S	Garmin

3.2 Methodology

3.2.1 Desk Studies

This was done to understand the technical know-how of the MASW method and also the geology of the area

3.2.2 Reconnaissance visit

This was done to map out the profiling of the survey area and to take their respective location coordinates.

3.2.3 Data Acquisition

The MASW overall setup is presented schematically in Figure 3.1. A 24-channel seismograph (ABEM Terraloc Pro) was used for data acquisition along seven profiles within the survey area (Figure 1.1). The aim is to estimate the shear wave velocity of the subsurface layers to a depth of 30m. In order to achieve this, a lower frequency geophone is required to obtain phase velocities at longer wavelengths (Figure 2.2b), which implies a deeper depth of penetration. Therefore, 10 Hz geophones were used, which is capable of investigating up to a depth of 30m (Park *et al*., 2002). A record length of 1024 ms was employed to yield good results, as a higher number of samples and shorter sampling interval influences good yield (Abubakar *et al*., 2019). The stacking number of four (4) was employed to ensure good quality of the result.

The MASW field acquisition parameters are of necessity to achieving the desired objectives. This comprises the offset distance, the receiver spacing, the spread length, and the source. The MASW method requires the analysis of plane waves of Rayleigh waves (fundamental-mode). Surface waves become stabilized or planar upon traveling a certain distance from the source, this distance is a function of wavelength (Park *et al*., 1999).

The geometry for the acquisition is summarized in the table below. The offset and the geophone spacing were varied within the recommended field parameters by Geometrics (2009) and park *et al*. (2002) for comparison. Before the acquisition, quiet times were waited for before shots were made.

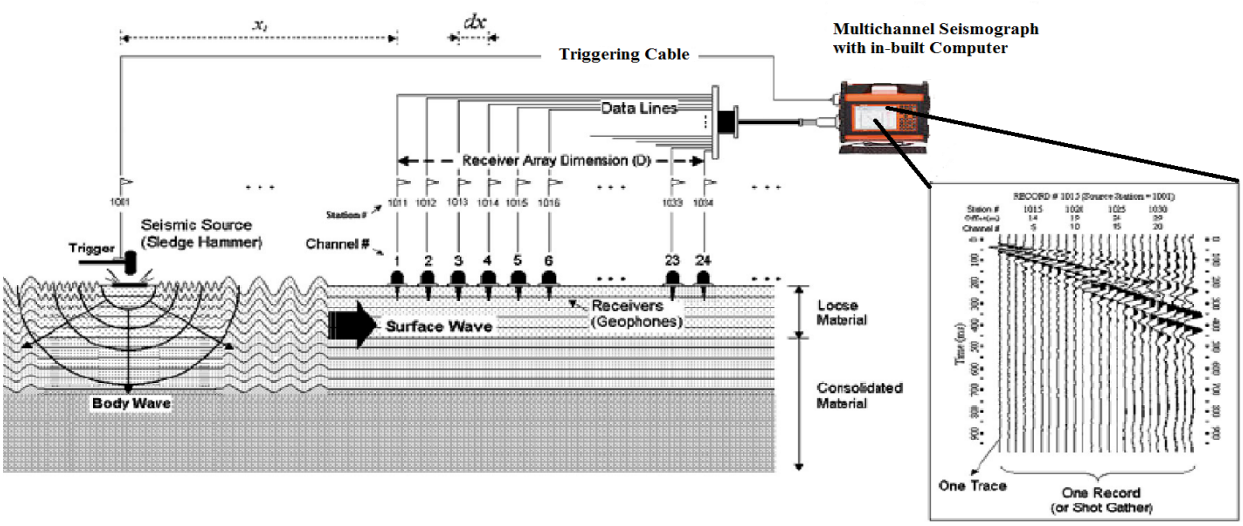


Figure 3.2: Schematic illustration for the Multi-channel Analysis of Surface Waves (MASW) data acquisition for 1-D and 2-D shear wave velocity determination.

Since the survey profile lines (mapped out) extends to about 100 m, to acquire an effective-continuous shot gather, the standard roll-along technique (Figure 3.2) was employed. However, this configuration enables the 2-D MASW survey to be achieved.

Table 3.2: Acquisition parameters

S/N	Profile	Offset distance (m)	Geophone spacing (m)	Shot interval (m)	No. of stacking
1	A-A[1]	-10	2	4	4
2	B-B[1]	-5	1	4	4
3	C-C[1]	-5	2	4	4
4	D-D[1]	-5	1	4	4
5	E-E[1]	-5	1	4	4
6	F-F[1]	-10	2	4	4
7	G-G[1]	-10	1	4	4

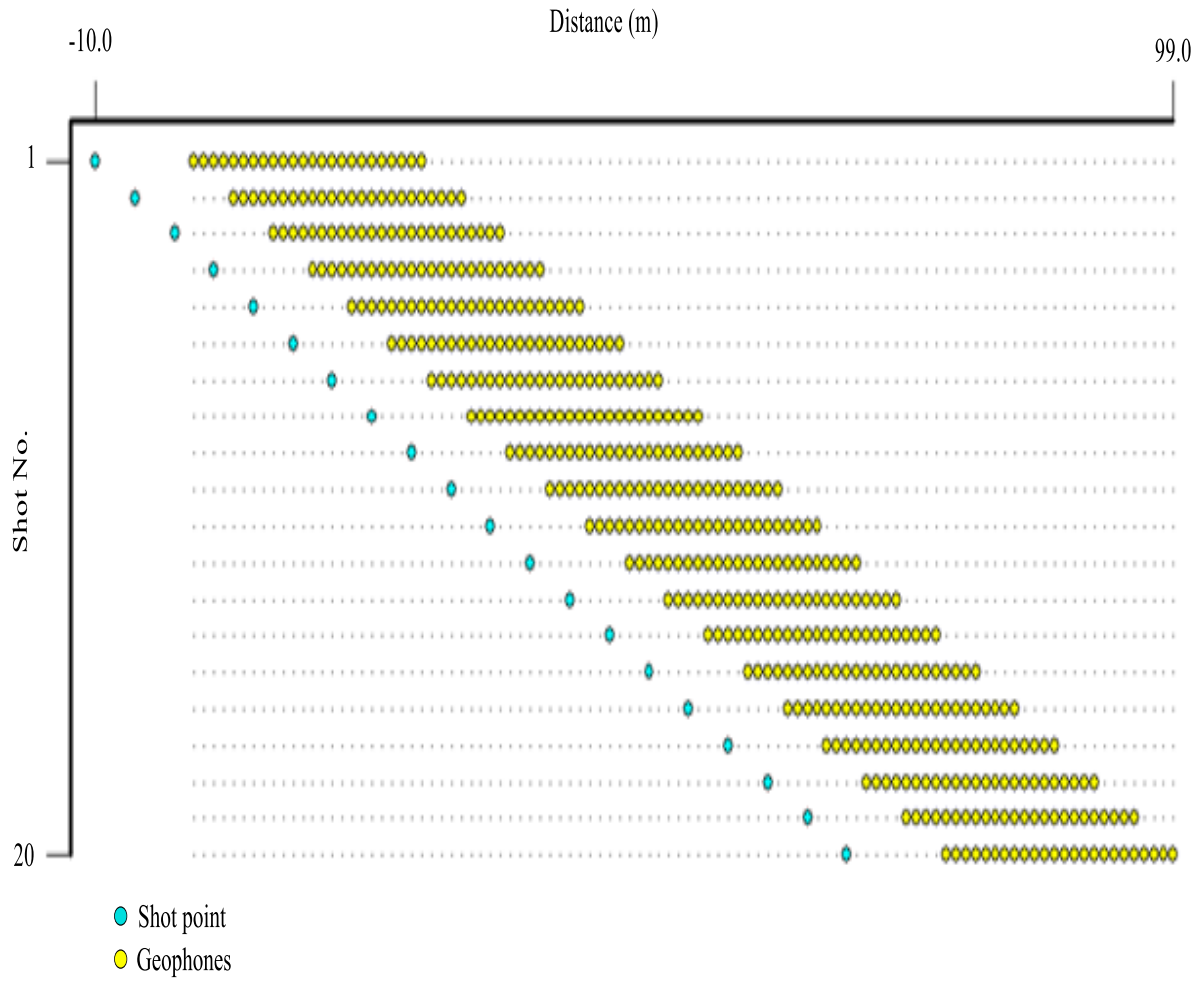


Figure 3.2: Standard roll-along configuration for 2-D MASW survey. The geophone spacing for this configuration is 1 m and an offset of 10 m was employed.



Plate 3.1: Seismic survey (a) 24 groups of 10 Hz geophones (b) Cable reel (c) Seismograph (Abem terraloc pro) in use (d) data acquisition setup in progress (e) Seismograph (Abem terraloc pro)

CHAPTER FOUR

4.0 DATA PROCESSING, RESULTS, AND INTERPRETATION

4.1 Data Processing

The MASW data was processed using "Seisimager/SW software". The software has three modules (integrated); PickWin, WaveEq, and GeoPlot. ReflexW was also used to have a better view of the shot gather.

A combination of series of geophone trace is called shot gather. The shot gathers (Figure 4.1-1 to Figure 4.1-6; Appendix I) (in Sg2 format) was inputted and processed into a file. The geometry of field data acquisition, which includes the geophone and the source coordinates was assigned to the data, which in turn arranges the data into the roll along (Figure 3.3) data configuration as acquired. The common mid-point (CMP) is a combination of traces having the same mid-point, which is the concept adopted by the reflection method. Every pair of traces in a shot record is cross-correlated, the correlation traces are gathered by CMP, and traces with equal spacing are stacked in the time domain (Hayashi and Suzuki, 2004). The CMP cross-correlation gather is calculated. Additionally, this improves the original MASW technique by effectively increasing the accuracy of the final shear wave velocity cross-section and also the lateral resolution.

After the CMP cross-correlation gathers are assembled, the parameters for phase velocity-frequency transformation are set to transform the time-domain gathers to the frequency domain, this is aimed at calculating the phase velocity for each frequency. 0 – 1000 m/sec and 0 – 40 Hz were employed for both phase velocity and frequency respectively. 1000 m/sec is used, being the maximum phase velocity expected for the site, while the 40 Hz is used as the maximum, to see the extent of the fundamental mode velocity.

Mathematically,

$$U(x,w) = \int u(x,t)e^{iwt}dt \quad 4.1$$

where $U(x,t)$ is a shot gather in the offset-time domain, $U(x,w)$ is a shot gather in the offset-frequency domain after applying Fourier transform to $U(x,t)$. $U(x,w)$ can be expressed as the multiplication of the phase and amplitude spectrum (Xia *et al*., 2000).

$$U(x,w) = e^{-i\Phi x}A(x,w) \quad 4.2$$

$$\Phi = \frac{w}{c_w} \quad 4.3$$

w is the frequency in radian and c_w is phase velocity for frequency (w).

Upon generating the dispersion spectrum (phase velocity-frequency plot) (Figure 4.1-1 to Figure 4.1-6), the curves for the Rayleigh-wave fundamental mode were picked (Appendix II). The output curve is examined to ensure the best curves are picked, the curves that represent the best choice are curves with a high signal-to-noise ratio. The dispersion curves (Appendix III) are individually inverted to generate an initial 1-dimensional (1D) shear-wave velocity model.

The average Vs model down to a depth of 30m (V_{s30}) is generated for the soil using the equation:

$$Average\ V_s = \frac{\sum d_i}{\sum(d_i/v_i)} \quad 4.4$$

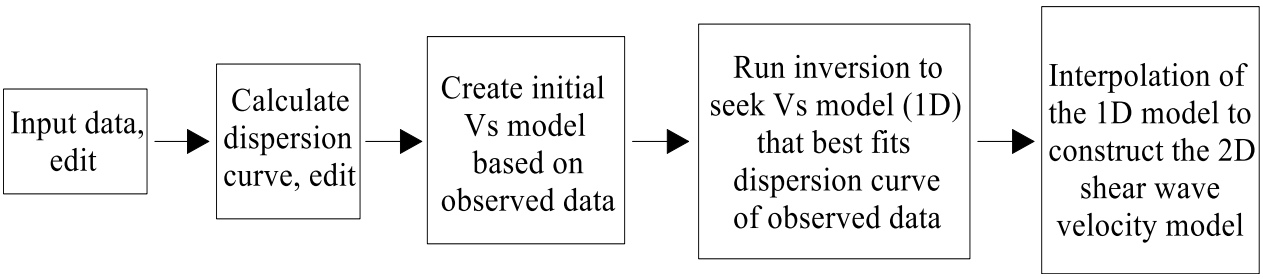
where $\sum d_i$ is the cumulative depth in meters, d_i is the thickness (in meters) of the ith layer and v_i is the shear wave velocity of the ith layer.

Therefore, $$V_{s30} = \frac{30}{\sum_{i=1}^{N}(d_i/v_i)} \quad 4.5$$

Where N represents the total number of layers.

The program utilizes the observed dispersion curve to calculate a theoretical dispersion curve by estimating the set of parameters that describe the soil column. As such, the theoretical and the observed dispersion curves are compared to measure the discrepancy in terms of root-mean-square error (RMSE) (Table 4.3). If the error is greater than 5% (as stipulated by software control parameters), the inversion algorithm is employed to modify the shear wave velocity profile to converge on the best fit of the initial model with the observed data, thereby, recalculating the RMSE (Geometrics, 2009). The circle of this process of modification and recalculation is referred to as iteration. Firstly, this is done continuously to reduce the degree of mismatch, thus, meeting the requirement of the control parameters. Secondly, to produce a realistic final velocity model. If the degree of mismatch is high above the tolerable limit, the initial set of model parameters is changed and the process re-run to improve the match. The RMSE serves as a guide, a lower RMSE suggests a high level of confidence in the estimation of the site's shear wave velocity. The RMSE is automatically saved in a text file format.

The generated 1-dimensional shear wave velocity models (Fig. 4.1-1c to 4.1-6c) are interpolated to produce a 2D shear-wave velocity model. This model is produced for each profile layout on the site. The data processing flow can be summarized as follows:



4.2 Results and Interpretation

The data acquired were subjected to the above data processing flow.

Figure 4.1-1a to 4.1-6a shows the shot gather analysis. It can be seen from the traces of the shot gather that the Rayleigh wave amplitudes which travel along the layer boundaries decay rapidly in depth. As the soil column approaches the bedrock, the surface waves become less prominent. This implies that surface waves are strongly dispersive in a low-velocity soil column with a high-velocity contrast at the soil-bedrock interface, and weakly dispersive in a high-velocity soil column (Fig. 4.1-1a to 4.1-6a).

The dispersion spectra (Fig. 4.1-1b to 4.1-6b) show clearly that each frequency component of the Rayleigh waves travels with a different horizontal phase velocity, which in turn, is the dispersive characteristics of the waves within the soil column. From the dispersion curve, the maximum depth to which the shear wave velocity can be investigated is approximately half the maximum wavelength (maximum picked phase velocity/respective minimum frequency) and the minimum depth of investigation corresponds to approximately half the minimum wavelength (minimum picked phase velocity/ respective maximum frequency) (Park *et al*., 1999). These criteria favor the yield (i.e. an investigation of about 30m), which is the interest of a geotechnical engineer.

The 1-dimensional shear wave velocity model (Figure 4.1-1c to 4.1-6c) shows the average shear wave velocity to a depth of 30 m. The average shear wave velocity at depth of 3 m, 7.5 m, 13.5 m, and 21.0 m are revealed at the right end of the model.

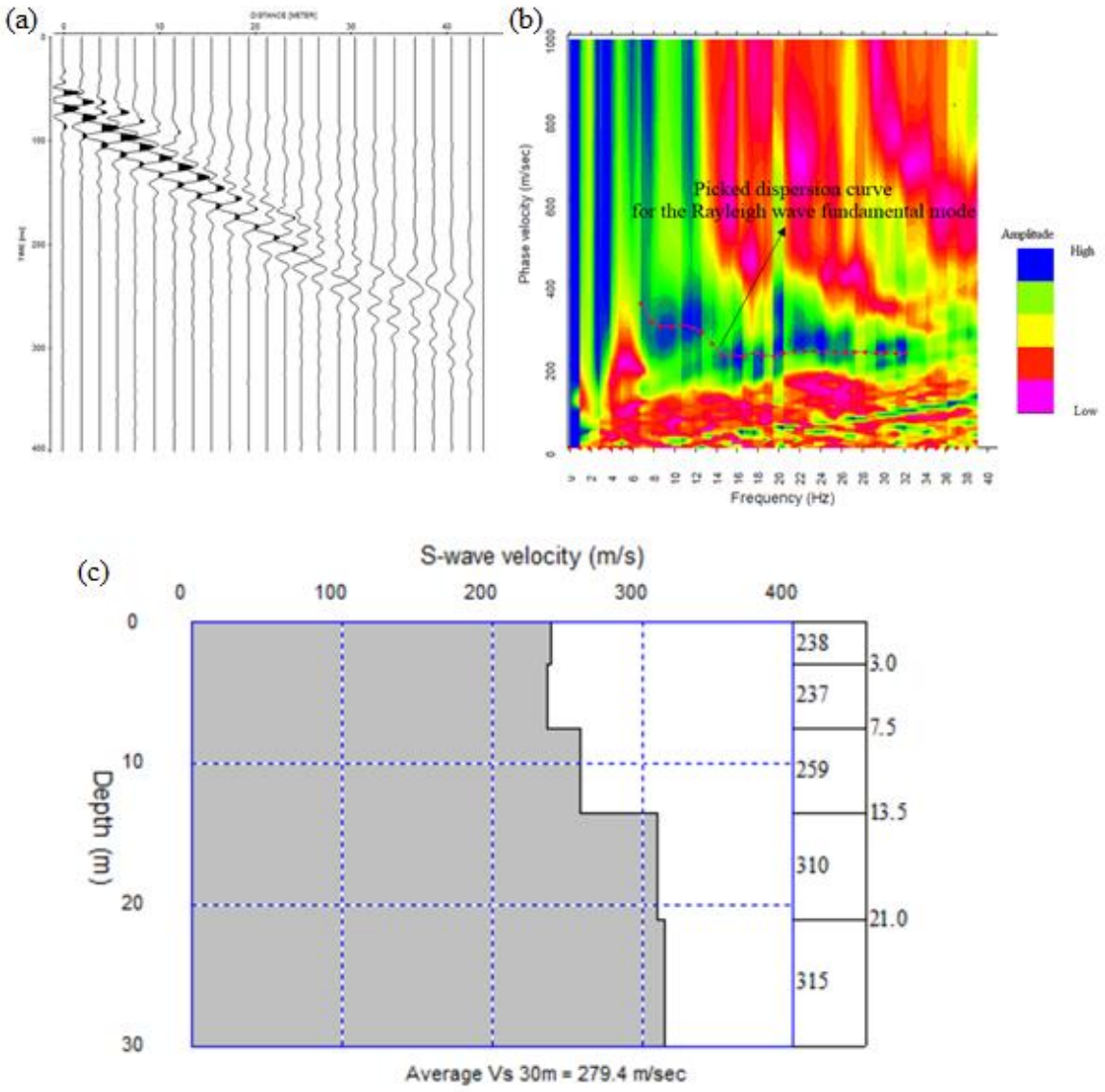


Figure 4.1-1: Profile 1 (A-A[1]), 1st shot gather analysis. (a) shot gathers (b) The dispersion spectrum. (c) 1D S-wave velocity model.

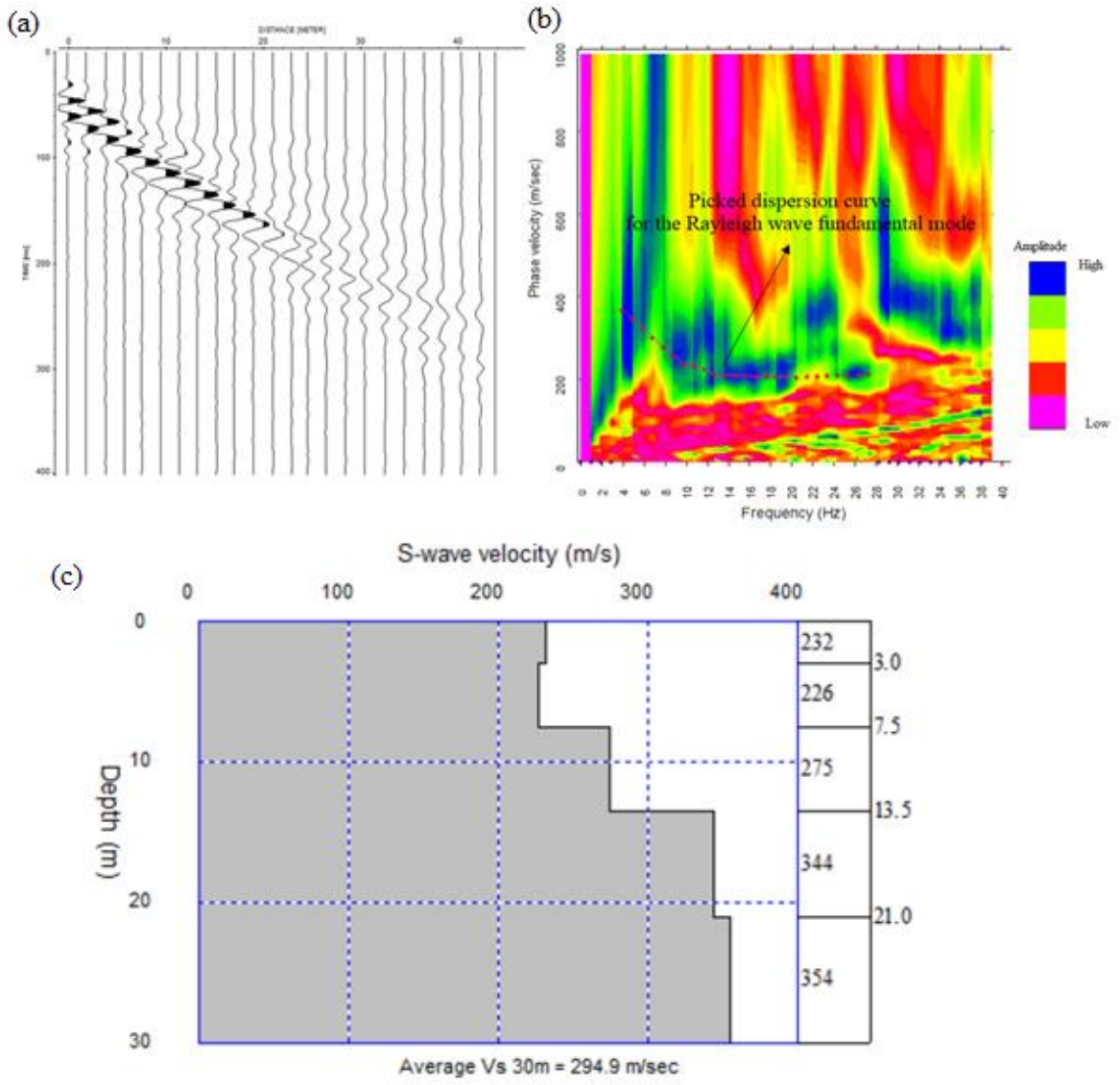


Figure 4.1-2: Profile 1 (A-A[1]), 10th shot gather analysis. (a) shot gathers (b) The dispersion spectrum. (c) 1D S-wave velocity model.

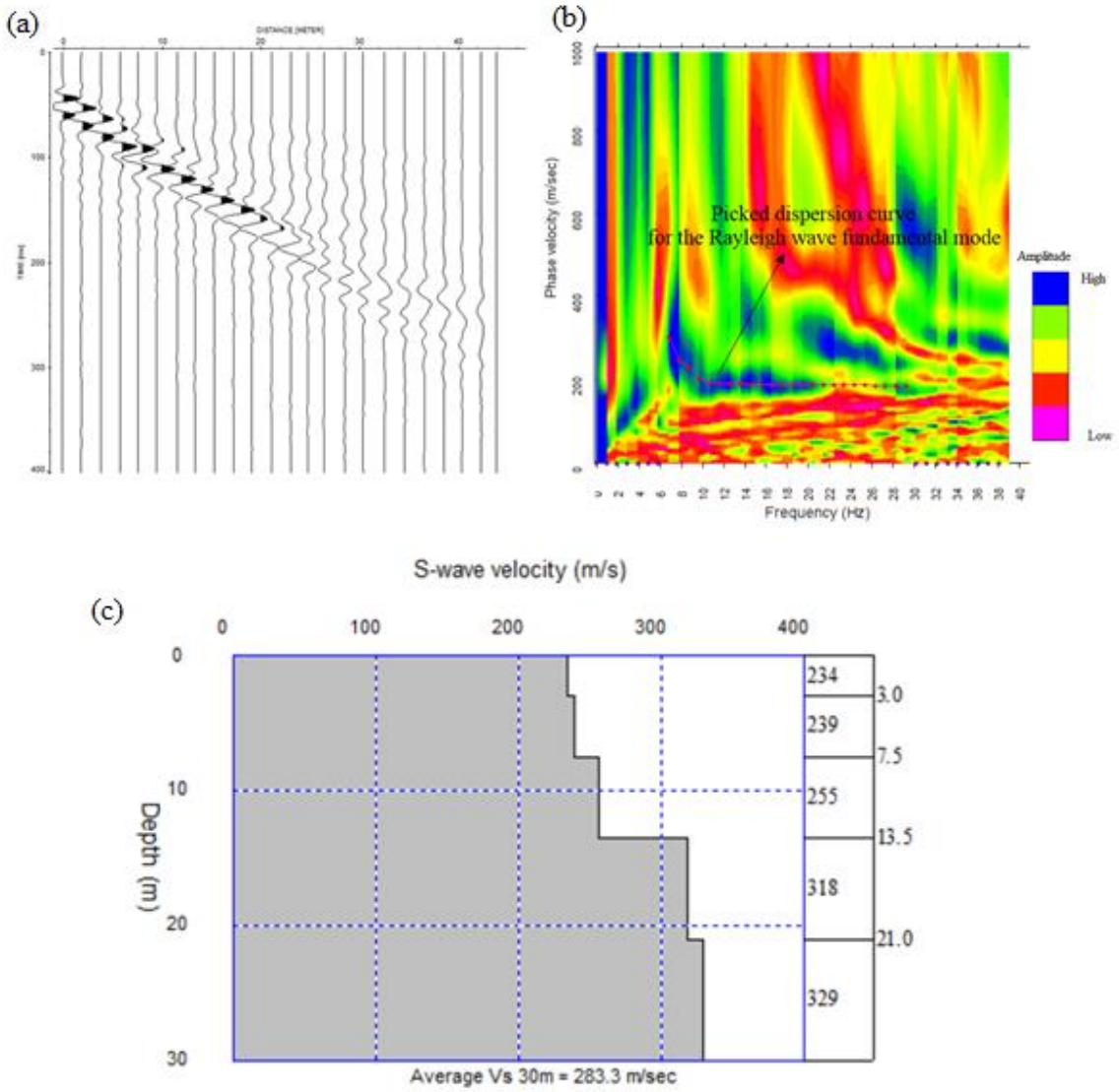


Figure 4.1-3: Profile 1 (A-A[1]), 15[th] shot gather analysis. (a) shot gathers (b) The dispersion spectrum. (c) 1D S-wave velocity model.

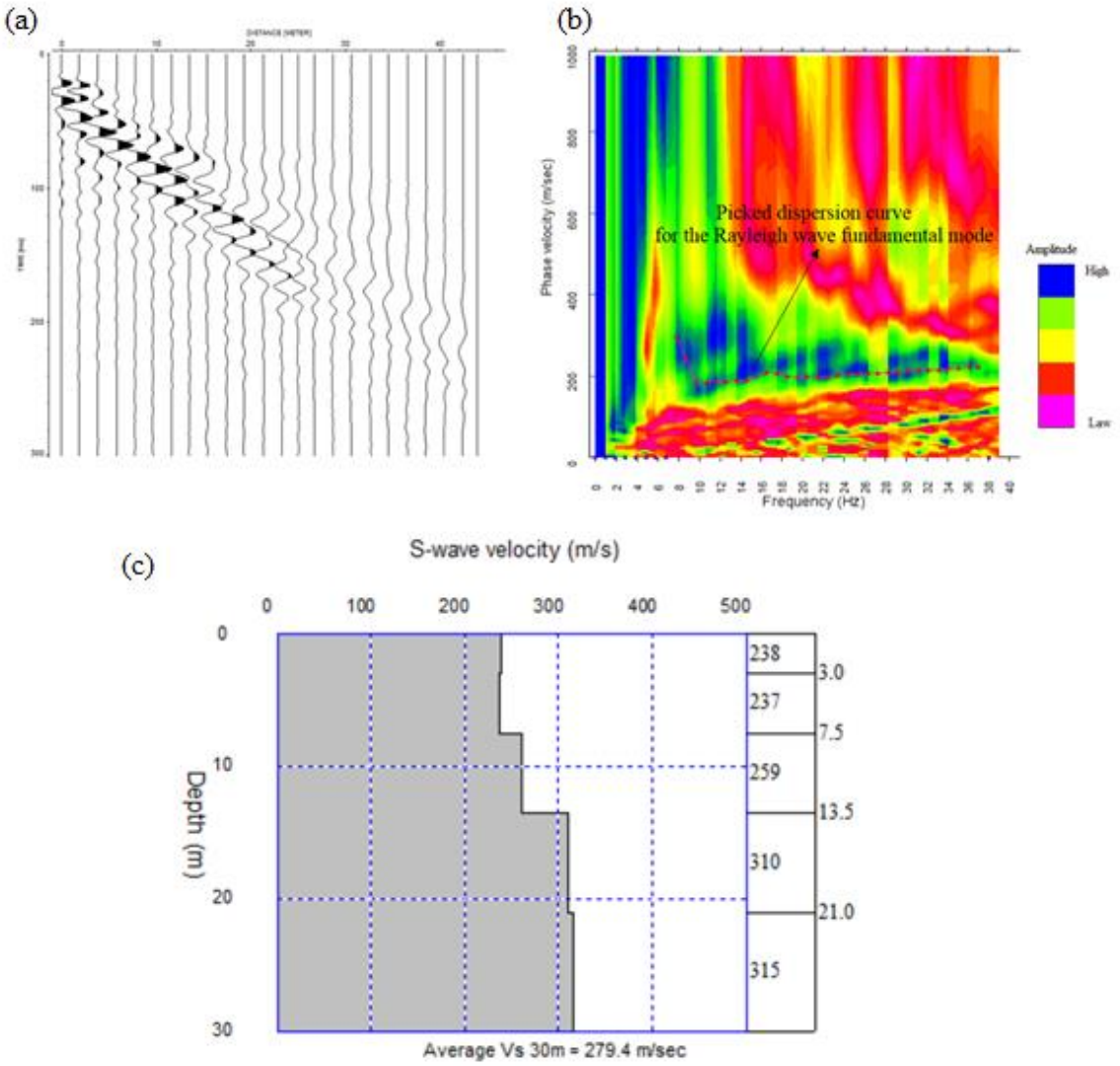


Figure 4.1-4: Profile 3 (C-C[1]), 1st shot gather analysis. (a) shot gathers (b) The dispersion spectrum. (c) 1D S-wave velocity model.

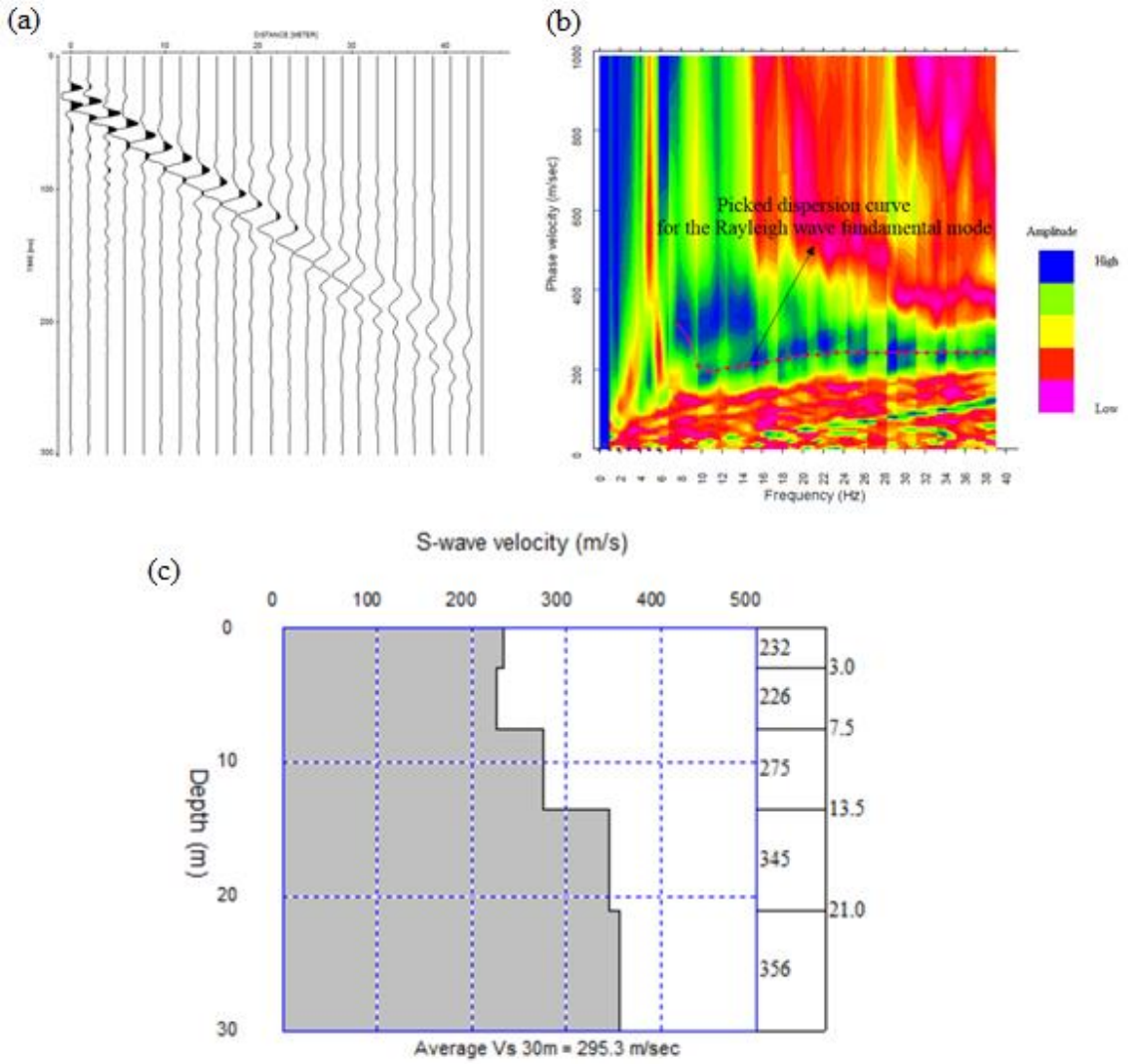


Figure 4.1-5: Profile 3 (C-C[1]), 7th shot gather analysis. (a) shot gathers (b) The dispersion spectrum. (c) 1D S-wave velocity model.

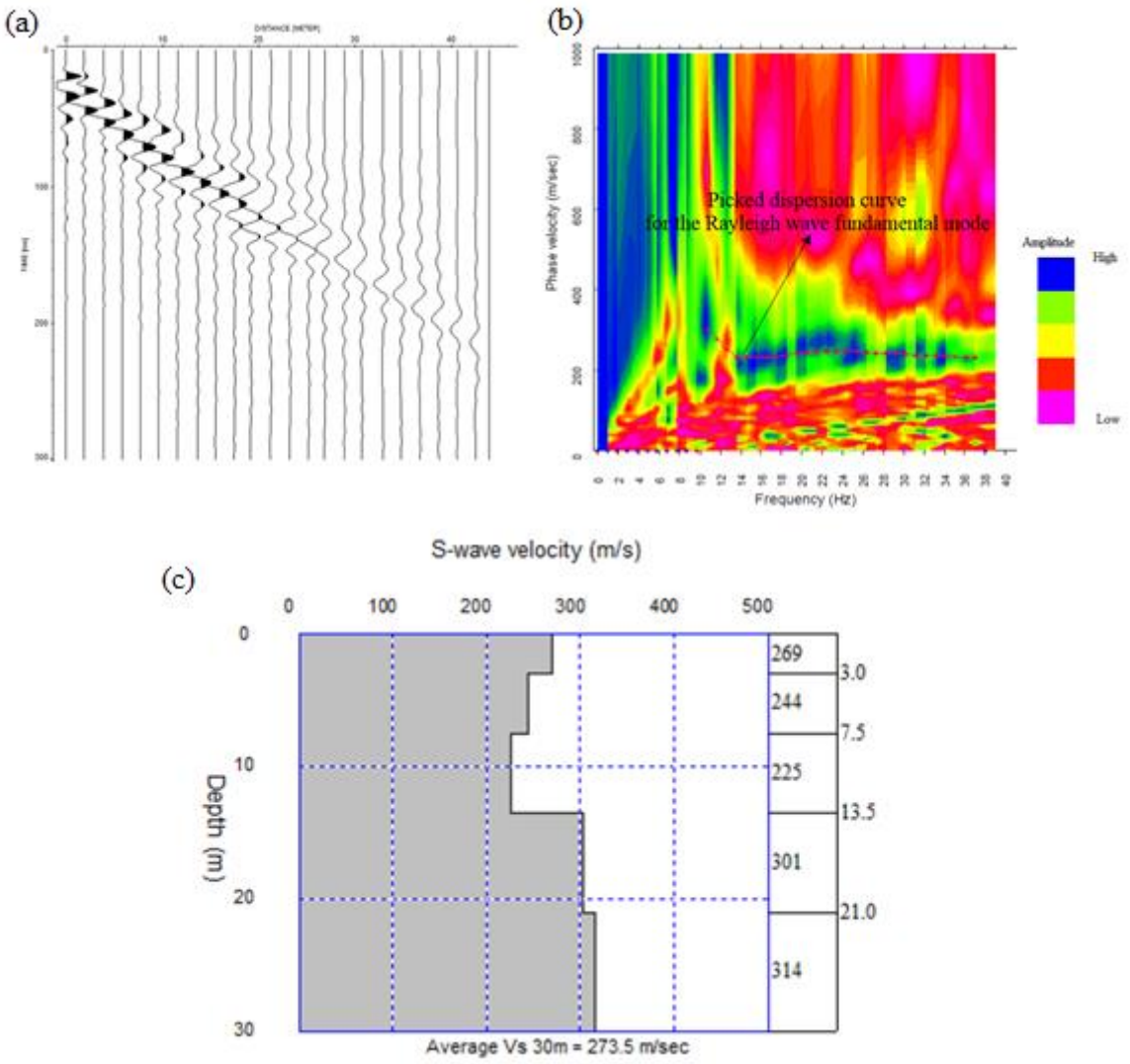


Figure 4.1-6: Profile 3 (C-C[1]), 15[th] (last) shot gather analysis. (a) shot gathers (b) The dispersion spectrum. (c) 1D S-wave velocity model.

The borehole log data (Fig. 4.2) was obtained from the National Water Resources Institute, Kaduna. The location of the borehole is within the same geology of the study area (Fig. 1.2)

In engineering seismology, civil engineering, earthquake geotechnical engineering, and environmental earth science studies, the elastic properties of the near-surface materials and their response to seismic wave propagation are very important. The seismic site

characterization used in estimating the seismic hazard is usually carried out based on the shear wave velocity values of the near-surface. The average shear wave velocity down to a depth of 30m (V_{s30}) is used for site classification based on the National Earthquake Hazards Reduction Program (NEHRP) provision (Table 4.1). The parameters employed to define the class of a site are based on the upper 30m (100ft) of the site profile (BSSC, 2003).

The 2-dimensional shear wave velocity models with the layers inferred (i.e. using both the borehole log data and the shear wave velocities observed) are illustrated in Figure 4.3-1 to 4.3-7. The models demonstrate a first layer (topsoil and laterite) with V_s in the range of 158 to 290 m/s and corresponding thickness of 0 to 6 m. The second layer (clayey sand) shows a V_s range of 180 to 270 m/s with a corresponding thickness of 2 to 7 m. The third layer, which is the weathered basement shows a V_s range of 250 to 500 m/s and a thickness range of 4 to 18 m. The fourth layer (fractured basement) has a thickness range of 2 to 8 m and V_s of 400 to 650 m/s. The fifth layer with the highest V_s (> 650 m/s) is assumed to be the fresh basement (bedrock). The depth of the engineering bedrock is determined in order to estimate the soil thickness beneath the MASW profiles. The areas with higher shear velocity values correspond to areas with lower soil thickness, while the areas with lower velocity values correspond to areas with higher soil thickness (Fig. 4.4). The depth of the fresh basement is 24 m in some of the areas (Fig. 4.3-4, Fig. 4.3-5, 4.3-6, and Fig. 4.3-7).

The V_{s30} values for the site vary between 273.5 m/s and 446.2 m/s based on the NEHRP standard (Table 4.2).

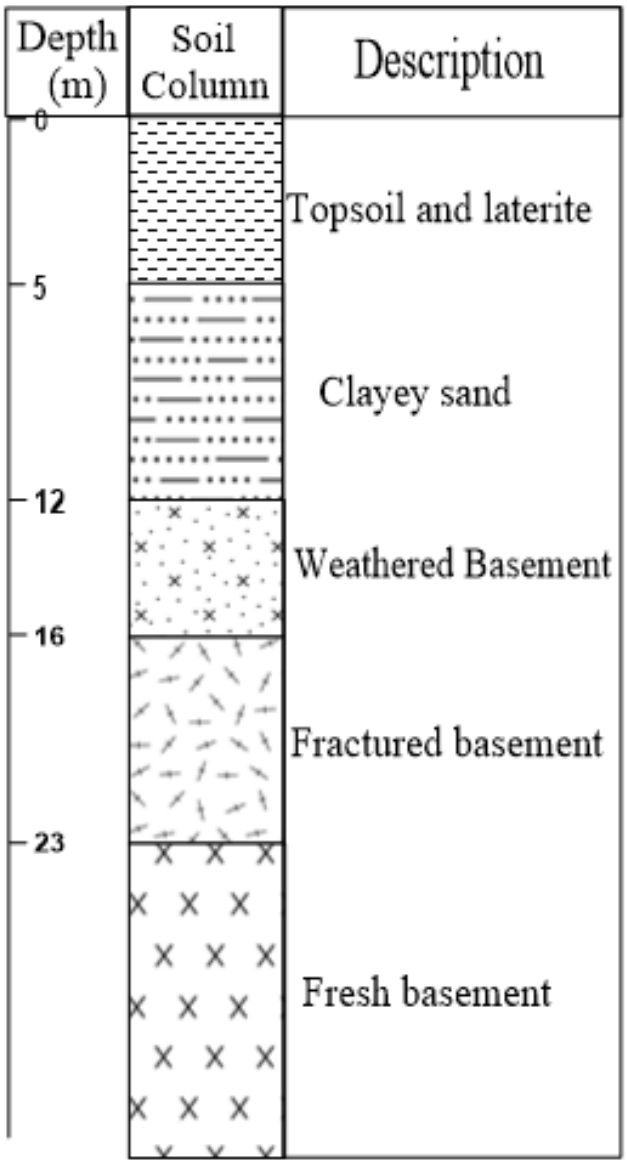


Figure 4.2: Borehole log (lithologic) data by the National water resources institute, Kaduna.

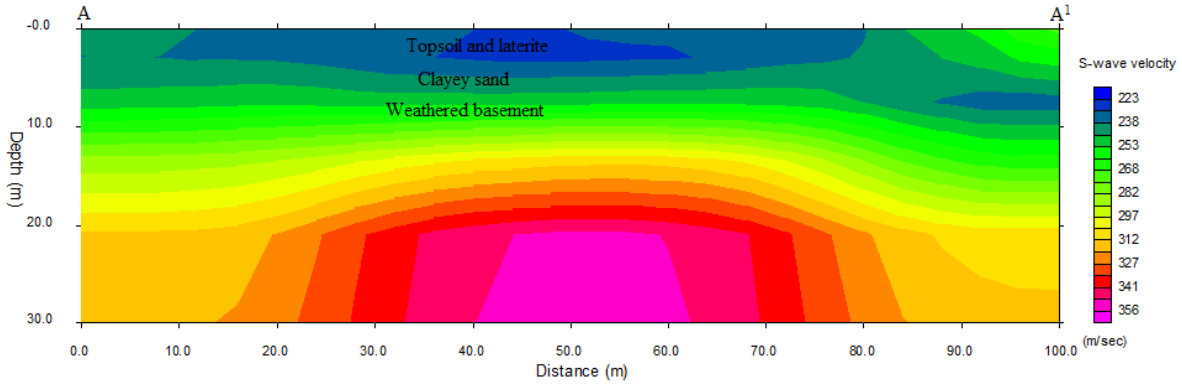


Figure 4.3-1: 2D shear wave velocity model with inferred layers for profile 1 (A-A^1)

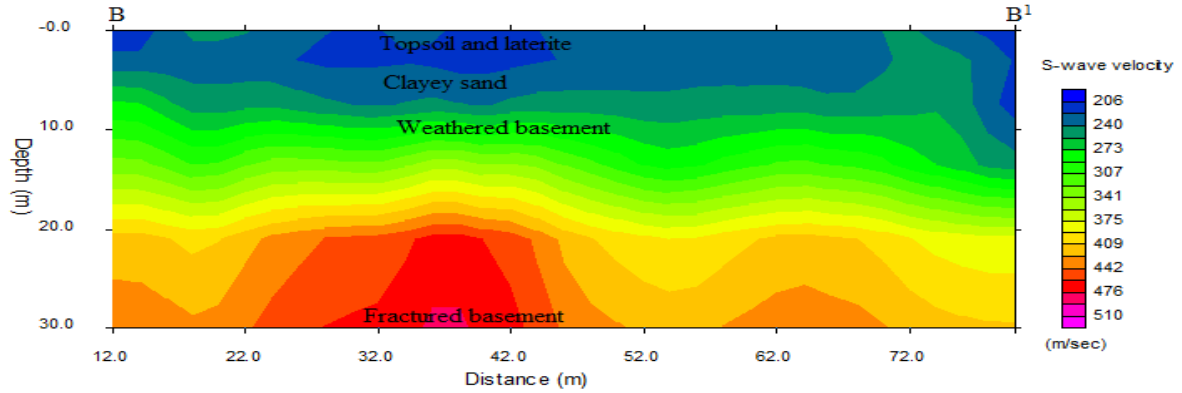


Figure 4.3-2: 2D shear wave velocity model with inferred layers for profile 2 (B-B^1)

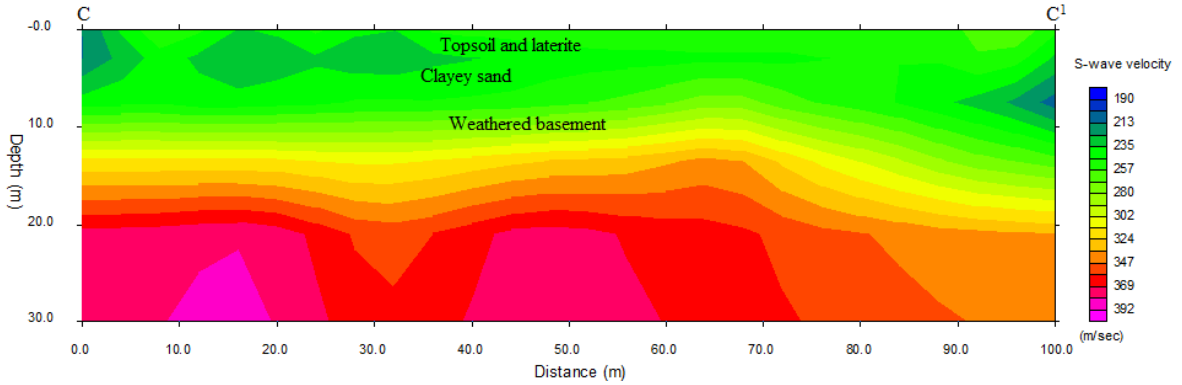


Figure 4.3-3: 2D shear wave velocity model with inferred layers for profile 3 (C-C^1).

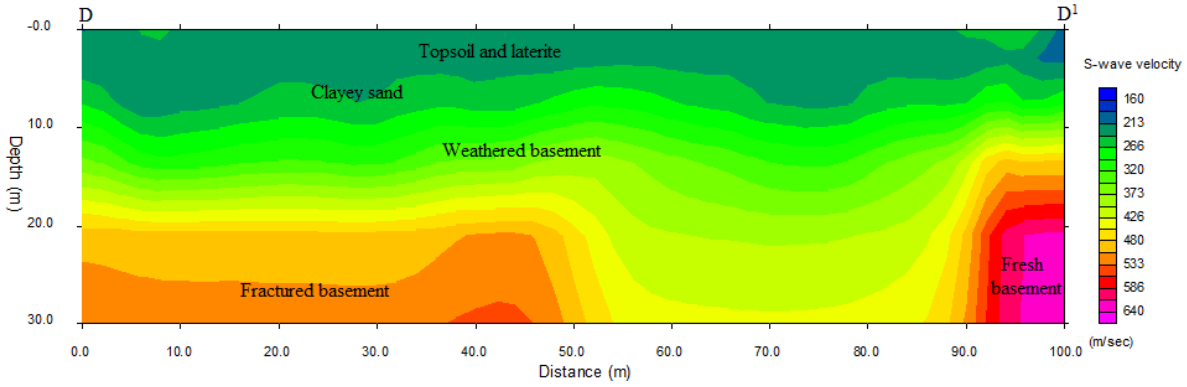


Figure 4.3-4: 2D shear wave velocity model with inferred layers for profile 4 (D-D^1).

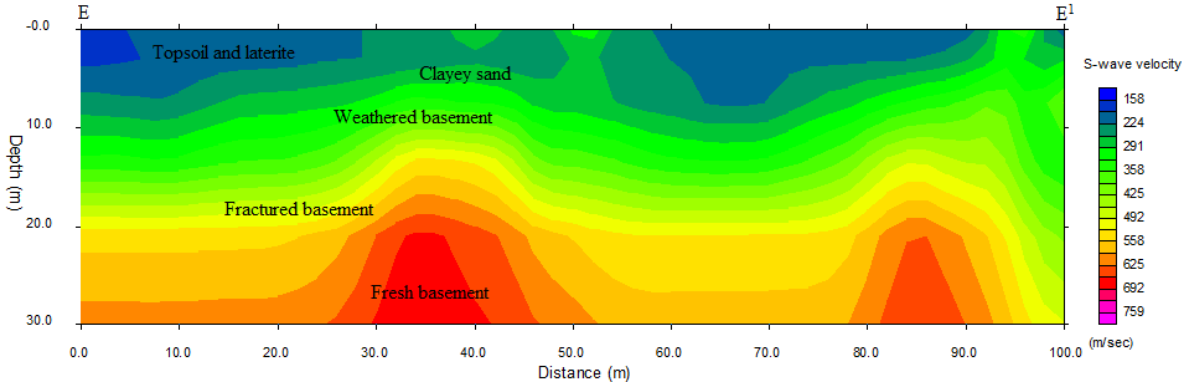


Figure 4.3-5: 2D shear wave velocity model with inferred layers for profile 5 (E-E^1).

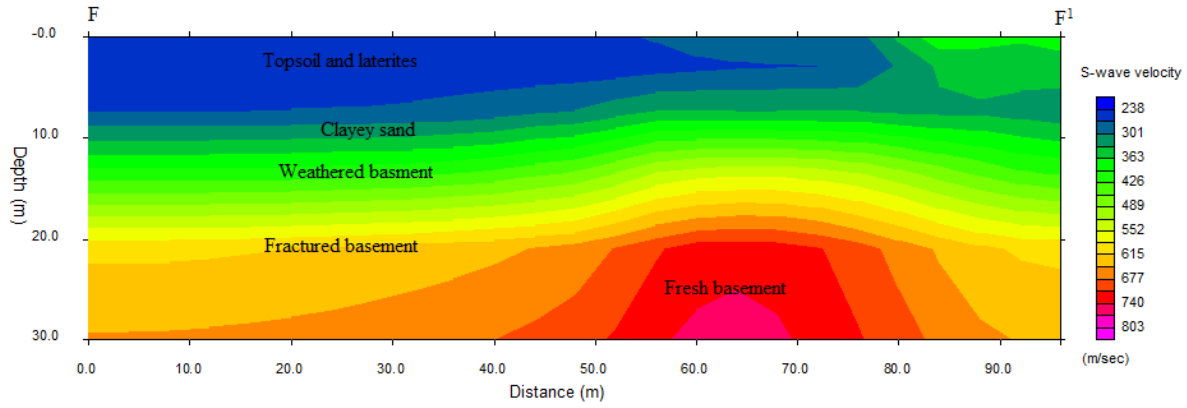


Figure 4.3-6: 2D shear wave velocity model with inferred layers for profile 6 (F-F^1).

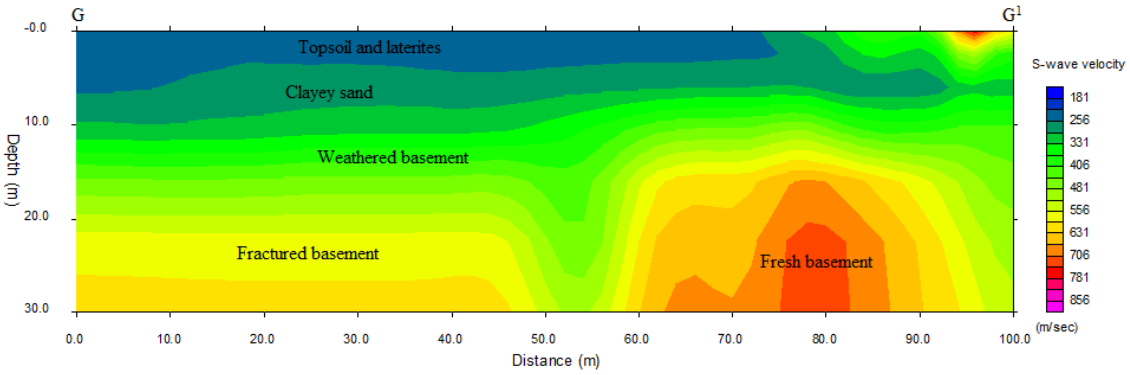


Figure 4.3-7: 2D shear wave velocity model with inferred layers for profile 7 (G-G[1]).

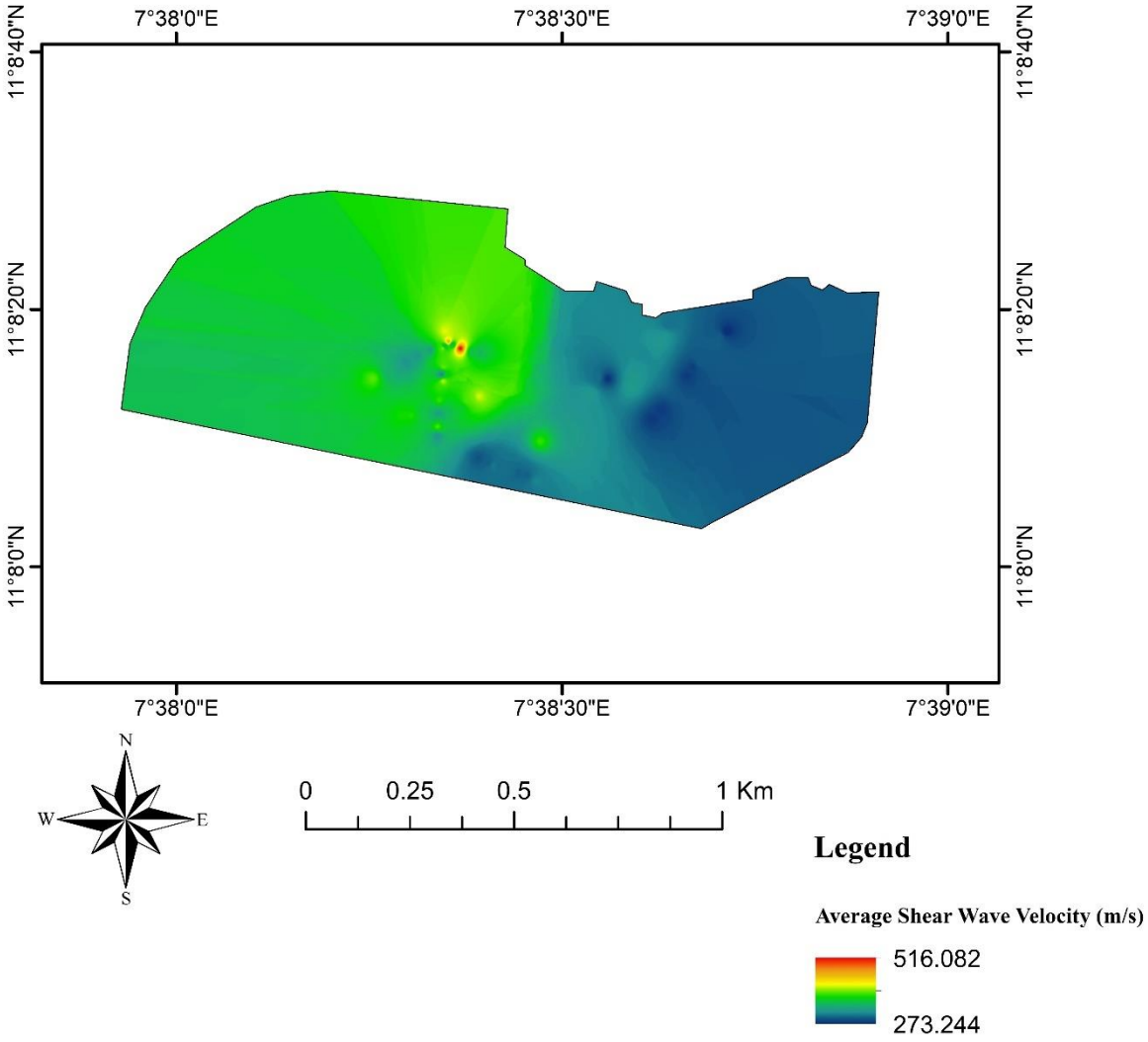


Figure 4.4: Map of the study area showing the average shear wave velocity distribution

Table 4.1: Site Classification, according to the NEHRP provisions (BSSC, 2003)

Site Class	Average shear wave velocity down to 30m (V_{s30})	Remarks
A	$V_{s30} > 1500\ (m/s)$	Hard rock
B	$760 \leq V_{s30} \leq 1500\ (m/s)$	Rock
C	$360 \leq V_{s30} \leq 760\ (m/s)$	Very dense soil or soft rock
D	$180 \leq V_{s30} \leq 360\ (m/s)$	Stiff soil
E	$V_{s30} < 180\ (m/s)$	Soil
F	$V_{s30} < 180\ (m/s)$	Soil requiring site-specific evaluation

Table 4.2: The site classification of the study area, based on the NEHRP provisions

S/N	Profile	Average V_{s30} (m/s)	Site class
1	A-A[1]	273.5	D
2	B-B[1]	301.6	D
3	C-C[1]	310.1	D
4	D-D[1]	352.6	D
5	E-E[1]	412.5	C
6	F-F[1]	414.5	C
7	G-G[1]	446.2	C

Table 4.3: RMSE for the 2D models (calculated for all data)

S/N	Profile	RMSE (in %)
1	A-A[1]	1.96
2	B-B[1]	3.28
3	C-C[1]	3.53
4	D-D[1]	2.83
5	E-E[1]	4.49
6	F-F[1]	3.39
7	G-G[1]	4.49

CHAPTER FIVE

5.0 DISCUSSION, CONCLUSION AND RECOMMENDATION

5.1 Discussion

The MASW method has displayed high accuracy in analyzing the properties of the near-surface and also very efficient in imaging the subsurface and detecting areas with high soil thickness. Higher velocity implies lower soil thickness and vice versa. The thickness of the soil increases eastwards as shown in the thickness distribution map (Fig. 4.4). Perhaps, this may be as a result of the proximity to the river channels (Fig. 1.2).

The method has shown great tolerance in the selection of field parameters that suit the survey. The profile F-F^1 and G-G^1 were acquired along the same profile but the geophone spacing of 2 m and 1 m respectively was used to ensure proper comparison. A similar result was obtained for both profiles. Although the result of G-G^1 yielded a higher resolution image of the subsurface. As observed from other 2-dimensional V_s models, the resolution of the subsurface images of data acquired using 1 m geophone spacing is higher than that acquired using 2 m. The offset distance varied using 5 and 10 m in some of the profiles has no significant effect in the resolution image of the subsurface.

Considering the 2-dimensional V_s models (Fig. 4.3-1 to 4.3-7), the inference of the layers was made using the borehole log data. But, priority was also given to the shear wave velocity revealed. The color does not really depict different layers, because there is considerable overlap between the shear wave velocity of several layers. The topsoil and laterite and the clayey sand displayed similar V_s. In some cases, the topsoil and laterites exhibit higher shear wave velocity than the clayey sand (Appendix III). The results of the 2-dimensional shear

wave velocity models indicate that the area has undergone intense weathering due to the dominance in the distribution of the weathered materials.

5.2 Conclusion

The MASW method was employed to image the subsurface layers of the ABU phase II site for foundation studies. This was achieved by estimating the 1D and 2D shear wave velocities over the survey profiles.

The average shear wave velocity down to 30 m of the site varies between 273.5 m/s and 446.2 m/s, which is classified as site class of C and D according to the NEHRP provisions, which implies that the site can be assumed for engineering construction. The soil thickness increases eastwards and the depth to the basement is 24 m in some areas.

The MASW method has shown high tolerance in the selection of field parameters.

5.3 Recommendation

Considering the presence of the clayey material, we recommend that excavation or densification (where it occurs) might be necessary before the construction is assumed on the site.

REFERENCES

Abubakar, F., Ahmed, I. I., Aminu, A. L., and Lawal, K. M. (2019). 1-dimensional shear wave velocity analysis of the phase II site, Ahmadu Bello University, Zaria using multi-channel analysis of surface waves. *FUDMA Journal of Sciences*. Vol. 3, No.3, pp436-443.

Abubakar, F., Ahmed, I. I., Idogbe, E. A., Usman, M. T. and Momoh, K. O. (2020). Site characterization of the proposed agricultural complex, Ahmadu Bello University, Zaria, Northern Nigeria, using multi-channel analysis of surface waves. *Minna Journal of Geosciences (MJG)*, Vol. 4 No.2.

Adewoyin, O. O., Joshua, E. O. and Akinyemi, M. L. (2017). Application of geophysical and geotechnical methods to determine the geotechnical characteristics of a reclaimed land. Adapted from extended abstract prepared in conjunction with oral presentation given at AAPG/SPE 2016 International Conference & Exhibition, Barcelona, Spain. April 3-6, 2016.

Aki, K. I., and Richards, P. G. (1980). Quantitative seismology: W.H. Freeman and Co.

Anand, J. and Parul, B. (2018). Site characterization using Multi-channel Analysis of Surface Waves at various locations in Kumaon Himalayas, India. *Journal of Industrial Geophysics Union*. vol.22, no.3, pp:265-278.

Anbazhagan, P. and Sitharam, T.G. (2006). Evaluation of dynamic properties and ground profiles using MASW: correlation between V_s and N_{60}. 13^{th} symposium on Earthquake Engineering Indian Institute of Technology, Roorkee. Paper no. 008.

Anukwu, G. C., Khalil, A. E. and Abdullah, K.B. (2017). Evaluating the effectiveness of the MASW technique in a geological complex terrain. IOP Conf. Series: *Journal of Physics*. Conf. Series 995.

Arjwech, R. and Everett, M. E. (2015). Application of 2D electrical resistivity tomography to engineering projects: Three case studies. *Songklanakarin J. Sci. Technol*., 37 (6), 675-681, 2015.

Ashraf, M. A. M., Kumar, N.S., Yusoh, R., Hazreek, Z. A. M., and Aziman, M. (2017). Site classification using Multi-channel Analysis of Surface Wave (MASW) method on Soft and Hard Ground. IOP Conf. Series: *Journal of Physics*: Conf. Series 995. Doi: 10.1088/1742-6596/995/1/012108.

Ayolabi, E. A., Folorunso, A. F., and Jegede, O. E. (2012). An application of 2D electrical resistivity tomography in geotechnical investigations of foundation defects: A case study. *Journal of Geology and Mining Research, Vol*. 3(12) pp. 142-151.

Blyth FGH and de Freitas, M.H. (1984). A Geology for Engineers, London, Publisher: Edward Arnold.

Bolt, M.H.P. (1982). The Interior of the Earth. Edward Arnold, London.

Bolt, B. A. (1993). Earthquakes and geological discovery, Scientific American Library.

Bowles, J. E. (1984). Physical and geotechnical properties of soils, 2nd Edition. New York: McGraw-Hill, Inc.

BSSC (2003). NEHRP recommended provisions for seismic regulations for new buildings and other structures (FEMA 450), Part 1: Provisions: Building Seismic Safety Council, National Institute of Building Sciences.

Chiemeke, C. C. and Osazuwa, I. B. (2007). Application of seismic refraction tomography for subsurface imaging in central Northern Nigeria. *Nigerian Journal of Physics*. 19 (2), 247-252.

Claerbout, J. F. (1978). Snell waves: Standford exploration project report no. 15: Standford University, 57-72.

Coduto, D. P. (1999). Geotechnical engineering: Principles and practices: Prentice Hall.

Collins, C. C. (2014). Investigation of dam safety making use of Multi-channel Analysis of Surface Wave (MASW) Seismic method. *International Journal of Environmental and Ecological Engineering*. Vol. 8, No.1.

Duffy, B., Campbell, J., Finnemore, M. and Gomez, C. (2014). Defining fault avoidance zones and associated geotechnical properties using MASW: a case study on the Springfield fault, New Zealand. Engineering Geology 183 (2014) 216-229.

Egwuonwu, G. N. and Osazuwa, I. B. (2011). Geophysical and geotechnical investigation of the origin of structural instabilities shown on some low rise buildings in Zaria, North-western Nigeria. *The Pacific journal of science and technology*. Vol. 12, No. 2.

Egwuonwu, G. N., Ibe, S. O., Osazuwa, I. B. (2011). Geophysical Assessment of Foundation Depths around a Leaning Superstructure in Zaria Area, Northwestern Nigeria using Electrical Resistivity Tomography. *The Pacific Journal of Science and Technology*. Vol. 12. No. 1.

Eigbefo, C. (1978). Hydrogeology of the Kubani Drainage Basin, Zaria. Unpublished M. Sc. Thesis, Department of Geology, Ahmadu Bello University, Zaria.

Geometrics (2009). Seisimager/SW Manual, Windows Software for Analysis of Surface Waves. Pp 314.

Hayashi, K. and Suzuki, H. (2004). CMP cross-correlation analysis of multi-channel surface-wave data, Exploration Geophysics, 35: 7-13.

Ivanov J., Park C. B., Miller R. D., and Xia, J. (2000). Mapping Poisson's Ratio of Unconsolidated Materials from a Joint Analysis of Surface-Wave and Refraction Events. Proc. of the Symposium on the Application of Geophysics to Engineering and Environmental Problems, Arlington, Va., February 20-24.

Jimoh L. A. (2011). Geophysical Investigation of a Sewage Treatment Site at Ahmadu

Bello University, Zaria. Unpublished M. Sc. Thesis, Department of Physics,

Ahmadu Bello University, Zaria.

Kabir, S. A, Hossain, D. and Abdullah, R. (2011). 2D Electrical imaging in some Geotechnical investigation of Madhupur clays, Bangladesh. *Journal geological society of India, Vol*. 77, pp. 73-81.

Kalinina, A.V., and Ammosov, S. M. (2015). The study of velocity characteristics of soils according to the MASW method for solving seismic microzonation problems. ISSN 0747-9239, Seismic Instruments. Vol. 51, No.4, pp.358-366.

Kennett, B. L. N. and Clarke, T. J. (1983). Seismic wave in a stratified half-space- IV: P-Sv wave decoupling and surface wave dispersion: Geophysical Journal International, 72, 633-645.

Lin, C. P., Chang, C. C., Chang, T. S. (2004). The use of MASW method in the assessment of soil liquefaction potential. Soil dynamics and earthquake engineering, vol. 24, pp 689-698.

Long, M. and Donohue, S. (2007). In situ shear wave velocity from Multi-channel Analysis of Surface Waves (MASW) tests at eight Norwegian research sites, Canada. *Geotechnical Journal*. Vol 44.

Marquardt, D. W. (1963). An algorithm for least-squares estimation of nonlinear parameters: J. Soc. Indus. Appl. Math., **2**, 431–441.

McCurry, P. (1970). The Geology of Degree Sheet 21 Zaria. Unpublished M.Sc. Theses, Ahmadu Bello University Zaria 1970:20-22.

Miller, R. D., Xia, J., Park, C. B., and Ivanov, J. (1999). "Multi-channel Analysis of Surface Waves to Map Bedrock", The Leading Edge, 18(12), 1392-1396.

Mohamed, A. M. E., Abu El Ata, A. S. A., Azim, F.A., and Taha, M.A. (2013). Site-specific shear wave velocity investigation for geotechnical engineering applications using seismic refraction and 2D multi-channel analysis of surface waves. NRIAG *Journal of Astronomy and Geophysics*. vol.2, pp: 88-101.

Neelima, D. S. and Rao, K. S. (2008). Seismic site characterization in Delhi region using Multi channel Analysis of Shear Wave Velocity (MASW) Testing. EJGE vol. 13, Bund.L pp.17.

Officer, C. B. (1958). Introduction to the theory of sound transmission with application to the ocean: McGraw-Hill.

Oyawoye, M. O. (1964). Geology of the Nigerian Basement Complex. *Journal of Nigerian Mining, Geological and Metallurgical Society*. Pp 87-102.

Park, C. B., Miller, R. D. and Xia, J. (1997). Summary report on surface-wave project at Kansas Geological Survey (KGS). [Open-file Report]. Lawrence, KS: Kansas Geological Survey.

Park, C. B., Miller, R. D. and Xia, J. (1999). Multi-channel analysis of surface waves. Geophysics, 64 (3), pp 800-808.

Park, C. B., Miller, R. D., Xia, J., and Ivanov, J. (2000). Multi-channel seismic surface-wave methods for geotechnical applications. Proceedings of the First International Conference on the Application of Geophysical Methodologies to Transportation Facilities and Infrastructure, St. Louis, December 11-15, 2000.

Park, C. B., Miller, R. D. and Xia, J. (2001). Offset and resolution of dispersion curve in Multi-channel analysis of surface waves (MASW). Proceedings of the Symposium on the Application of Geophysics to Engineering and Environmental Problems (SAGEEP 2001), Denver, Colorado, SSM-4.

Park, C. B., Miller, R. D. and Miura, H. (2002). Optimum field parameters of an MASW survey. Expanded Abstracts, SEG-J, Tokyo, May 22-23, 2002.

Park, C. B. (2019). Multi-channel Analysis of Surface Waves (MASW). www.masw.com/services-TrainingCourse.html.

Physical planning and Municipal Services (2017). Ahmadu Bello University, Zaria.

Premium times (2018). Three killed in Zaria building collapse. https://www.premiumtimesng.com/regional/nwest/271678-three-killed-in-zaria building-collapse.html

Press, W. H., Teukosky, S. A., Vetterling, W. T. and Flannery, B. P. (1992). Numerical recipes in C: Cambridge Univ. Press.

Rayleigh, J. W. S. (1885). On waves propagated along the plane surface of an elastic solid: Proceedings of the London Mathematical Society, 17, 411.

Ryden, N. and Park, C. B. (2006). Fast simulated annealing inversion of surface waves on pavements using phase velocity spectra. Geophysics, 71(4). R49-R58.

Schroder, C. T. and Scott, W. R. (2001). On the complex-conjugate roots of the Rayleigh equation: the leaky surface wave. *Journal of the Acoustic Society of America*, 110, 2867-2877.

Schwab, F. A. and Knopoff, L. (1972). Fast surface wave and free mode computations, *in* Bolt,B. A., Ed., Methods in computational physics: Academic Press, 87–180.

Sheriff, R. E. and Geldart, L. P. (1982). Exploration Seismology (in 2 volumes). New York: Cambridge University Press.

Steeples, D. (2001). Engineering and environmental geophysics at the millennium. Geophysics. Pp 31-35.

Telford, W. M., Geldart, L. P. and Sheriff, R. E. (1990). *Applied Geophysics*. Cambridge University Press.

Tokarski, A. (1972). Heterogeneous terrace arrangement west of A.B.U. occasional paper No.2. Department of Geology, A.B.U., Zaria.

Truswell, J. F. and Cope, R. N. (1963). The geology of parts of Niger and Zaria Provinces, Northern Nigeria. Geological Survey, Nigeria. Bull. 29.

Udias, A. (1999). Principles of seismology: Cambridge University Press.

Watabe, Y. and Sassa, S. (2008). Application of MASW technology to identification of tidal flat stratigraphy and its geoenvironmental interpretation. Marine Geology. www.elsevier.com/locate/margeo.

Wright, J. B. and McCurry, P. (1970). The geology of Nigeria sheet 102 SW, Zaria and its regions. Edited by M.J. Mortimore. Department of Geography, occasional paper, No. 4, Ahmadu Bello University, Zaria.

Xia, J. (1986). Some problems in the interpretation of two-dimensional magnetic anomalies by nonlinear programming: Symposium of Geophysics and Geochem. Prosp., 174–187 (in Chinese).

Xia, J., Miller, R. D. and Park, C. B. (1999). Estimation of near-surface shear-wave velocity by inversion of Rayleigh waves. Geophysics, vol. 64, No. 3 p691-700.

Xia, J., Miller, R. D., Park, C. B. and Ivanov, J. (2000). Construction of 2-D vertical shear-wave velocity field by the Multi-channel analysis of surface waves technique. Proceeding of the Symposium of the Application of Geophysics to Engineering Environmental Problems (SAGEEP 2000) Arlington, VA., February 20-24, 1197-1206.

Xia, J., Miller, R. D., Park, C. B., Hunter, J. A., Harris, J. B. and Ivanov, J. (2002). Comparing shear-wave velocity profiles from Multi-channel analysis of surface wave with borehole measurements. Soil Dynamics and Earthquake Engineering, 22 (3), 181-190.

Xia, J., Miller, R. D., Park, C. B. and Tian, G. (2003). Inversion of high-frequency surface waves with fundamental and higher modes. *Journal of Applied Geophysics*, 52, 45-57.

Xia, J., Miller, R. D., Park, C. B. and Tian, G. (2004). Utilization of high-frequency Rayleigh waves in near-surface geophysics: The Leading Edge, 23, 753-759, http://dx.doi.org/10/1190/1.1786895.

Xia, J., Xu, Y., Miller, R. D., Cakir, R., and Zeng, C. (2012). Advantages of using Multi-channel analysis of love waves (MALW) to estimate near-surface shear-wave velocity: Survey in Geophysics, 33, 841-860. Springer.

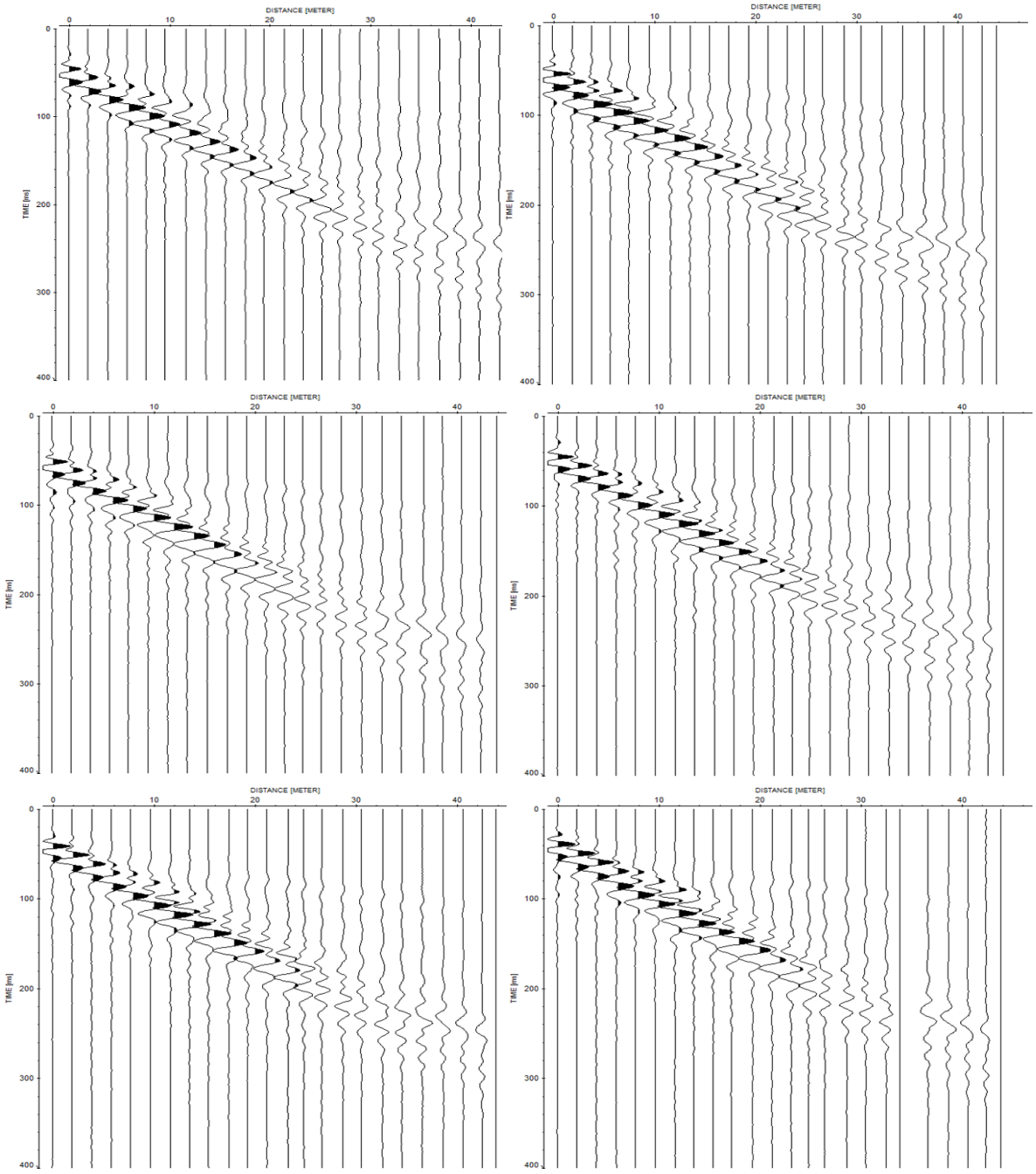
Yilmaz, O. (2001). Seismic data analysis: Processing, inversion, and interpretation of seismic data: SEG Investigations in Geophysics No. 10, http://dx.doi.org/10.1190/1.97815 60801580.

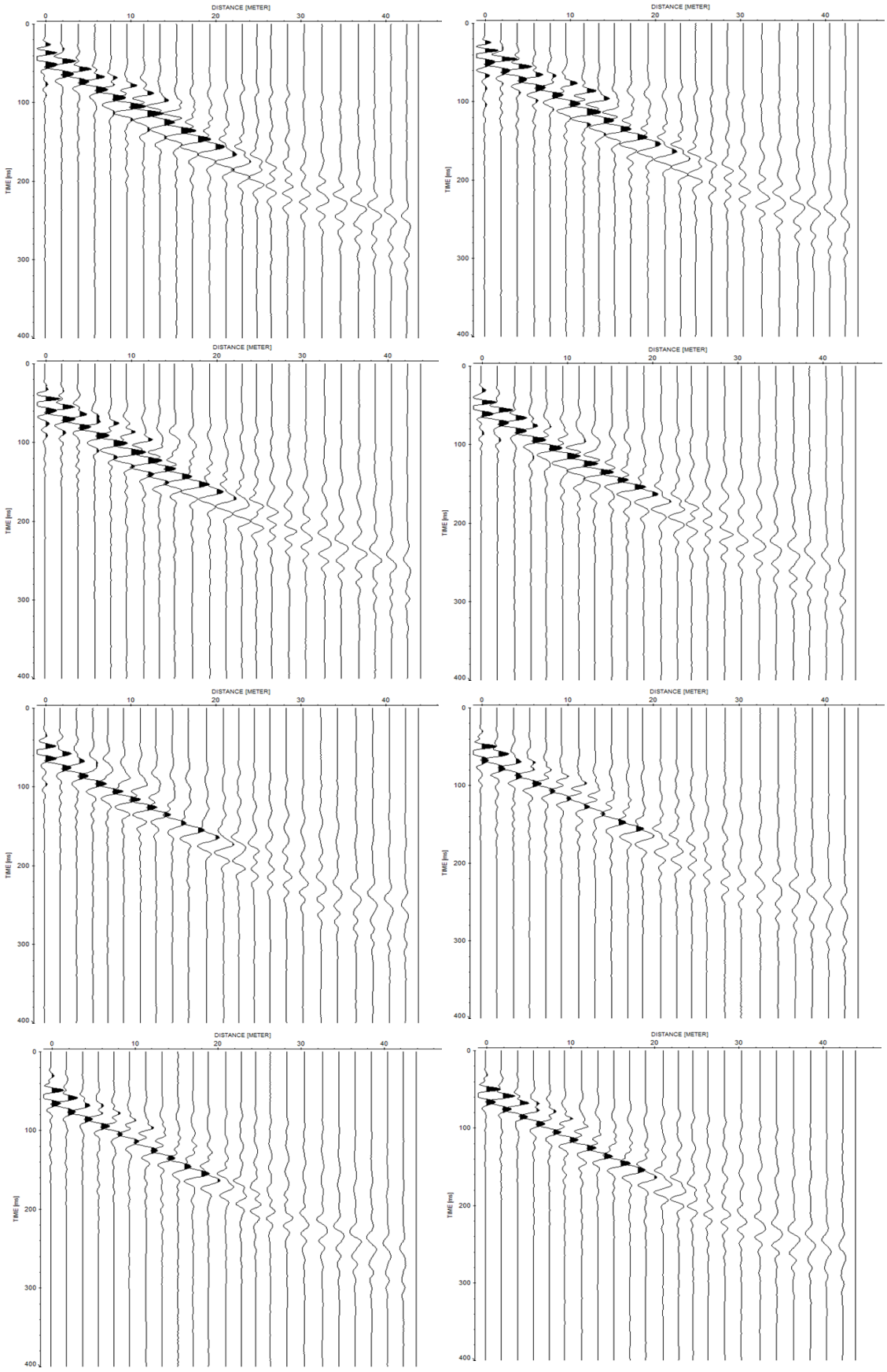
Yilmaz, O. (2015). Engineering Seismology with Applications to Geotechnical Engineering. Society of Exploration Geophysicists. *The international society of applied geophysics*. Tulsa, Oklahoma, U.S.A. Investigation in Geophysics Series No. 17.

APPENDIX I

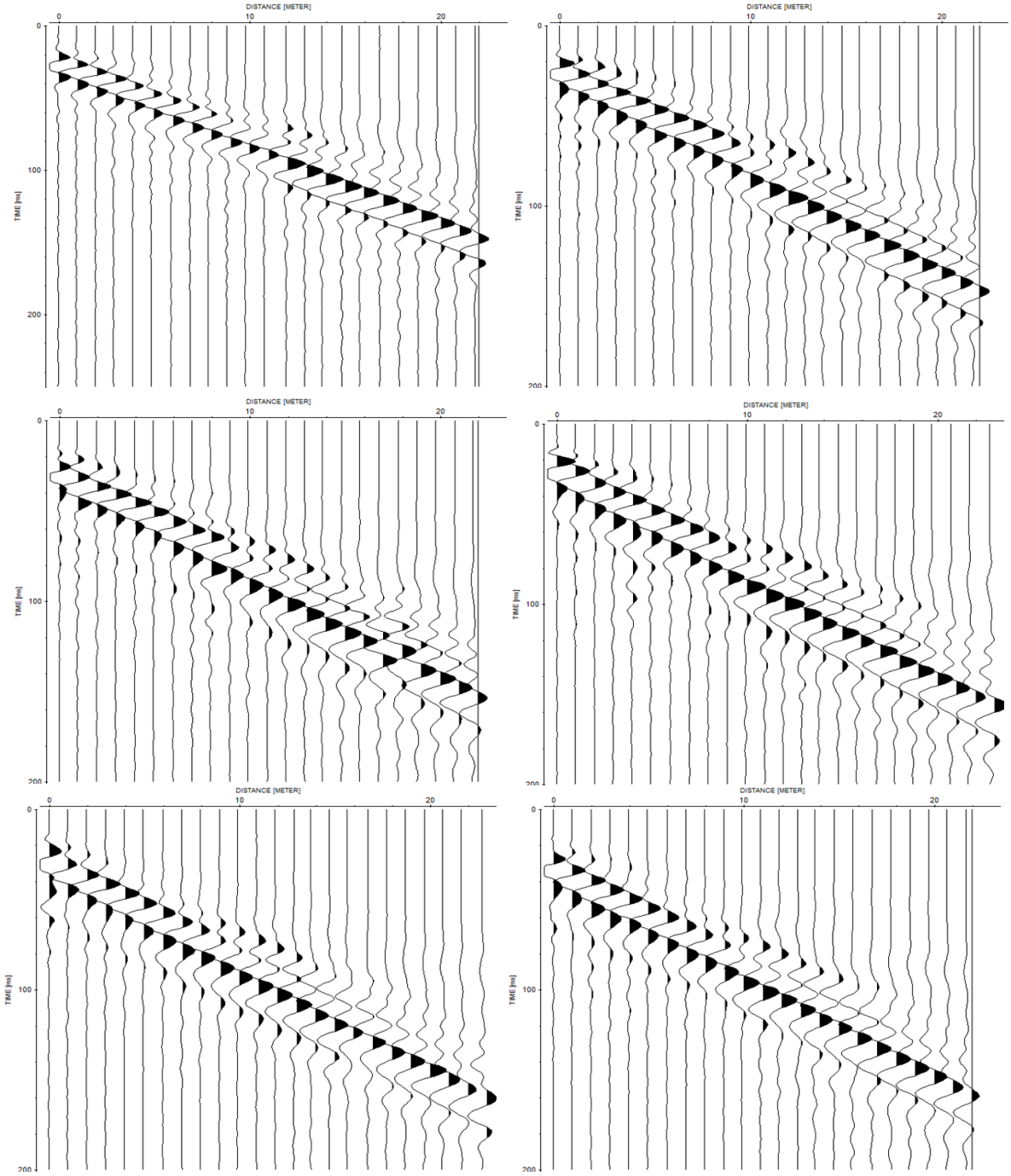
SHOT GATHER

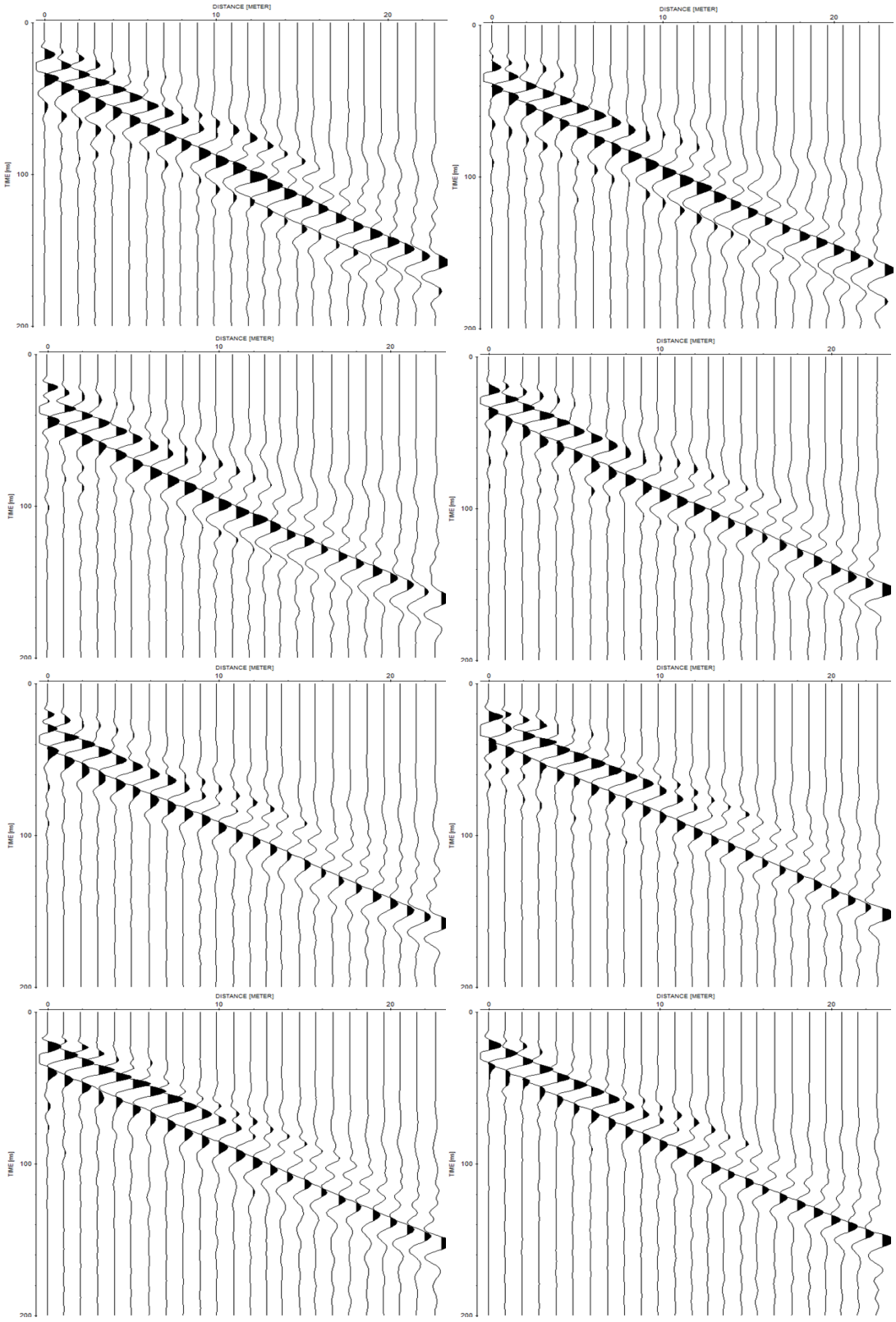
Profile 1 (A-A^1)



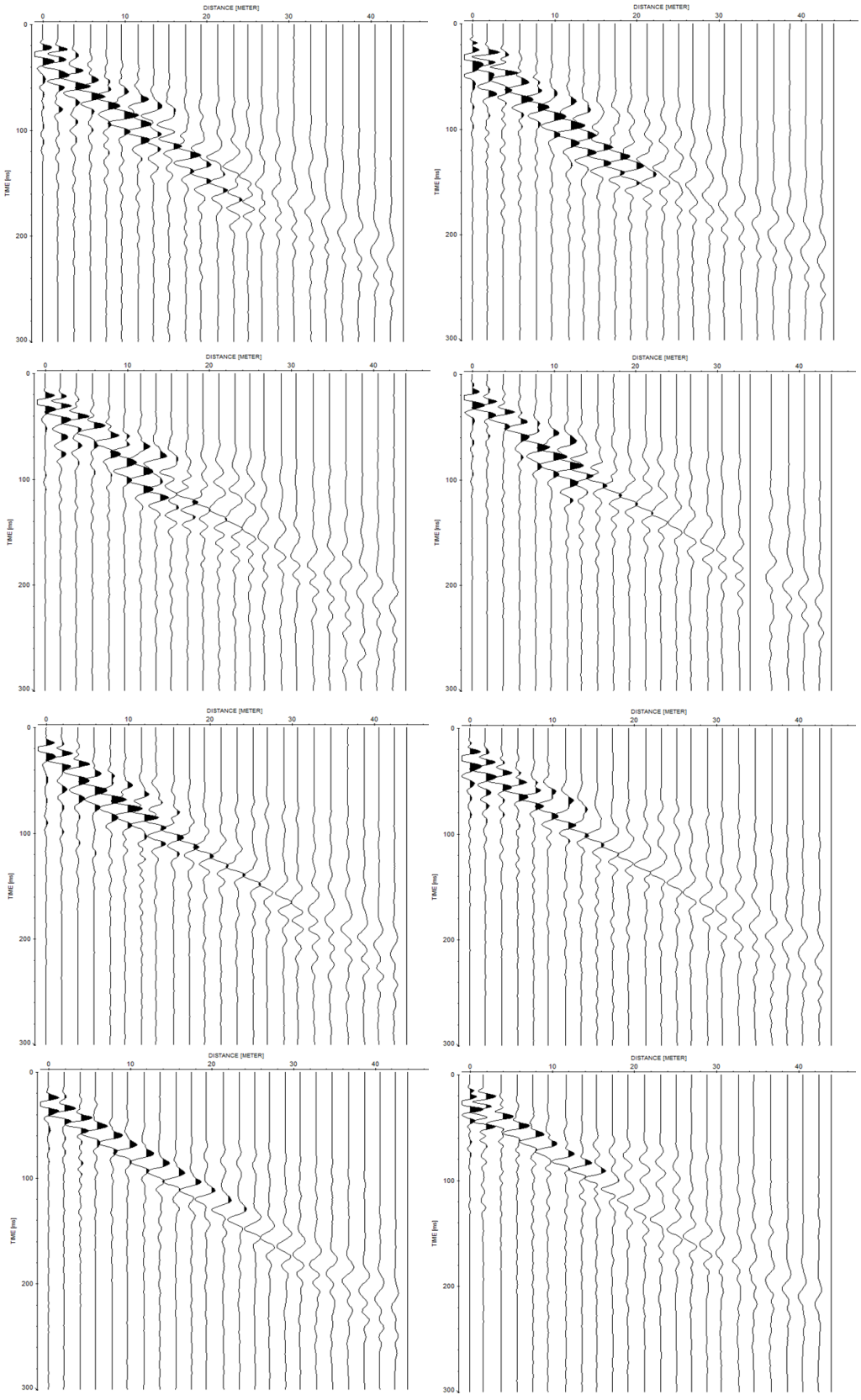

DISTANCE [METER]
0
10
20
30
40
TIME [ms]
0
100
200
300
400

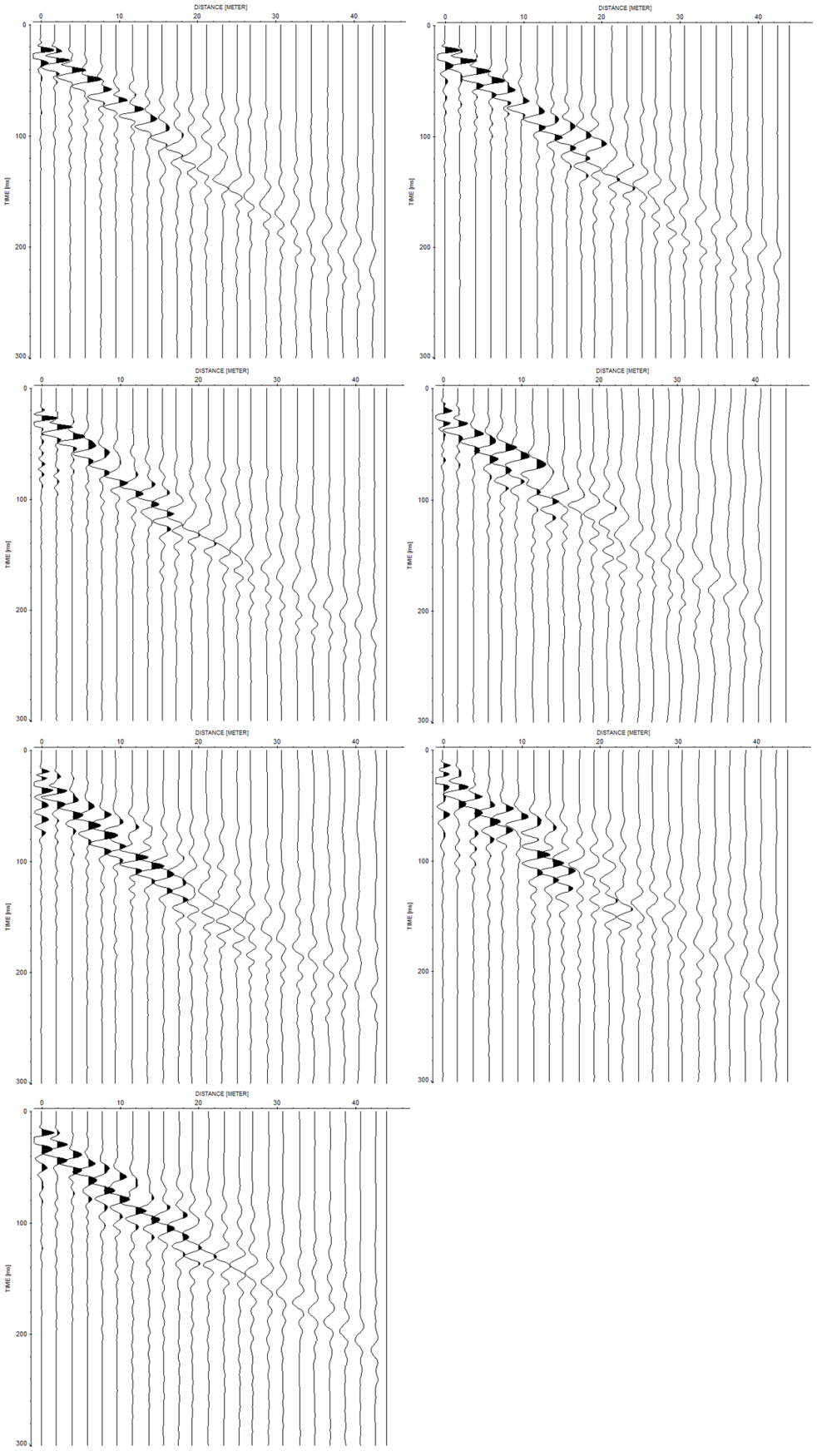
Profile 2 (B-B^1)



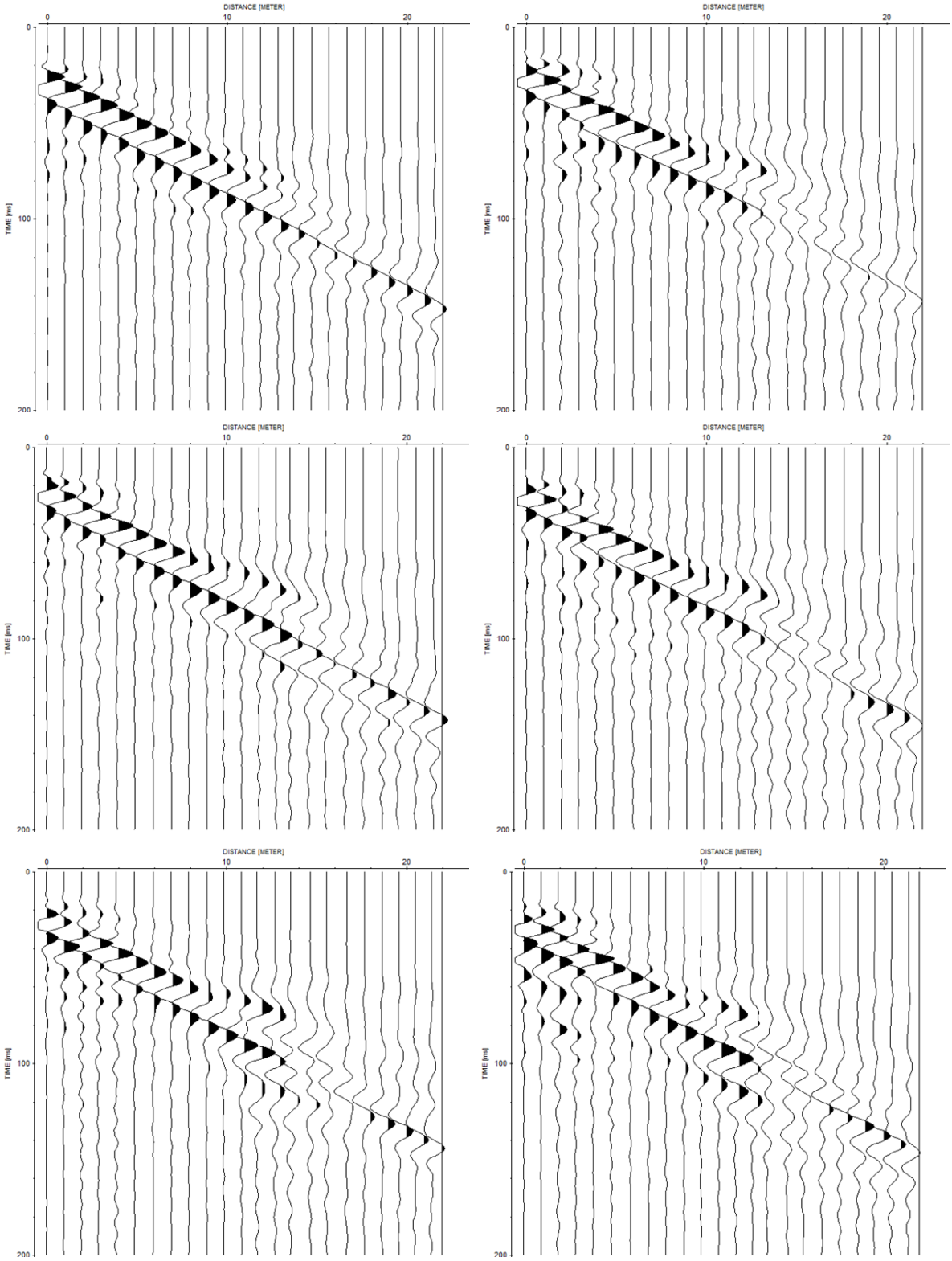

DISTANCE [METER]
0
10
20
TIME [ms]
0
100
200

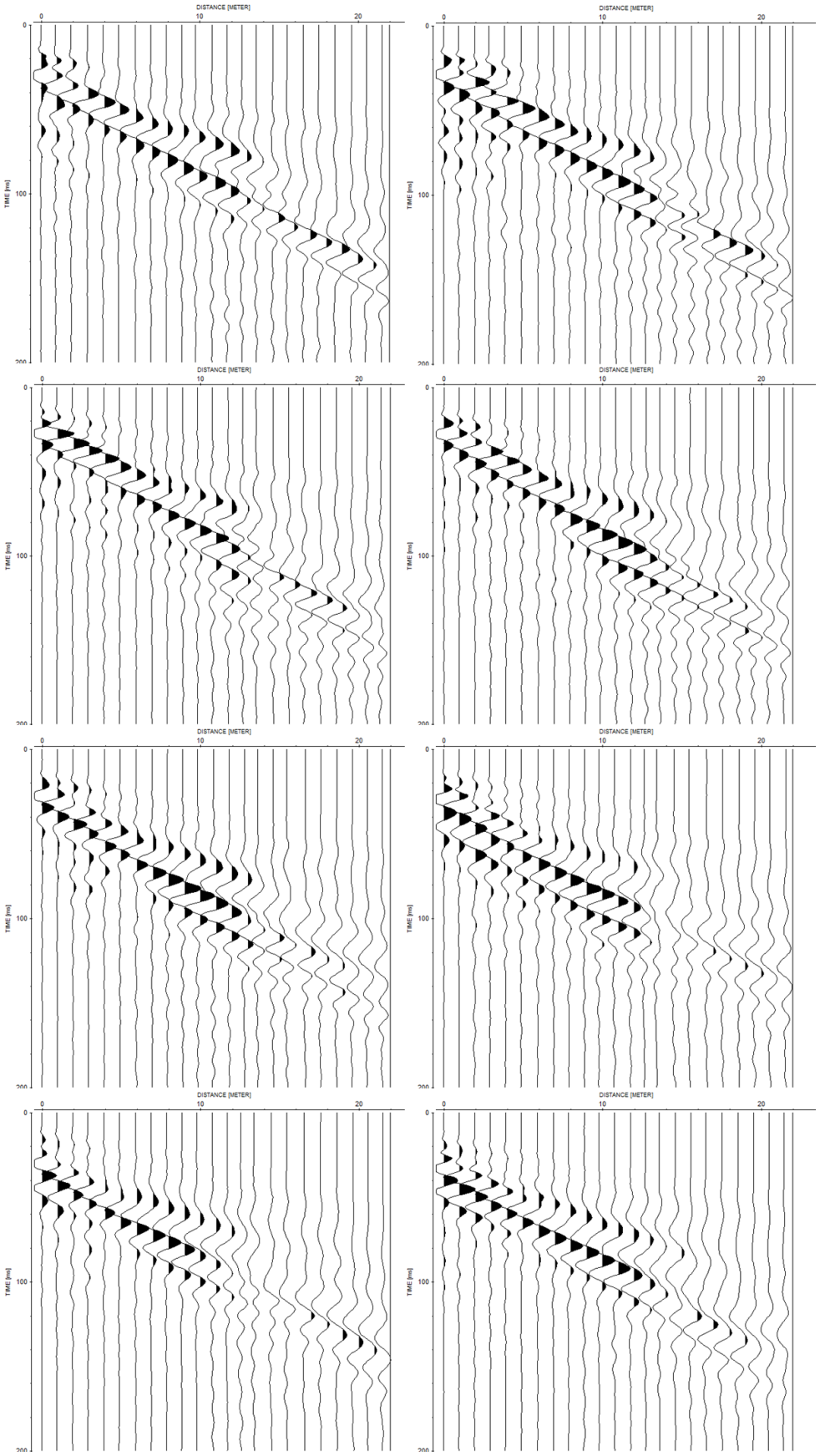
Profile 3 (C-C[1])

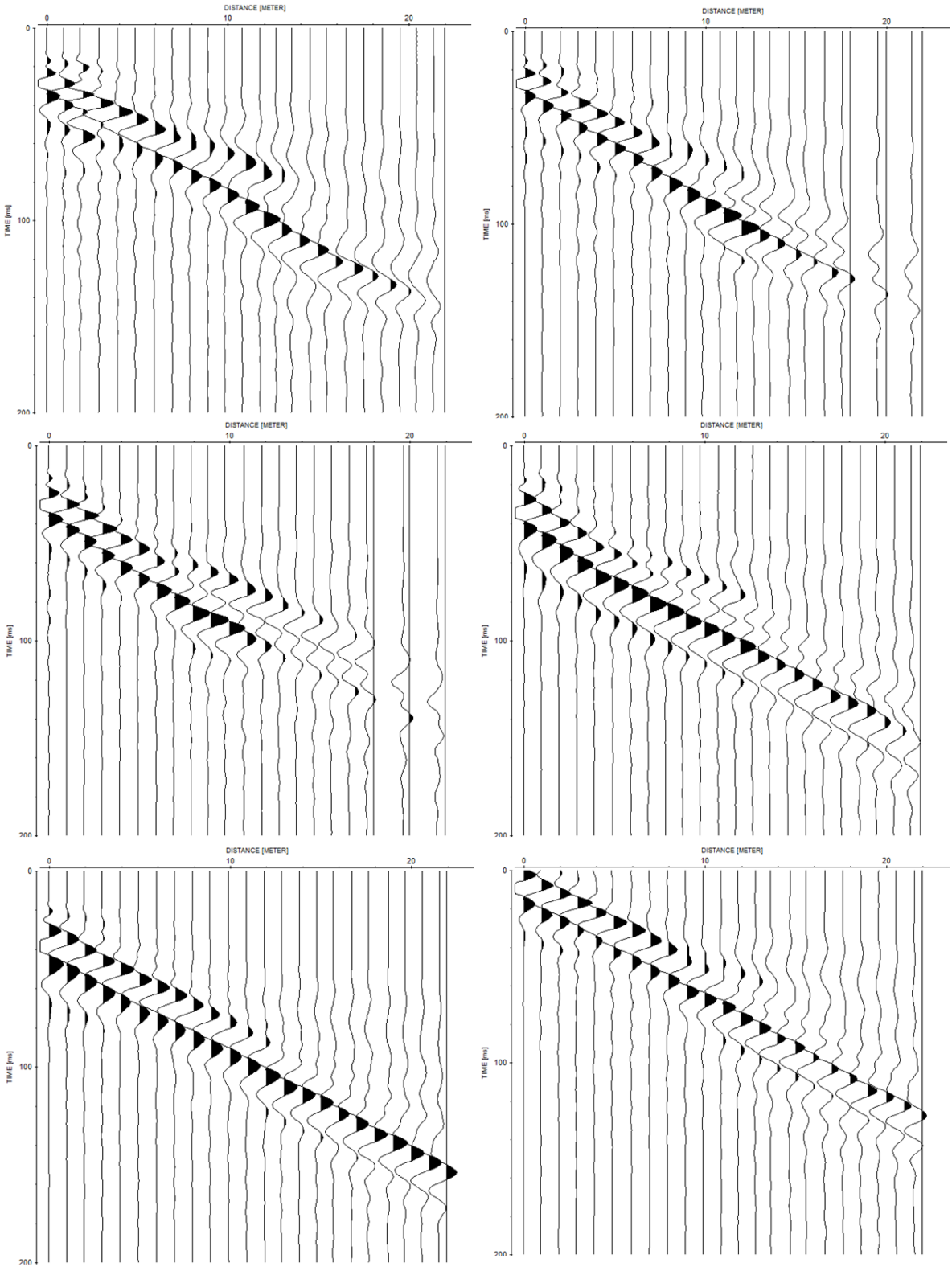



DISTANCE [METER]
0
10
20
30
40
TIME [ms]
0
100
200
300

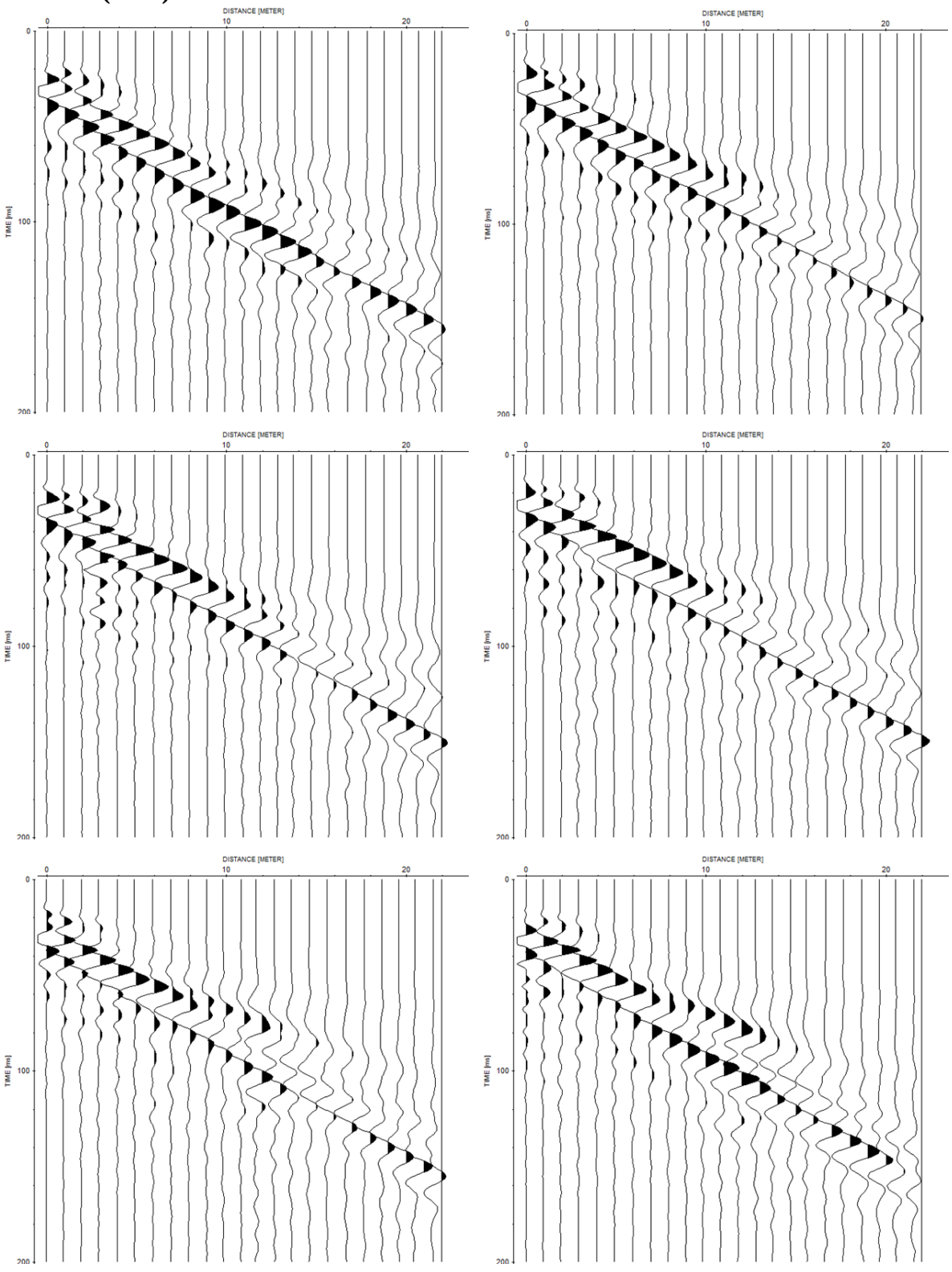
Profile 4 (D-D[1])

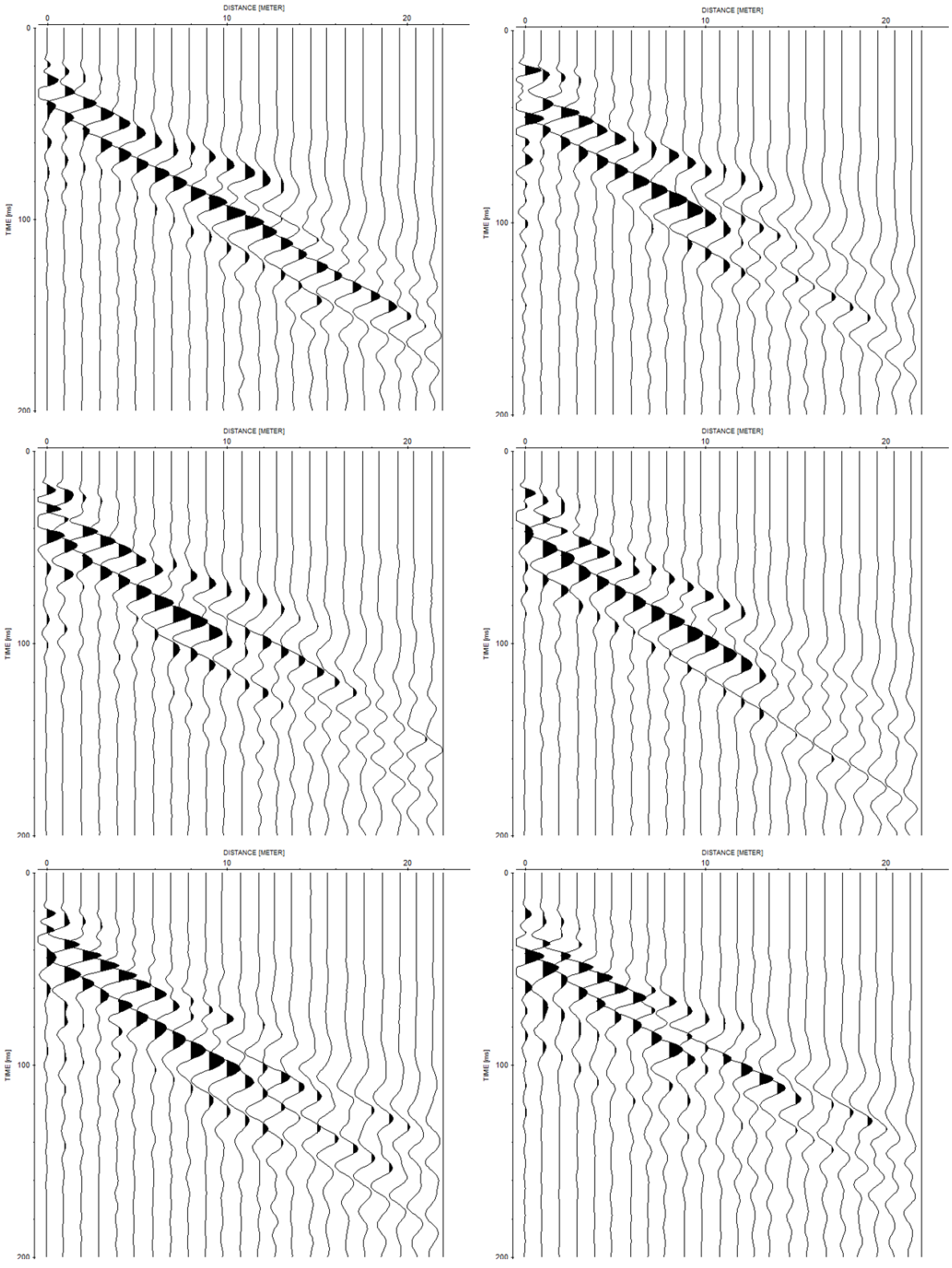


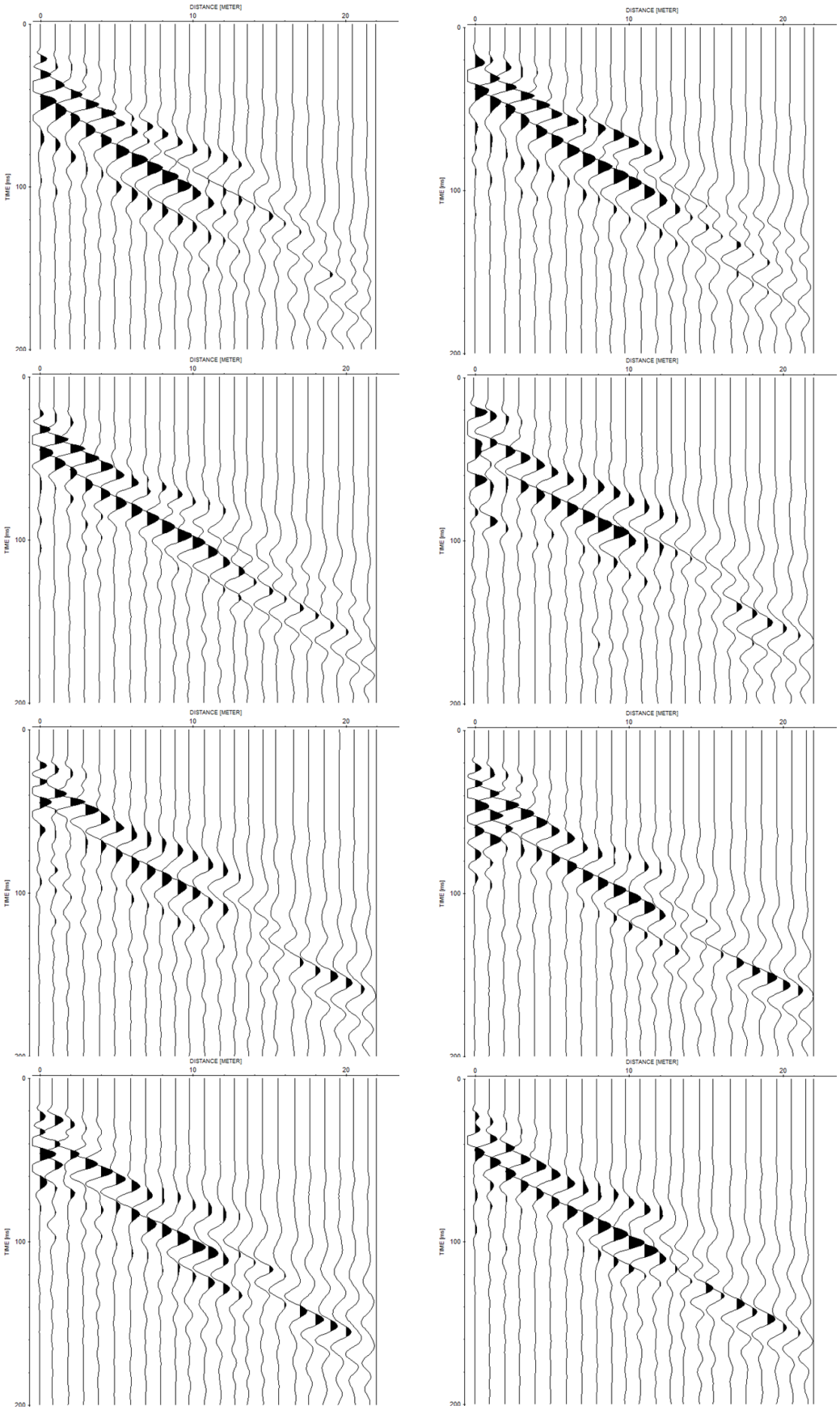

DISTANCE [METER]
0
10
20
TIME [ms]
0
100
200


DISTANCE [METER]
0
10
20
TIME [ms]
0
100
200

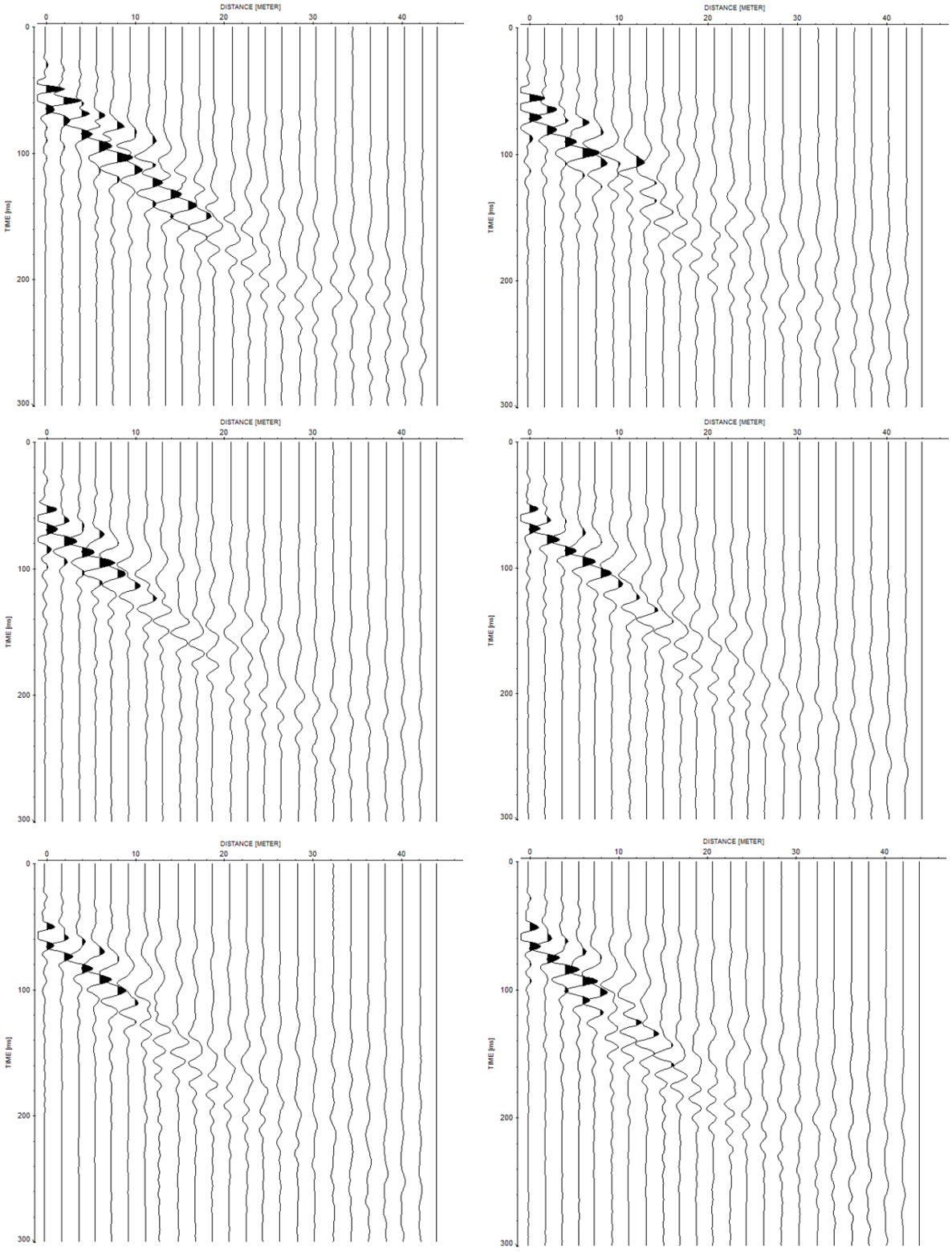
Profile 5 (E-E[1])

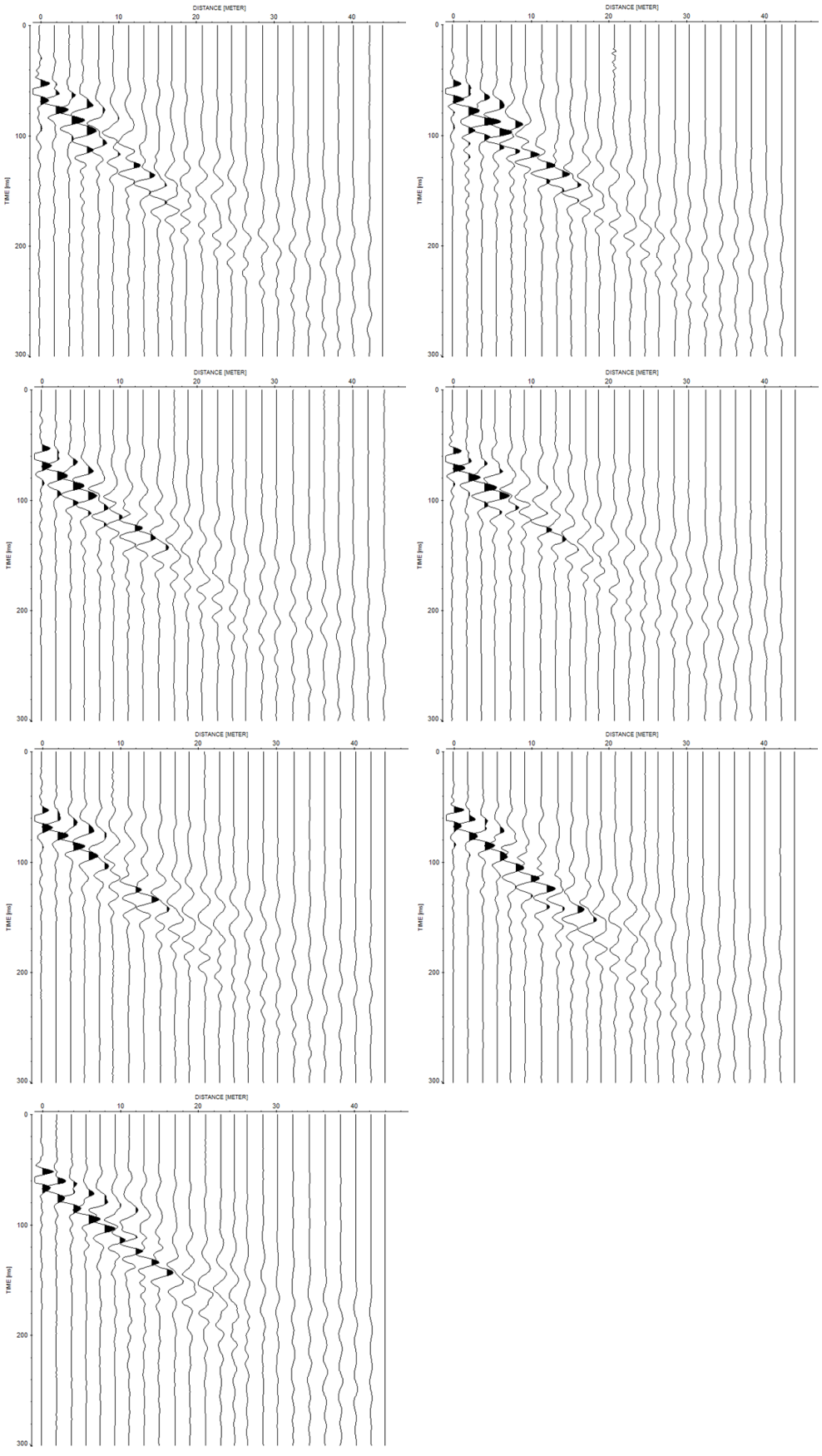



DISTANCE [METER]
0
10
20
TIME [ms]
0
100
200

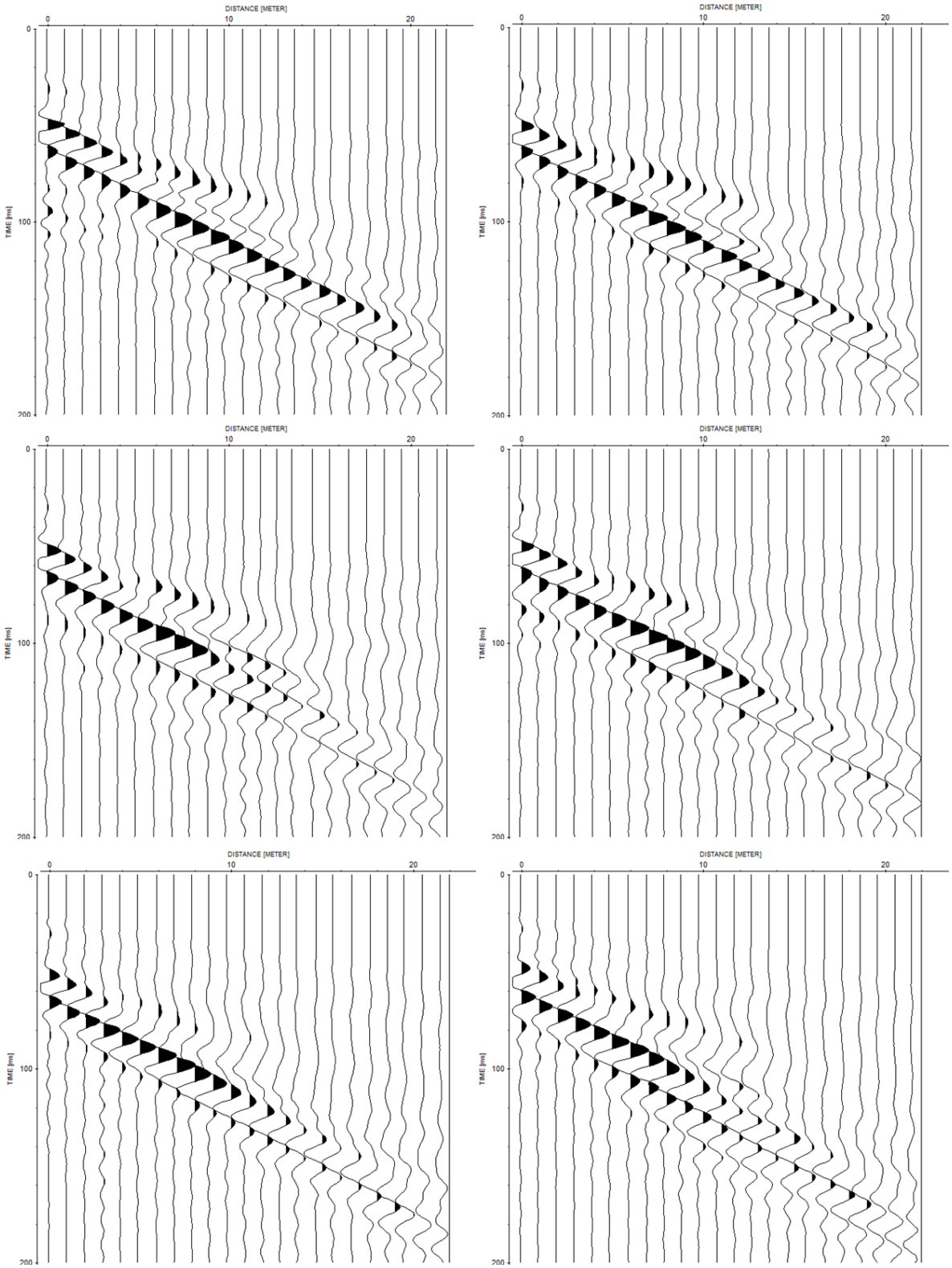

DISTANCE [METER]
0
10
20
TIME [ms]
0
100
200

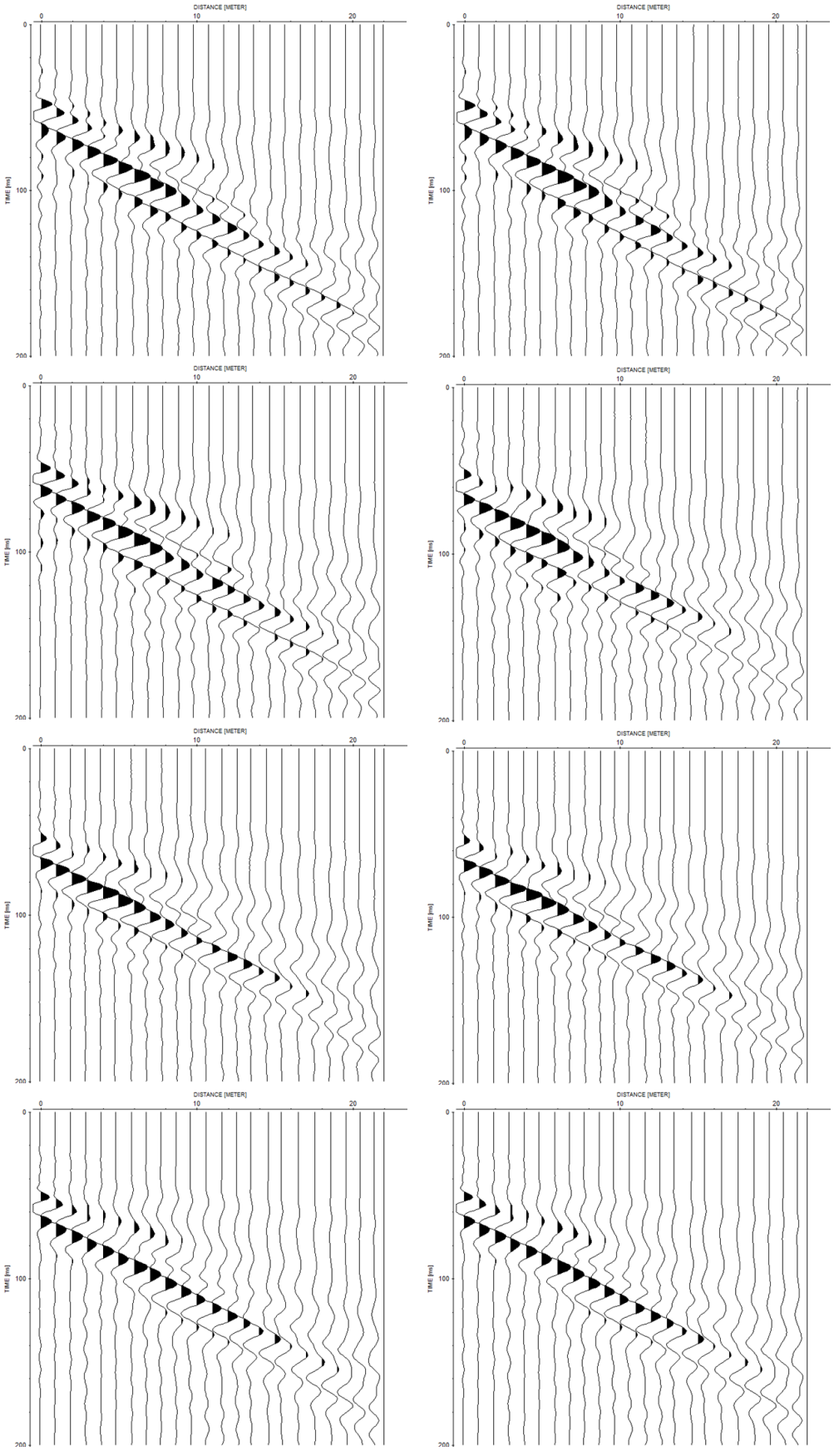
Profile 6 (F-F[1])

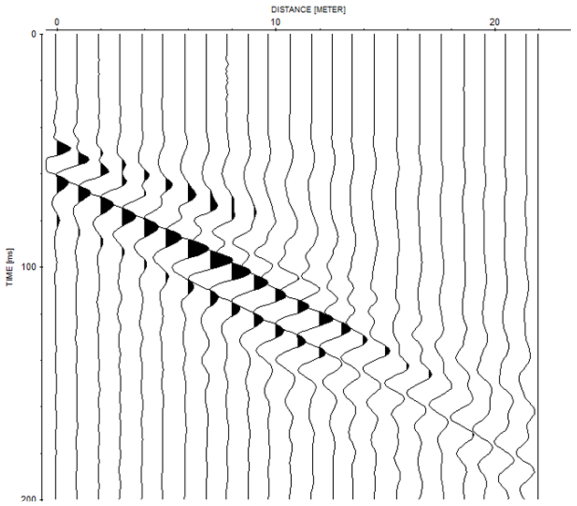


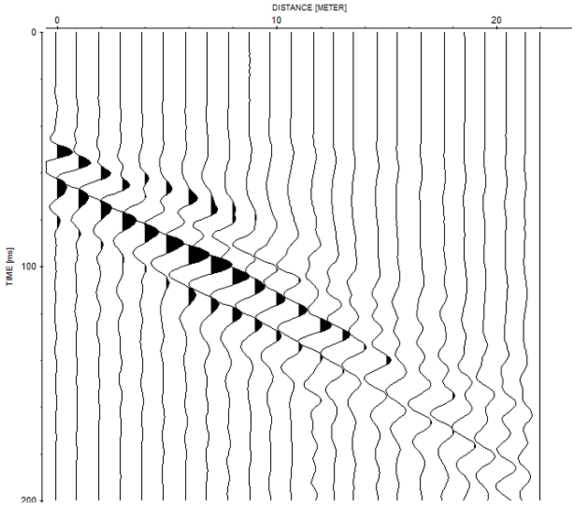

DISTANCE [METER]
0
10
20
30
40
TIME [ms]
0
100
200
300

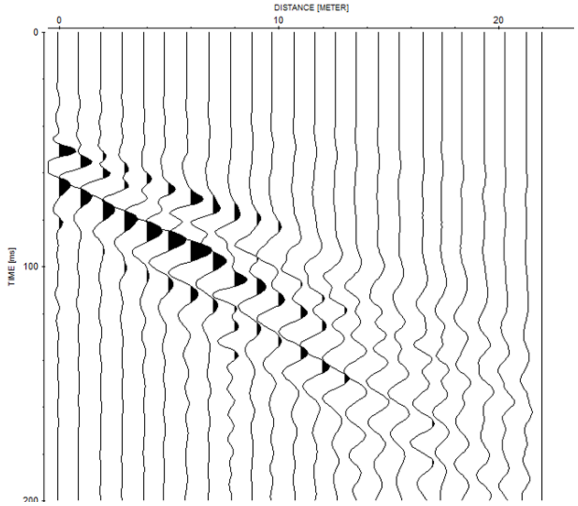
Profile 7 (G-G[1])

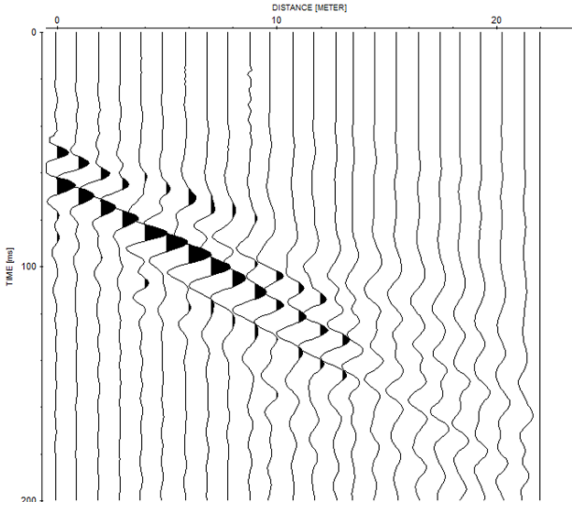


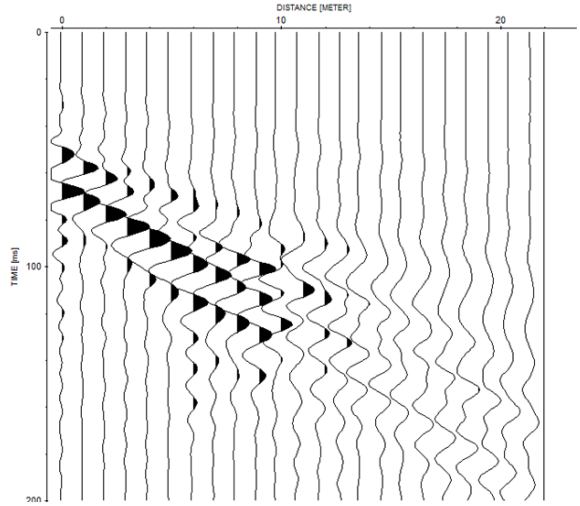

DISTANCE [METER]
0
10
20
TIME [ms]
0
100
200

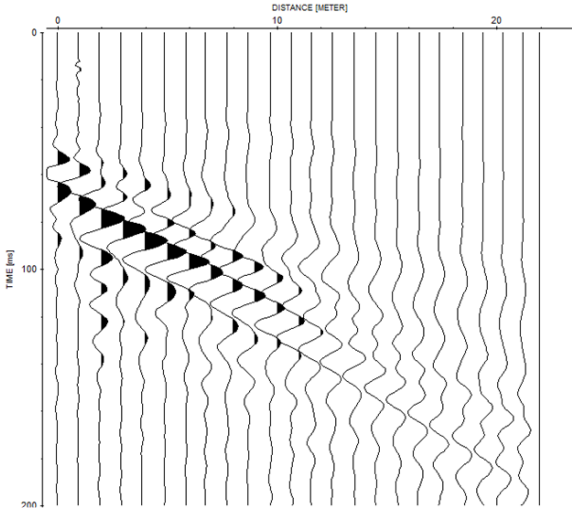

DISTANCE [METER]
0
10
20
TIME [ms]
0
100
200


DISTANCE [METER]
0
10
20
TIME [ms]
0
100
200


DISTANCE [METER]
0
10
20
TIME [ms]
0
100
200


DISTANCE [METER]
0
10
20
TIME [ms]
0
100
200

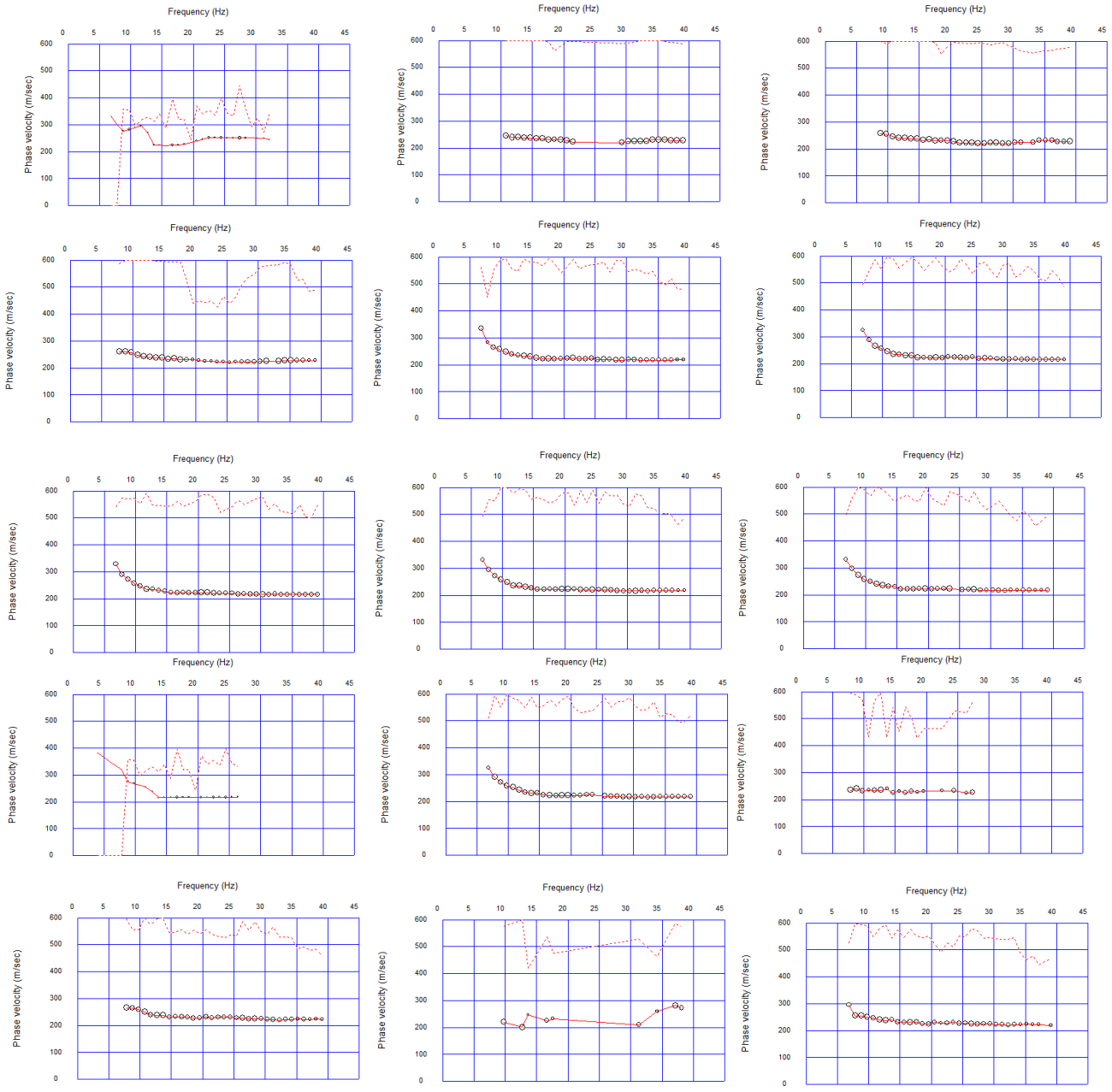

DISTANCE [METER]
0
10
20
TIME [ms]
0
100
200


DISTANCE [METER]
0
10
20
TIME [ms]
0
100
200

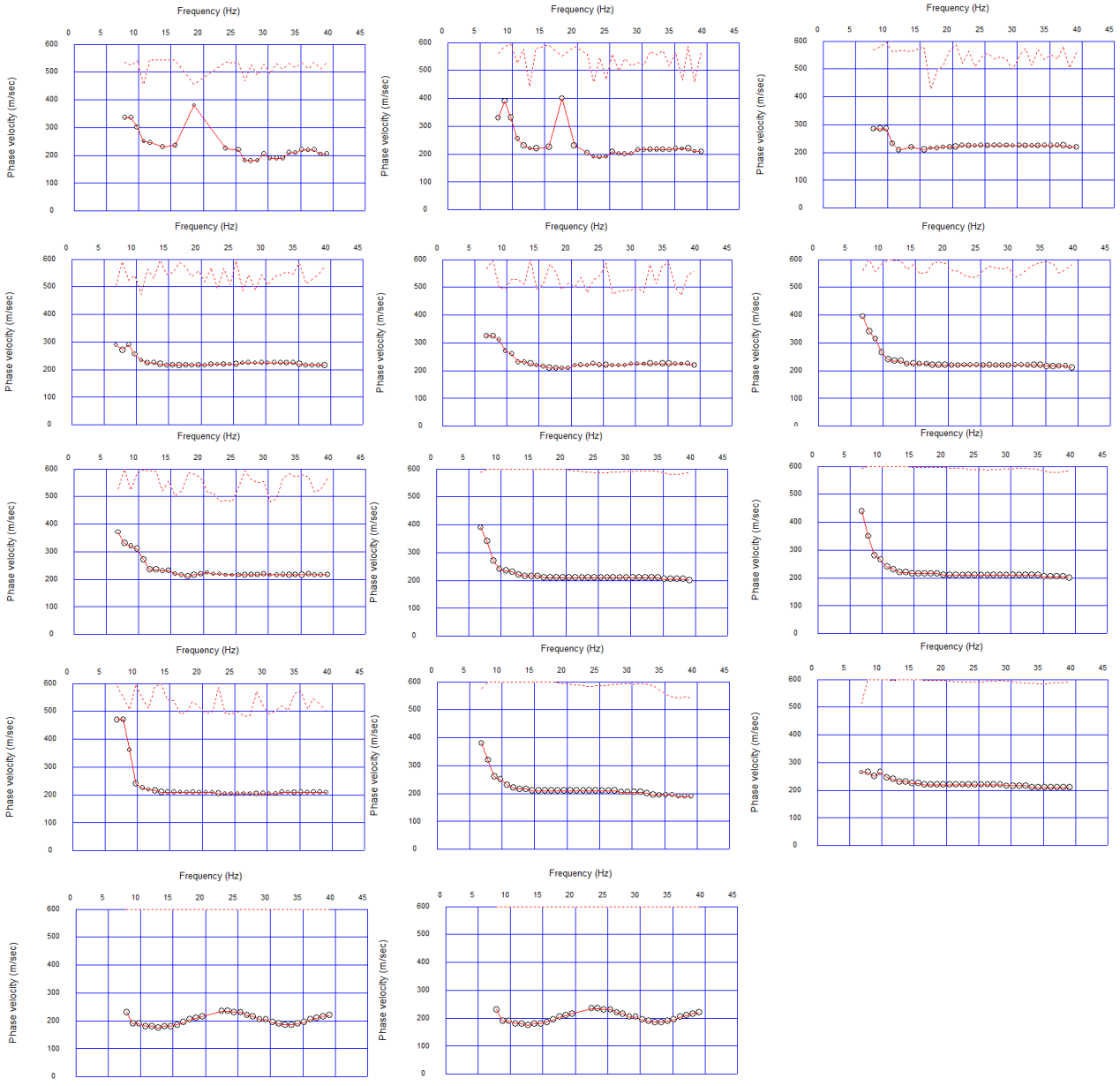
APPENDIX II

PICKED RAYLEIGH WAVE FUNDAMENTAL MODE (DISPERSION CURVE)

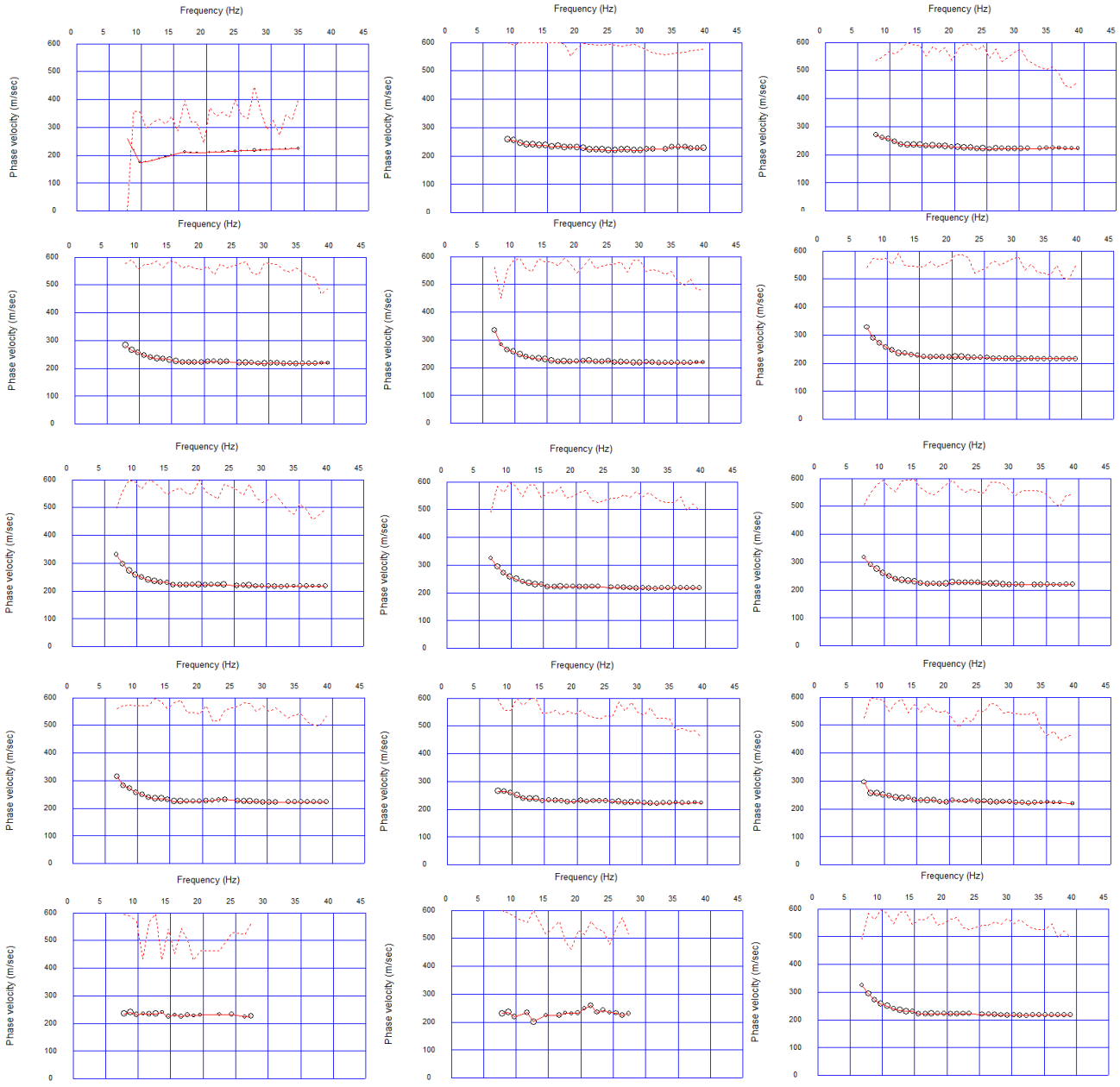
Profile 1 (A-A^1)



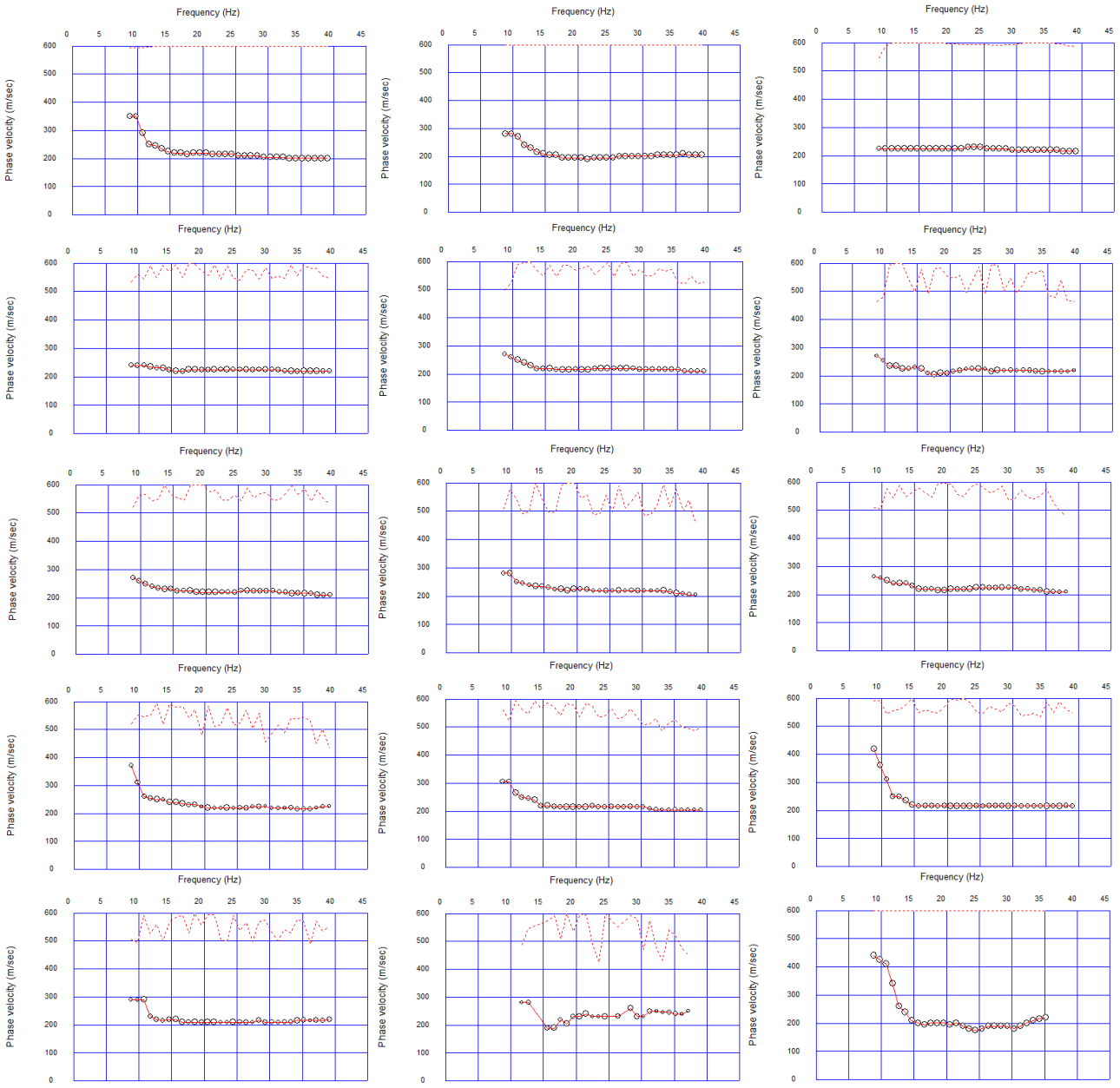
Profile 2 (B-B[1])



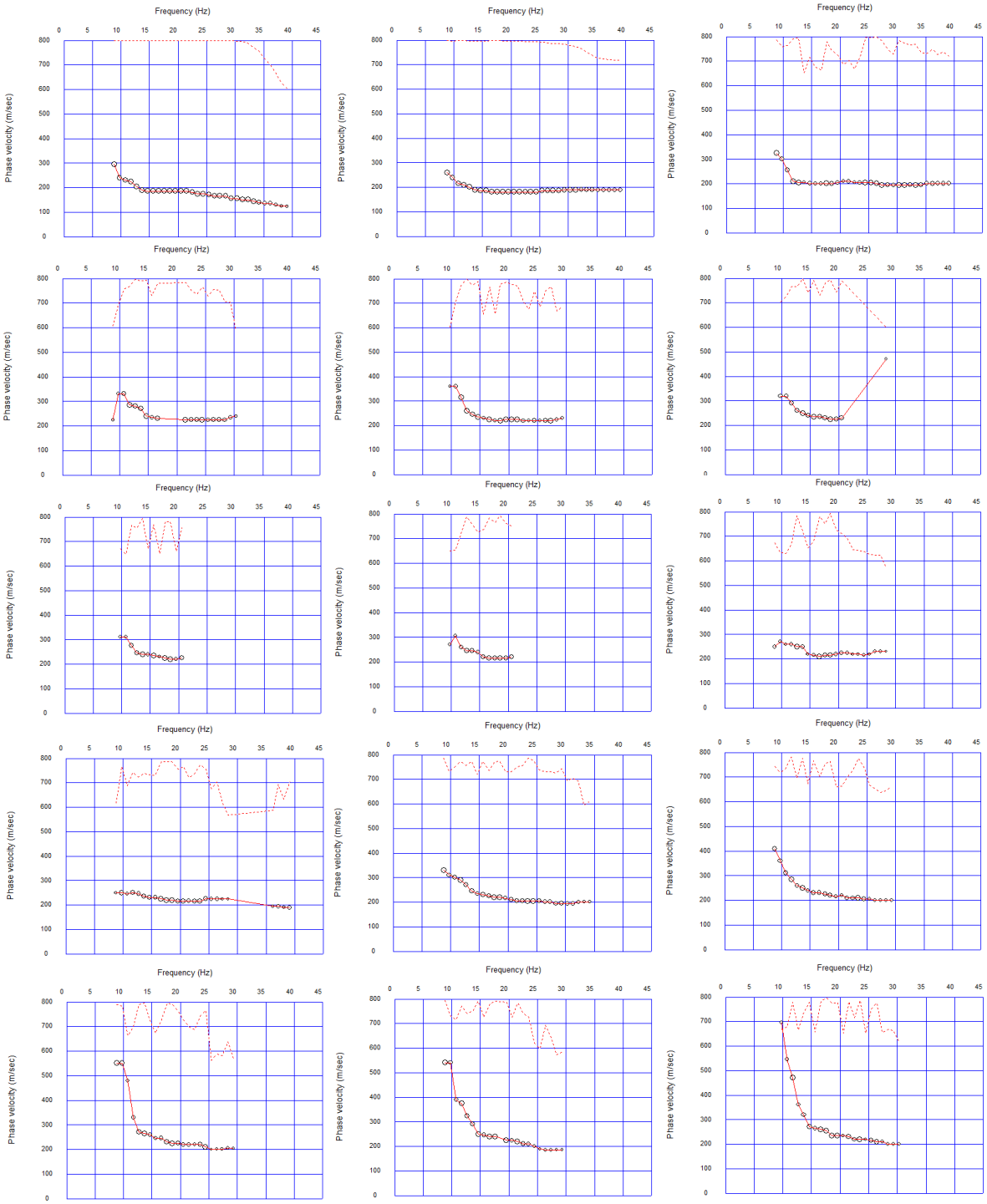
Profile 3 (C-C[1])

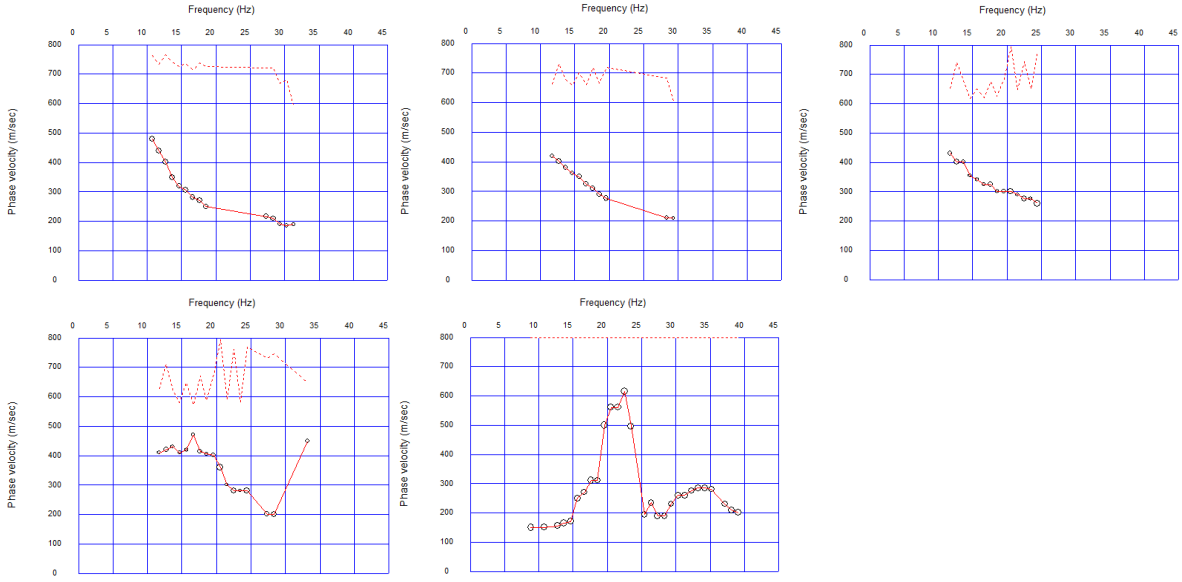


Profile 4 (D-D[1])

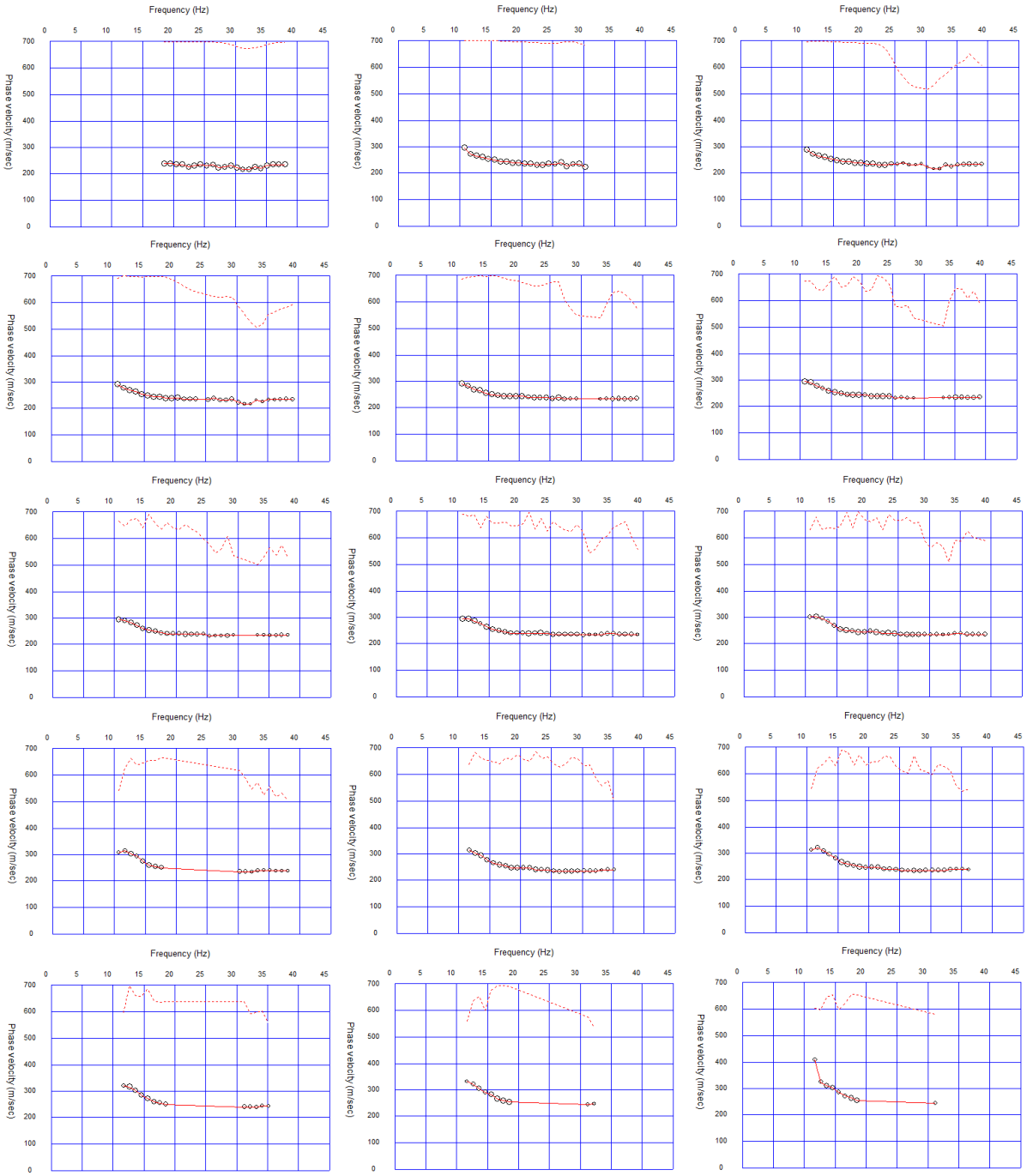


Profile 5 (E-E[1])

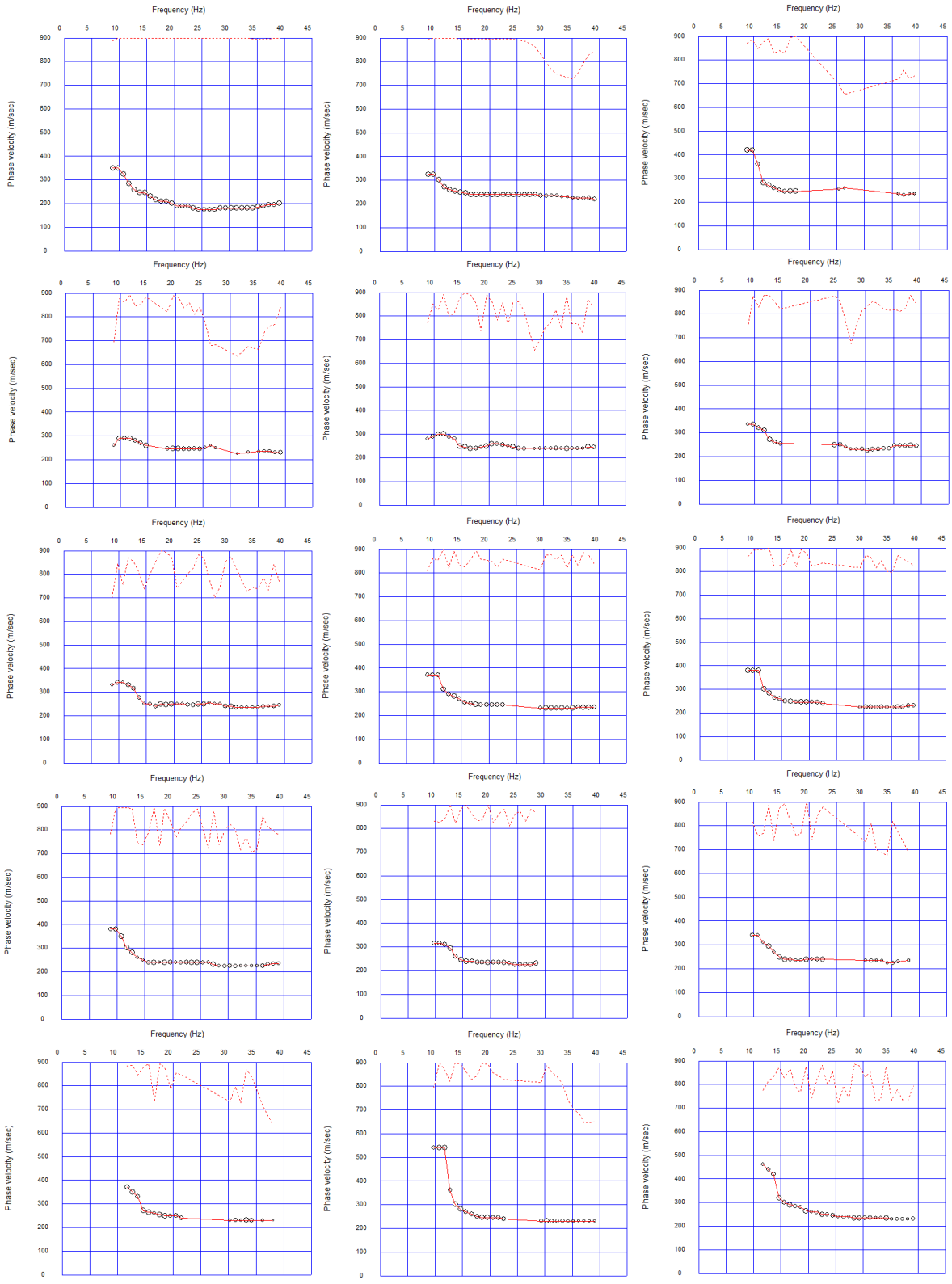


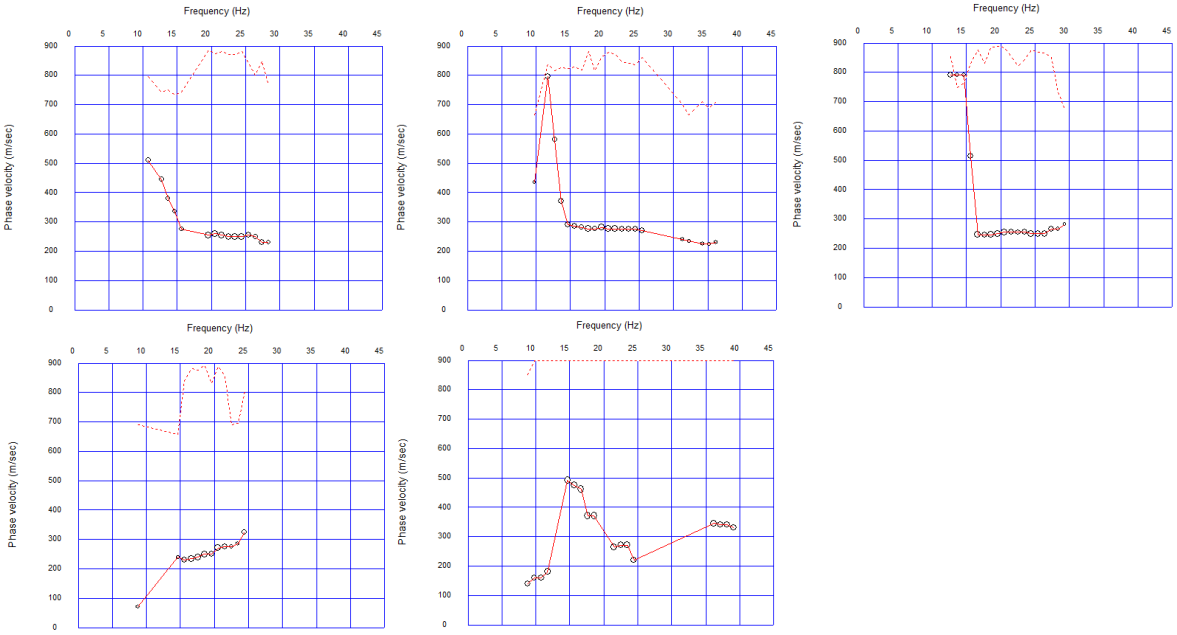

Frequency (Hz)
Phase velocity (m/sec)
0 5 10 15 20 25 30 35 40 45
0 100 200 300 400 500 600 700 800

Profile 6 (F-F[1])



Profile 7 (G-G[1])

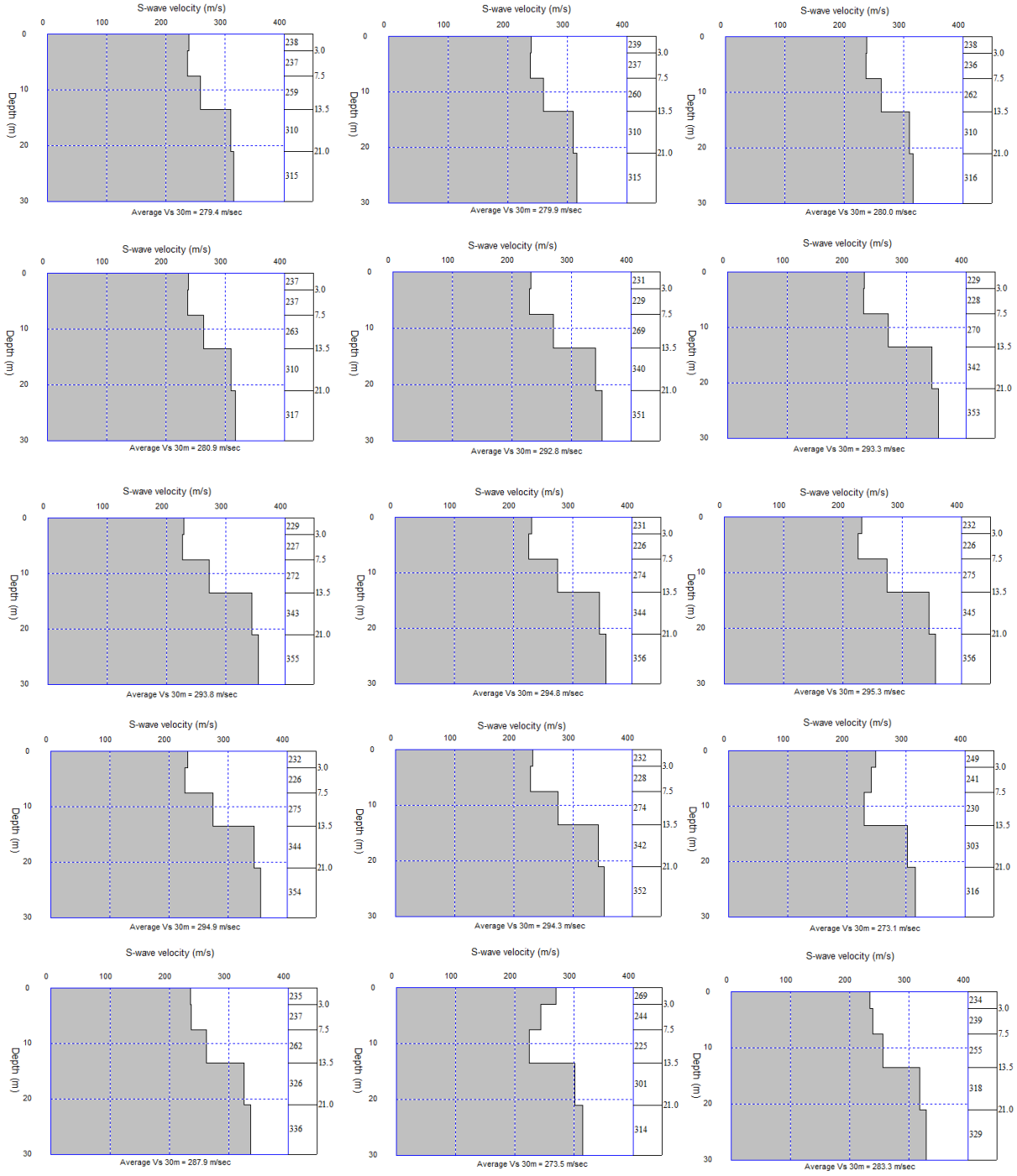



Frequency (Hz)
Phase velocity (m/sec)
0 5 10 15 20 25 30 35 40 45
0 100 200 300 400 500 600 700 800 900

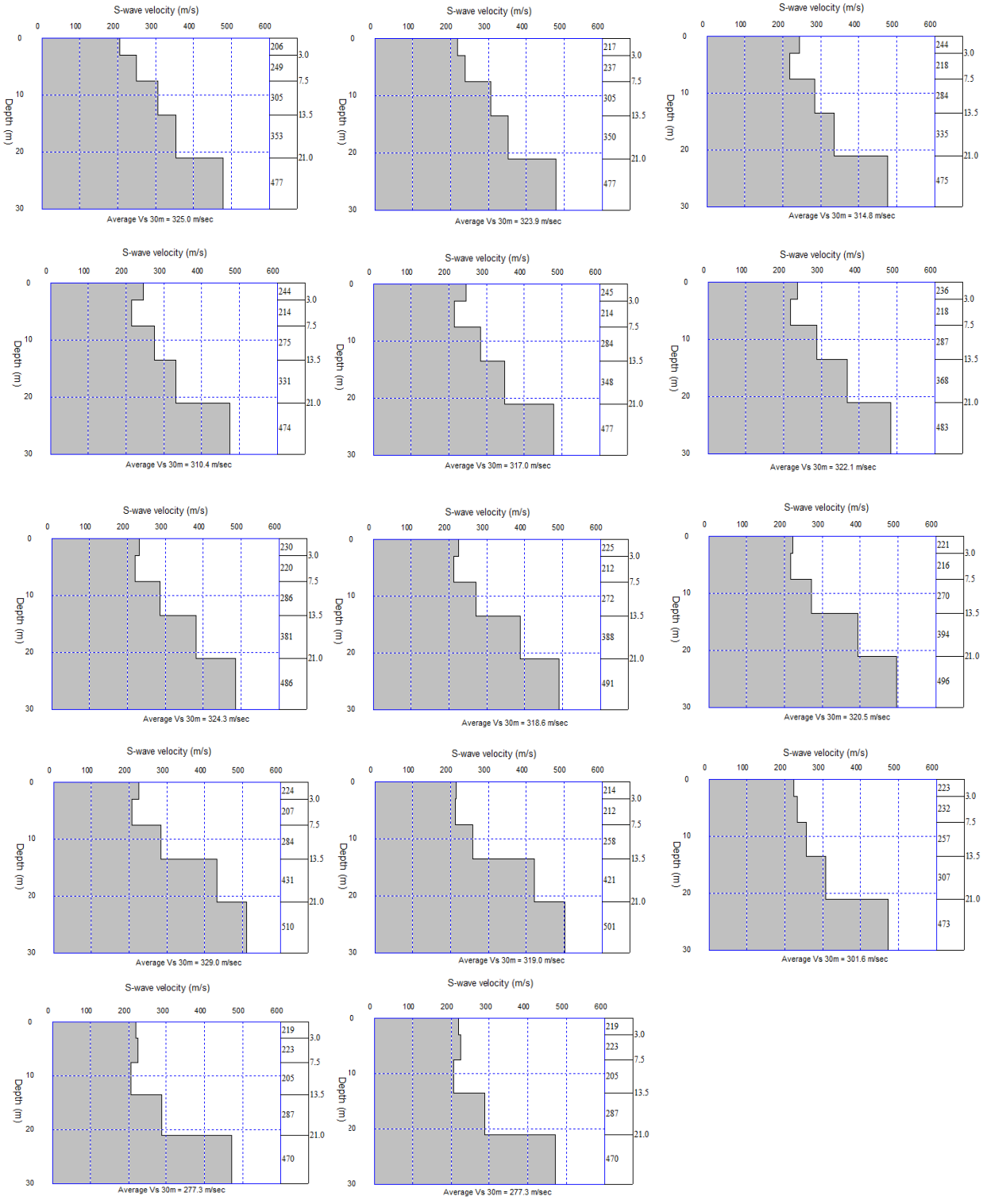
APPENDIX III

1-DIMENSIONAL SHEAR WAVE VELOCITY MODEL

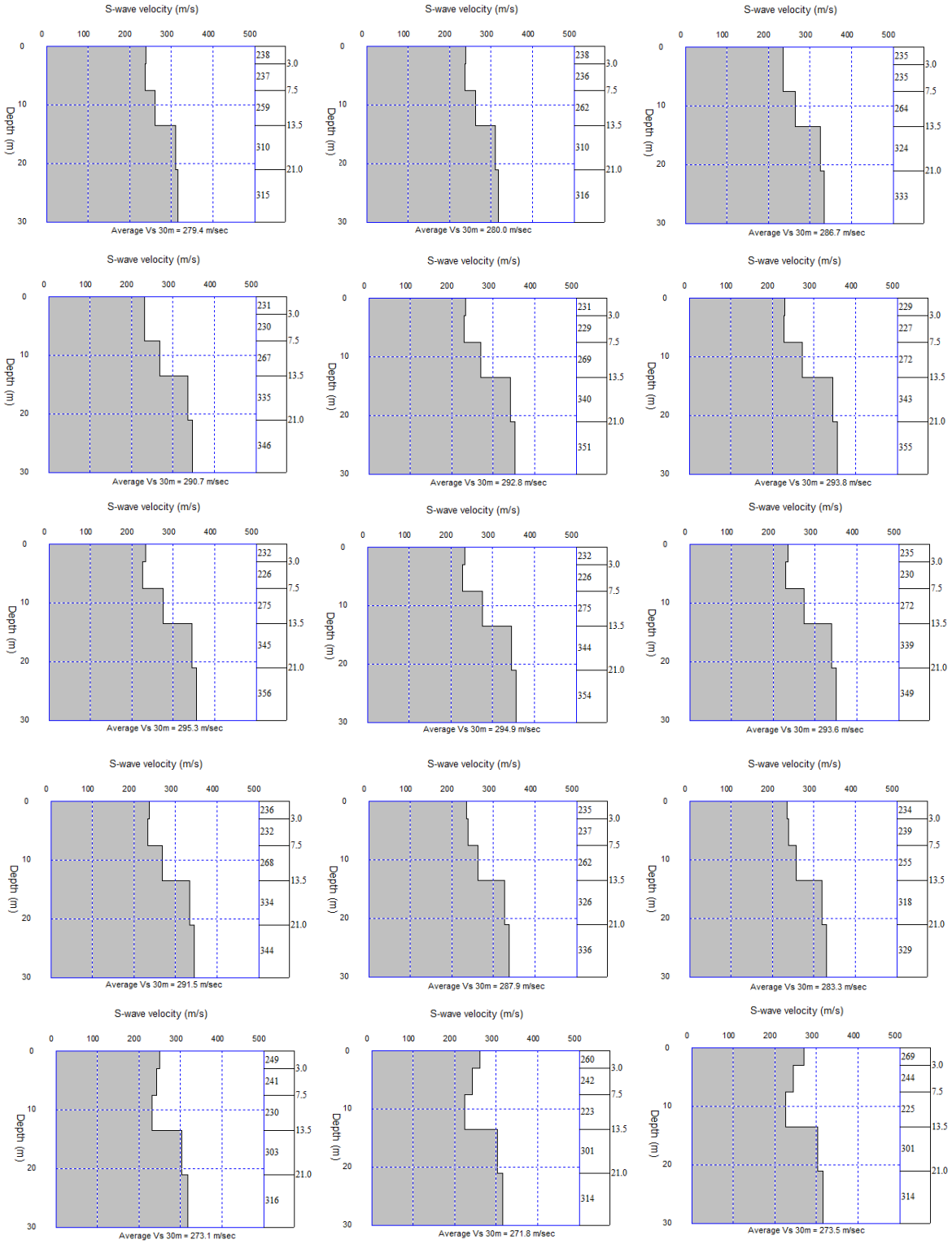
Profile 1 (A-A^1)



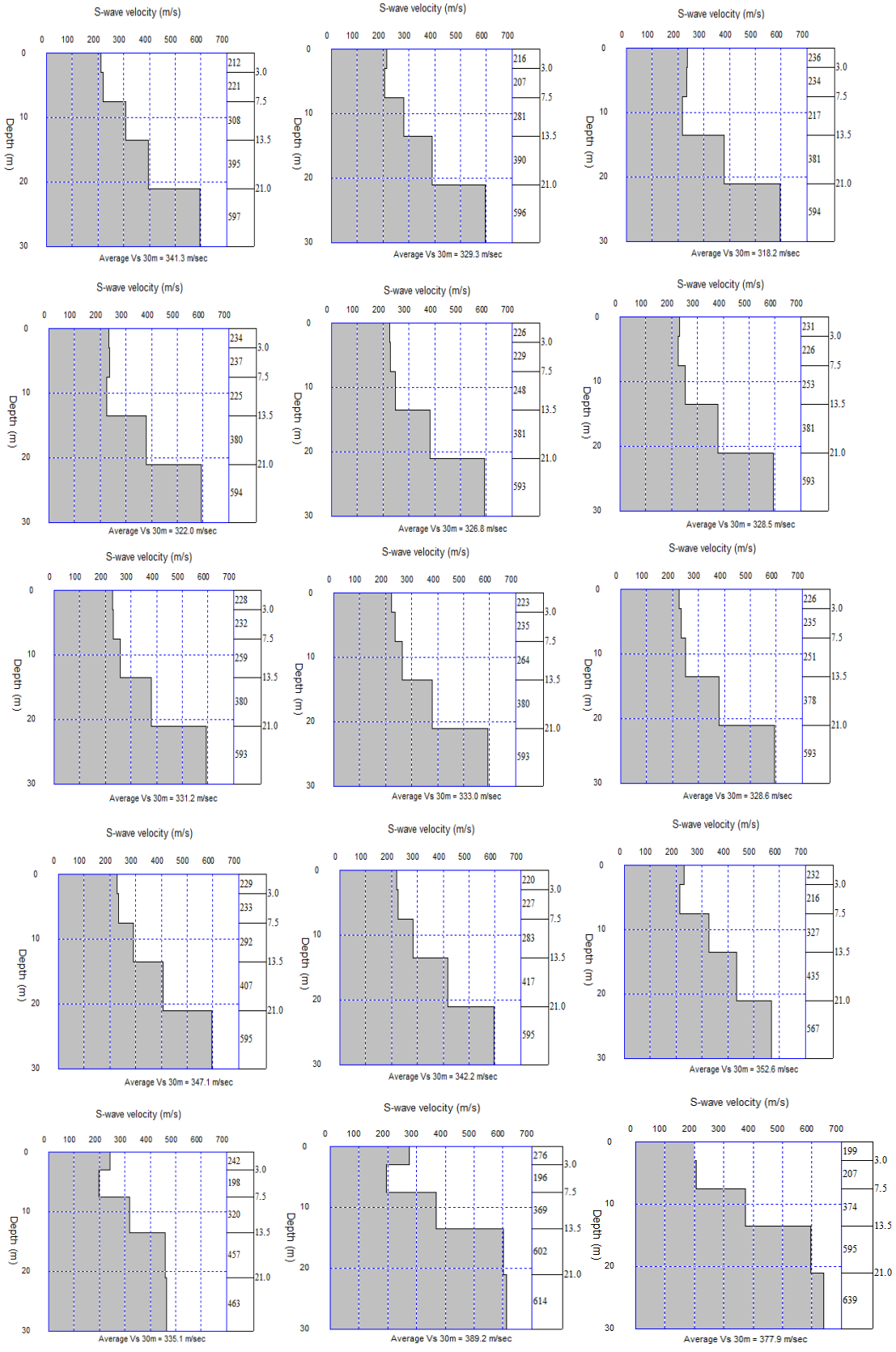
Profile 2 (B-B^1)



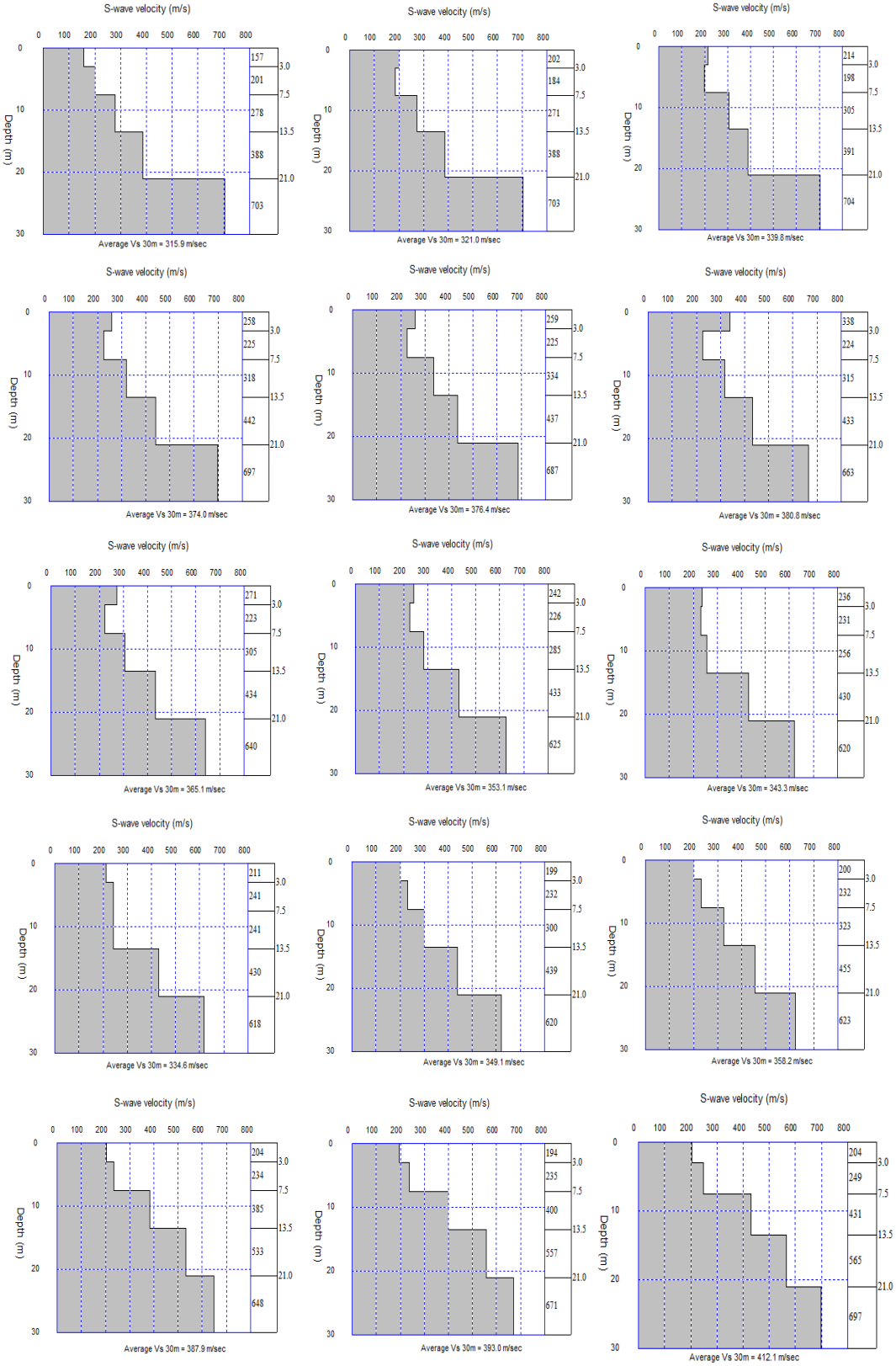
Profile 3 (C-C[1])

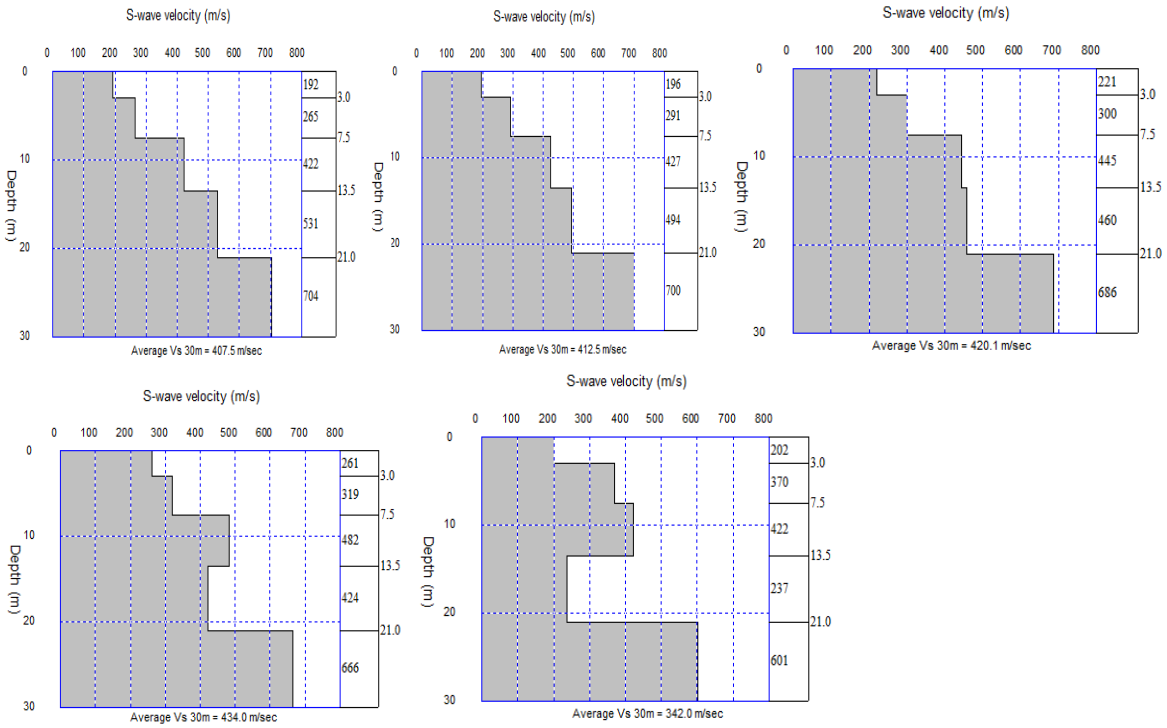


Profile 4 (D-D[1])

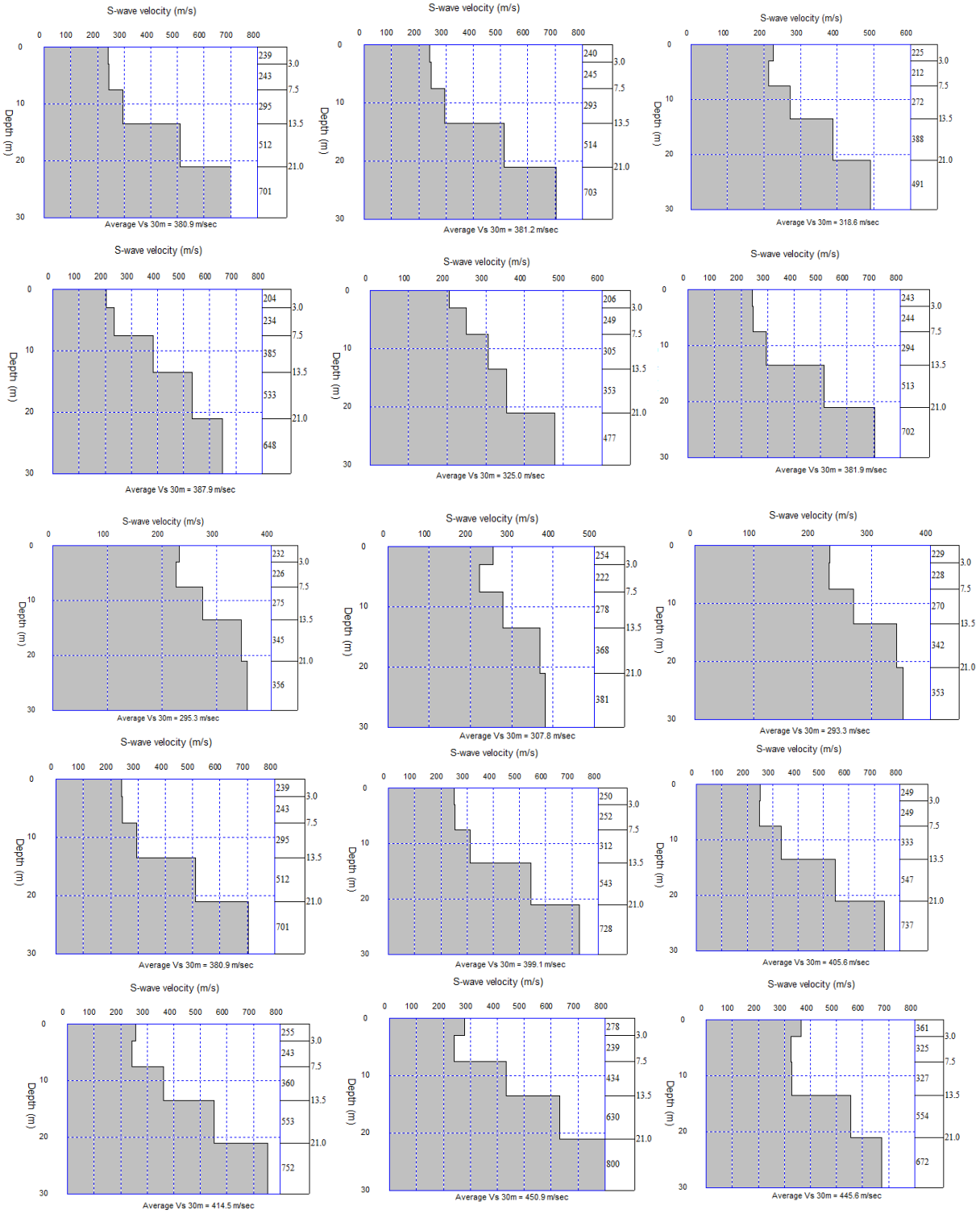


Profile 5 (E-E[1])

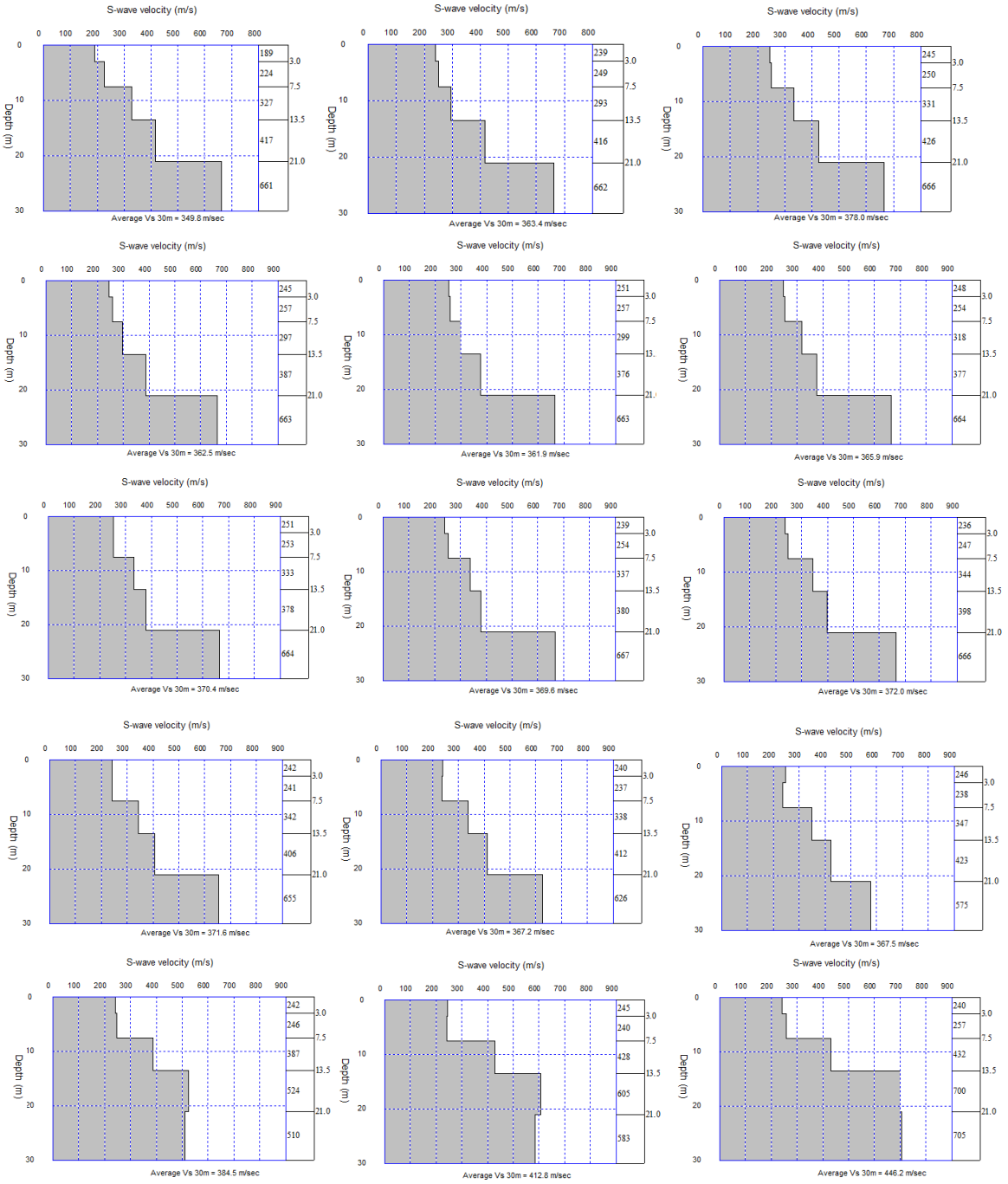


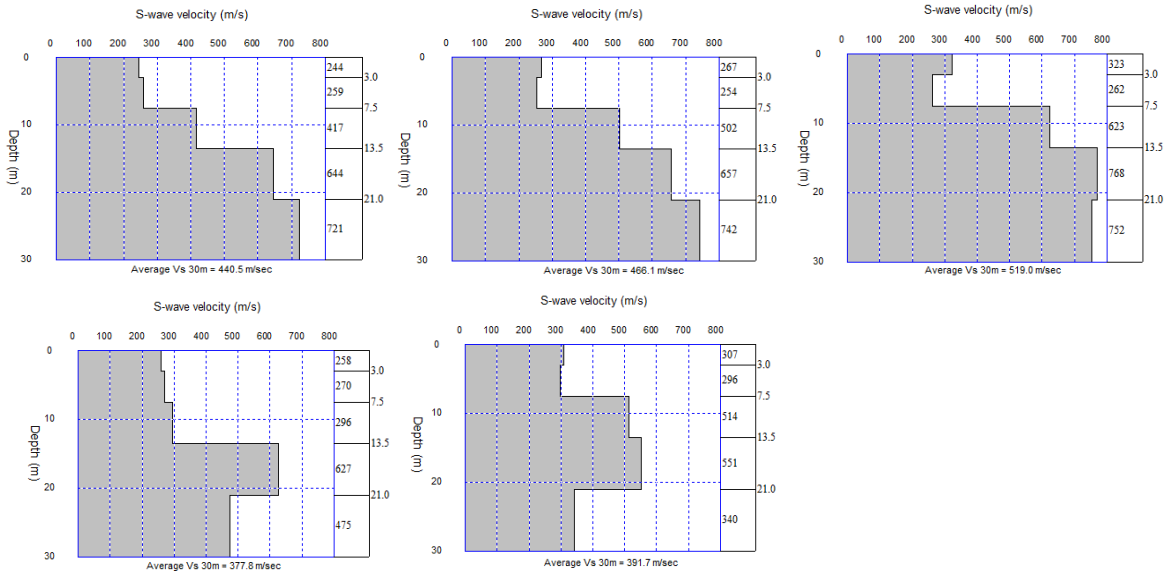

S-wave velocity (m/s)
0 100 200 300 400 500 600 700 800
Depth (m)
0 10 20 30
192 265 422 531 704
3.0 7.5 13.5 21.0
Average Vs 30m = 407.5 m/sec
S-wave velocity (m/s)
0 100 200 300 400 500 600 700 800
Depth (m)
0 10 20 30
196 291 427 494 700
3.0 7.5 13.5 21.0
Average Vs 30m = 412.5 m/sec
S-wave velocity (m/s)
0 100 200 300 400 500 600 700 800
Depth (m)
0 10 20 30
221 300 445 460 686
3.0 7.5 13.5 21.0
Average Vs 30m = 420.1 m/sec
S-wave velocity (m/s)
0 100 200 300 400 500 600 700 800
Depth (m)
0 10 20 30
261 319 482 424 666
3.0 7.5 13.5 21.0
Average Vs 30m = 434.0 m/sec
S-wave velocity (m/s)
0 100 200 300 400 500 600 700 800
Depth (m)
0 10 20 30
202 370 422 237 601
3.0 7.5 13.5 21.0
Average Vs 30m = 342.0 m/sec

Profile 6 (F-F[1])



Profile 7 (G-G[1])




S-wave velocity (m/s)
0 100 200 300 400 500 600 700 800
Depth (m)
0 10 20 30
244 259 417 644 721
3.0 7.5 13.5 21.0
Average Vs 30m = 440.5 m/sec
S-wave velocity (m/s)
0 100 200 300 400 500 600 700 800
Depth (m)
0 10 20 30
267 254 502 657 742
3.0 7.5 13.5 21.0
Average Vs 30m = 466.1 m/sec
S-wave velocity (m/s)
0 100 200 300 400 500 600 700 800
Depth (m)
0 10 20 30
323 262 623 768 752
3.0 7.5 13.5 21.0
Average Vs 30m = 519.0 m/sec
S-wave velocity (m/s)
0 100 200 300 400 500 600 700 800
Depth (m)
0 10 20 30
258 270 296 627 475
3.0 7.5 13.5 21.0
Average Vs 30m = 377.8 m/sec
S-wave velocity (m/s)
0 100 200 300 400 500 600 700 800
Depth (m)
0 10 20 30
307 296 514 551 340
3.0 7.5 13.5 21.0
Average Vs 30m = 391.7 m/sec